AD-A025 668

COHERENT OPTICAL ADAPTIVE TECHNIQUES (COAT)

ROCKWELL INTERNATIONAL CORPORATION

PREPARED FOR
ROME AIR DEVELOPMENT CENTER
DEFENSE ADVANCED RESEARCH PROJECTS AGENCY

FEBRUARY 1973

RADC-TR-73-95
Final Technical Report
February 1973

COHERENT OPTICAL ADAPTIVE TECHNIQUES (COAT)

North American Rockwell
Electronics Group
Research Division

Sponsored by
Defense Advanced Research Projects Agency
ARPA Order No. 1279, Amendment 5

Approved for public release;
distribution unlimited.

The views and conclusions contained in this document are those of the authors and should not be interpreted as necessarily representing the official policies, either expressed or implied, of the Defense Advanced Research Projects Agency or the U. S. Government.

Rome Air Development Center
Air Force Systems Command
Griffiss Air Force Base, New York

UNCLASSIFIED

Security Classification

DOCUMENT CONTROL DATA - R & D

(Security classification of title, body of abstract and indexing annotation must be entered when the overall report is classified)

1. ORIGINATING ACTIVITY (Corporate author)
North American Rockwell Electronics Group
3370 Miraloma Avenue
Anaheim, California 92803

2a. REPORT SECURITY CLASSIFICATION
UNCLASSIFIED

2b. GROUP

3. REPORT TITLE
Coherent Optical Adaptive Techniques (COAT) (U)

4. DESCRIPTIVE NOTES (Type of report and inclusive dates)
Final Technical Report

5. AUTHOR(S) (First name, middle initial, last name)
C. L. Hayes, et al.

6. REPORT DATE	7a. TOTAL NO OF PAGES	7b. NO OF REFS
Febraury 1973	115	4

8a. CONTRACT OR GRANT NO.	9a. ORIGINATOR'S REPORT NUMBER(S)
F30602-72-C-0417	C72-731/501 ✓
b. PROJECT NO.	
c. Program Code Number 2E20	9b. OTHER REPORT NO(S) (Any other numbers that may be assigned this report)
d. ARPA Order Number 1279, Amend. 5	RADC-TR-73-95 ✓

10. DISTRIBUTION STATEMENT
APPROVED FOR PUBLIC RELEASE;
DISTRIBUTION UNLIMITED.

SUPPLEMENTARY NOTES	12. SPONSORING MILITARY ACTIVITY
Monitored by R.F. Ogrodnik (315) 330-2747 RADC (OCTM-1) GAF, NY 13440	Advanced Research Projects Agency Washington D.C. 20301

13. ABSTRACT

COAT (Coherent Optical Adaptive Techniques) is the name given to an optical phased array transceiver system which automatically compensates for atmospheric distortion along the propagation path of the beam(turbulence, thermal blooming, laser amplifier). Based upon the principal of transmitting a wavegront which is the phase conjugate of the received wavefront, the COAT system can lock onto and track a target of very small dimension under conditions in which a conventional single-element system would fail or perform poorly. That is, energy can be focused at the target. A previous experiment successfully demonstrated the concept for a two-element system. This report describes the implementation and test results of a multiaperture (1x6) array operating at a wavelength of 10.6μm. Temporal and spatial information from the intensity distributions developed at ranges of 1 km and 10 km are presented as an evaluation of system performance. A theoretical prediction of system operation through computer simulation has also been made and shows the system to be operating near the theoretical limit.

DD FORM 1 NOV 68 1473

UNCLASSIFIED

Security Classification

14 KEY WORDS	LINK A		LINK B		LINK C	
	ROLE	WT	ROLE	WT	ROLE	WT
Adaptive Array						
Coherent Optical Techniques						
Target Re-imaging						

COHERENT OPTICAL ADAPTIVE TECHNIQUES (COAT)

C. L. Hayes, et al

Contractor: North American Rockwell - Electronics Group - Research Division
Contract Number: F30602-72-C-0417
Effective Date of Contract: 20 March 1972
Contract Expiration Date: 23 February 1973
Amount of Contract: $213,500.00
Program Code Number: 2E20

Principal Investigator: C. L. Hayes
Phone: 714 632-2239

Program Manager: R. A. Brandewie
Phone: 714 632-3682

Project Engineer: R. F. Ogrodnik
Phone: 315 330-2747

Approved for public release;
distribution unlimited.

This research was supported by the Defense Advanced Research Projects Agency of the Department of Defense and was monitored by R. F. Ogrodnik under Contract F30602-72-C-0417.

FOREWORD

This final technical report is submitted to the Rome Air Development Center in partial fulfillment of the requirements of Contract F30602-72-C-0417, "Coherent Optical Adaptive Techniques." The program was initiated on 20 March 1972.

The work described in this report was performed by the Lasers and Advanced Radiation Systems Group; Research and Technology Division; Electronics Group of North American Rockwell; 3370 E. Miraloma Avenue, Anaheim, California.

Major contributors to this effort are:

C. L. Hayes: Principal Investigator
R. A. Brandewie
W. C. Davis
G. E. Mevers
J. SooHoo
J. Yamamoto

This technical report has been reviewed and is approved

Robert F. Ogrodnik
RADC Project Engineer

Arthur J. Frohlich
ARTHUR J. FROHLICH
Chief, Techniques Branch
Surveillance & Control Division

ACKNOWLEDGMENTS

At this time, we gratefully acknowledge the assistance and cooperation of Mr. G. Ochs and Dr. R. Lawrence of NOAA for the use of their equipment in collecting atmospheric data.

Also, a special note of appreciation is directed to Mr. L. Lawrence of WPAFB Avionics Laboratory for the timely delivery of material needed to pursue the laboratory tests on this program.

In addition, the use of PbSnTe detectors furnished by Drs. A. Joseph, J. Lango, and M. Andrews of the Rockwell International Corporation's Science Center is gratefully noted.

We are indebted to Mr. R. F. Ogrodnik of the Rome Air Development Command for his concise and constructive suggestions offered during the execution of this program and preparation of reports.

TABLE OF CONTENTS

I. INTRODUCTION AND SUMMARY

A. Introduction

This report is concerned with experimental demonstration and test of a linear (1 x 6) array phase conjugation COAT system. COAT stands for Coherent Optical Adaptive Technique, an infrared or optical phased array method which was invented by North American Rockwell almost ten years ago. This device, which retransmits the phase conjugate of the received wavefront, can be used for correction of atmospheric inhomogenities (blooming, turbulence) as well as for automatic target acquisition, pointing and tracking.

The basic method is illustrated in Figure I-1. There, an array of laser beams, derived from a single laser source, is shown with provision for measuring the phase of the wave which returns from a target(s), and adjusting the phase of the wave which is transmitted. Suppose that the phase adjusters are set to produce a plane wave. After traversing the optical system, which is no doubt vibrating, and the atmosphere, which is certainly turbulent and perhaps blooming, the wave is no longer planar, and energy is going in various directions other than toward the target(s), which, of course, is where we want to concentrate energy.

COAT makes use of the fact that the return from any one target point is spherical in nature. Thus, the return wave, after traversing the

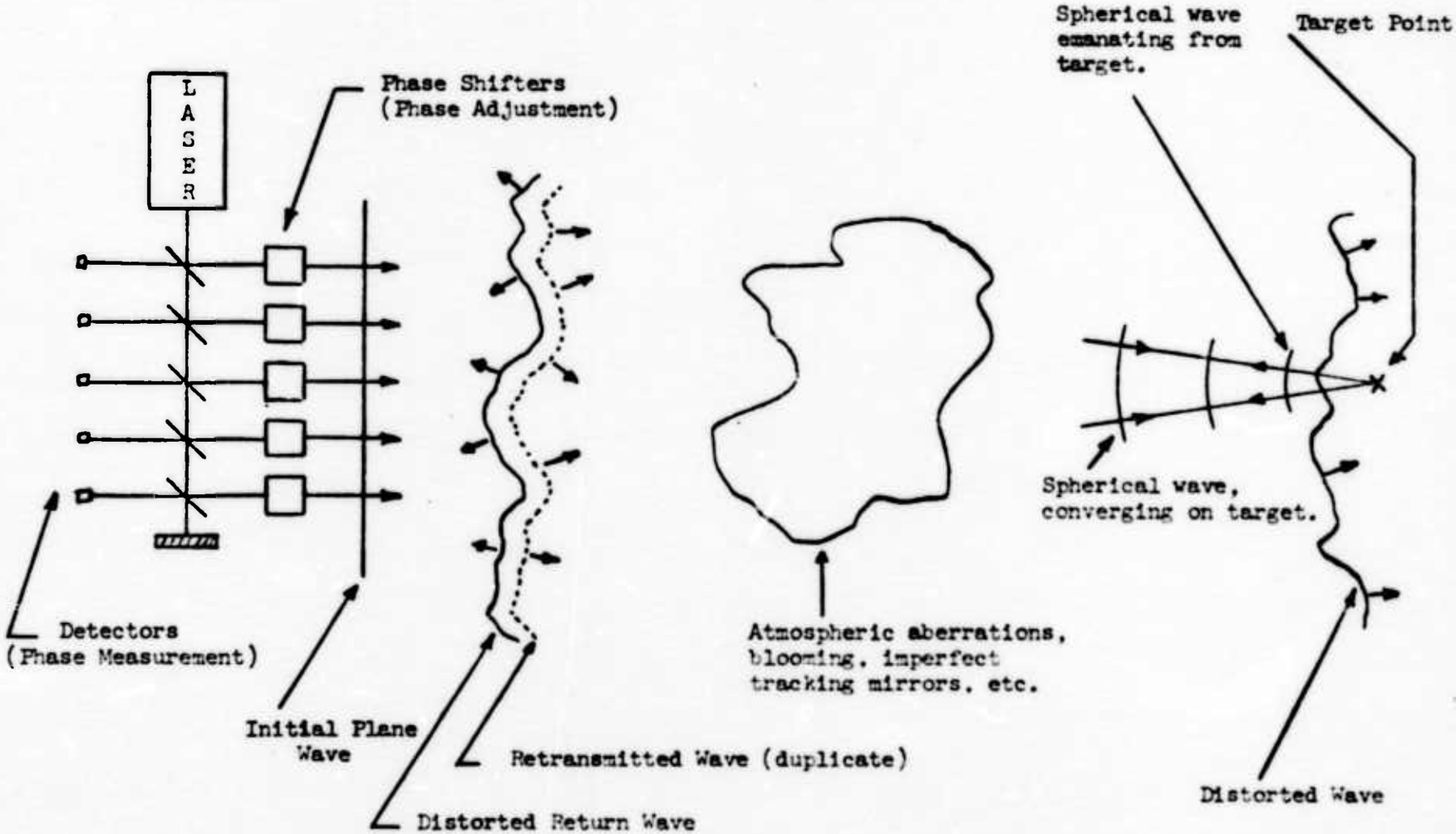

Figure I-1. Illustrating the Operation of Phase Conjugation COAT

atmosphere or other perturbations, is sampled by the phase measurement detectors which determine the spatial distribution of the return wavefront. Since we know a priori that this wavefront should have been spherical, the phase measurement gives sufficient information for correction of the intervening turbulence, blooming, vibrations, or other perturbations. It is only necessary to transmit the duplicate of the received wavefront toward the target, and the reciprocity principle assures us that a properly focused spherically converging wave will arrive at the target point. The mathematical expression for this operation is "phase conjugation," and we therefore refer to this system as phase conjugation COAT.

It can be seen from Figure I-1 that phase conjugation COAT will produce a spherically converging wave on the target point no matter where the target is located within the array field of view. Therefore, COAT can also function both as a target locating device, and as a target tracking device. If a target suddenly appears anywhere within the COAT field of view, the adaption process described above will lock the system onto the target automatically. Furthermore, once the system is locked-on, the target will be tracked across the field of view. All of this is performed automatically, with no mechanical or electronic time lags. The only limitation is the transit time of light to and from the target point.

Further, analysis shows that the phase conjugation principle is selective in adapting to a multiglint target. That is, repeated transmission of compensated wavefronts to the multiglint target reinforces energy buildup on the point of highest reflectivity. This is an important consideration when concerned with real targets which are normally characterized by a multitude of glint sources.

North American Rockwell recognized the potential of COAT almost a decade ago. Our first patent disclosure on COAT was prepared early in 1963. The first demonstration of a COAT system in the infrared was achieved at NR in 1968, under the sponsorship of Rome Air Development Command (RADC). Using a two-element array, experiments were performed at ranges of 150 m and 4.6 km. These experiments are described in detail in our final report.[1]

Following the successful experimental demonstration of COAT using a two-element array, NR performed a detailed computer analysis and trade-off study of multi-element COAT systems for complex targets. This work was performed under ARPA/RADC sponsorhsip and is described in detail in our final contract report.[2] During the past year, again under ARPA/RADC sponsorship, we have fabricated and experimentally tested a six-element linear COAT system using advanced optical and electronic implementation methods. In the past years program we have experimentally demonstrated every important aspect of COAT operation, including atmospheric correction, target location, and target tracking. Specifically, we have demonstrated experimentally:

1. Compensation for atmospherically induced perturbations.
2. Lock to a single glint target centered in the field.
3. Lock to a single glint target at various locations within the field of view.
4. Lock to a moving glint target.
5. Lock to the glint of highest reflectivity in a multi-glint target environment.

6. Speed of adaptive acquisition limited only by transit time.

7. Improvement in array focusing capability.

Furthermore, all of the above experimental results have been found to be in excellent agreement with our theoretical and computer simulation predictions.

B. Summary

Propagation of coherent radiation through the atmoshpere is significantly affected by meterological phenomena and turbulence conditions. Thermal "blooming" of high energy beams is also known to present propagation problems. That is, induced wavefront distortion limits the ability of a system to bring such radiation to a focus as required for some laser systems. Theoretical calculations show that the ability of a fixed focus system to concentrate energy does not improve with ever-increasing aperture size as classical theory predicts due to these effects. Previous contractual effort[1,2] has shown that coherent optical adaptive techniques (COAT) can be used to overcome these problems. This is accomplished through the use of phase controlled multi-aperture arrays to compensate for all wavefront distortions - naturally occurring or induced. In addition, other benefits are derived from segmenting the aperture in that smaller, less expensive optical elements can be used with an attendant relaxation in pointing requirements, mounting, and pointing hardware. To this end, the current COAT program was directed toward the design, construction, and experimental demonstration of a multi-aperture optical

system which can effectively compensate for such atmospherically induced aberrations. Employing the phase conjugation principle for wavefront control, a six-element linear arry was fabricated for operation at a wavelength of 10.6μ meters. Detailed tests were conducted to evaluate performance with respect to the following primary objectives:

1. Compensate for atmospheric propagation effects at 10.6μ meters and provide improved focusing capability at the target for two ranges.
2. In a multiglint target scenario, establish the ability of the system to lock onto a single glint point.
3. Acquire and track a glint point which moves across the array field of view.

All of the tasks have been successfully demonstrated.

System operation and a detailed discussion of the optical configuration is presented in Section II. In designing the system, consideration was given to future operation at higher power levels and a self-compensating feature for the type of environment most likely to be encountered is discussed. A brief introduction to an analytical description of array operation is given as a prelude to examining the data obtained during the tests.

In Section III, each component is described along with the function each performs in the system. The range instrumentation as well as the target diagnostic equipment used to collect the data at the field sites are shown. Complete atmospheric data were also recorded for computation of the refractive index structure constant (C_n^2) and a description of this equipment is also given.

Section IV presents, chronologically as the data was recorded, the type of information used to evaluate system performance. This includes the temporal and spatial responses measured at the target for a variety of operational modes. That is, among the parameters varied were: the number of elements; the spacing of the elements; the number of targets; the reflectivity of the targets; and the target position in the array field of view. These data clearly indicate successful operation of the system.

In Section V, a direct comparison to a computer simulation is made. The simulation is done by codes previously developed which incorporate a model of the atmospheric turbulence into the computation. An exact intensity distribution of the propagated energy is defined in the target plane and shows a one to one correspondence with experiment.

Finally, Section VI presents some of the conclusions of this program and suggests a course of action for the future.

II. THEORY OF SYSTEM OPERATION

A. COAT Array for Phase Conjugate Operation

The COAT system is a multiple channel heterodyne transceiver employing common transmit/receive optics for each independent channel. In simplest terms, each channel samples the relative phase of the incoming wave and retransmits radiation having a conjugate phase relationship. In this way, compensation for atmospheric and other induced aberrations can be achieved. Of course, the normal "problems" associated with operation of this type of common aperture system must be considered. That is, surface scatter from components, optical isolation between channels, providing sufficient local oscillator power, component movement, etc., are factors which determine the optimum approach.

Basic operation of the system can best be understood by referring to the simplified optical diagram of Figures II-1 and II-2 and the hardware implementation shown in Figure II-3. The primary subsystems are denoted by the laser, beamsplitters, frequency modulator, output optics, and the detectors with associated processing electronics. By following the signal path in one arm, the conjugate compensation action of COAT can be described as well as the elimination of component scatter effects which experience obtained from various programs involving common aperture has shown can be a problem.

Consider that the transmitted waves for each channel are split-off by beamsplitters B_1 .... B_n. After leaving the beamsplitter B_1, the wave passes through the combination frequency shifter and phase modulator.

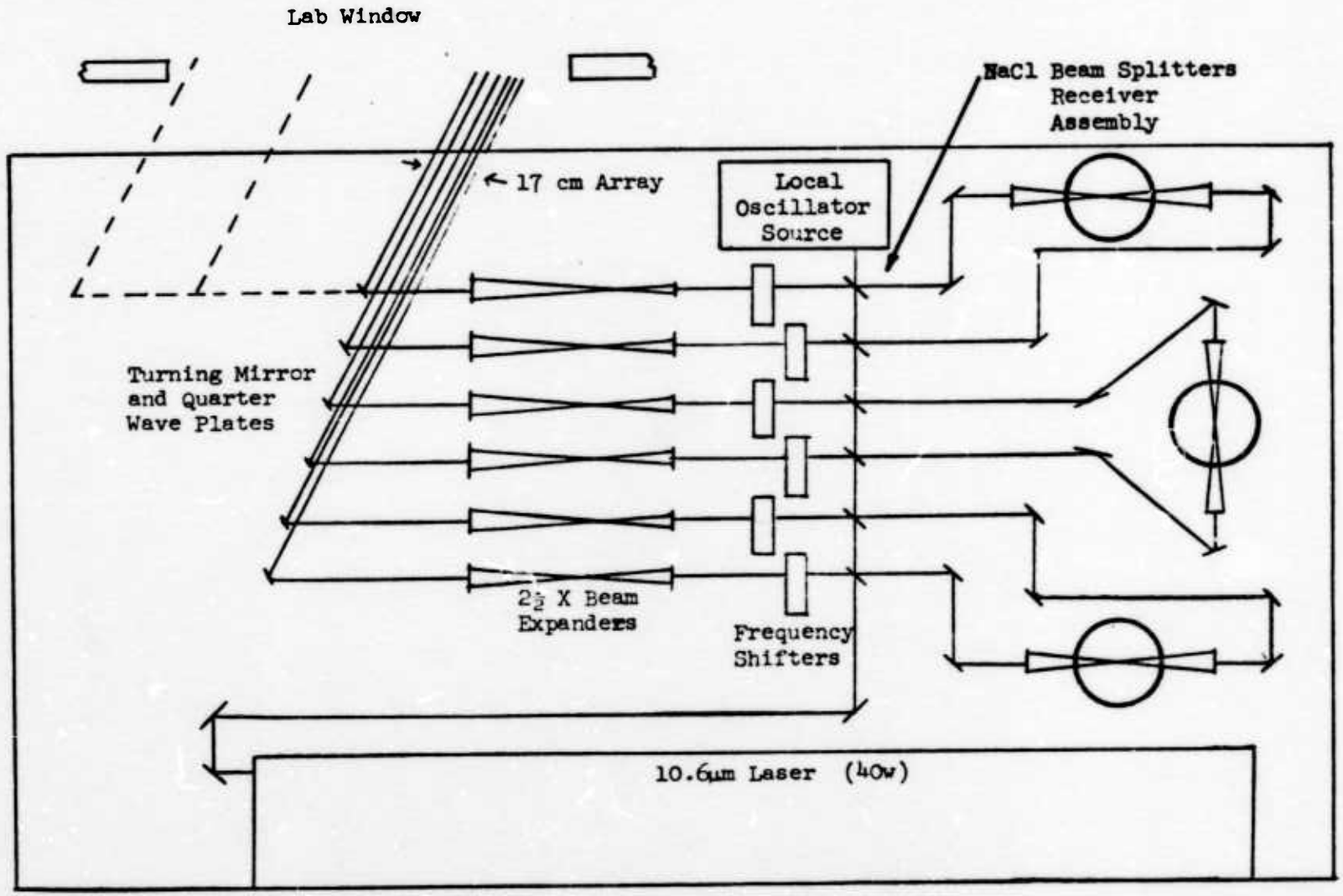

Figure II-1. Optical System Layout

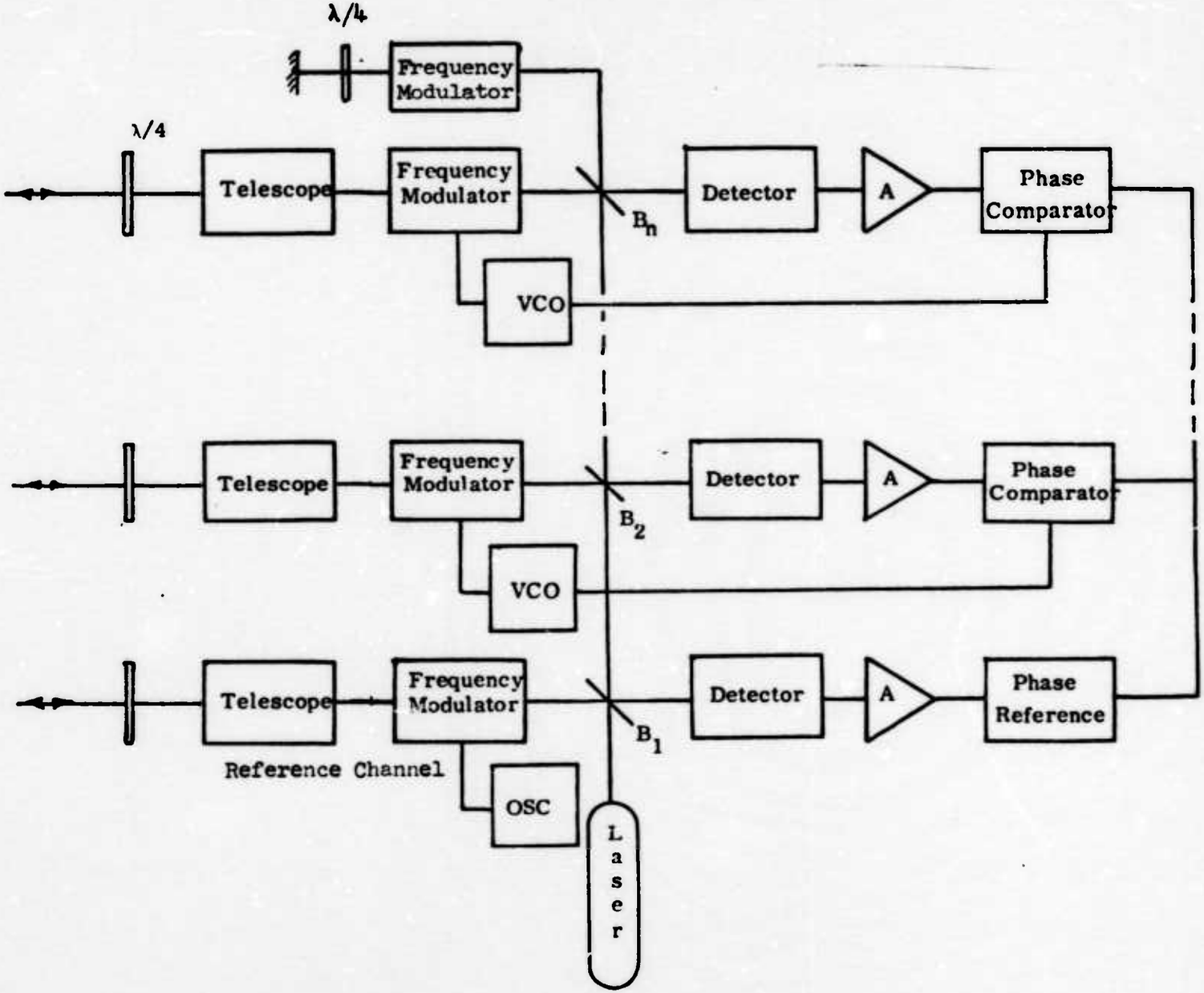

Figure II.2. Simplified COAT Optical Function Diagram

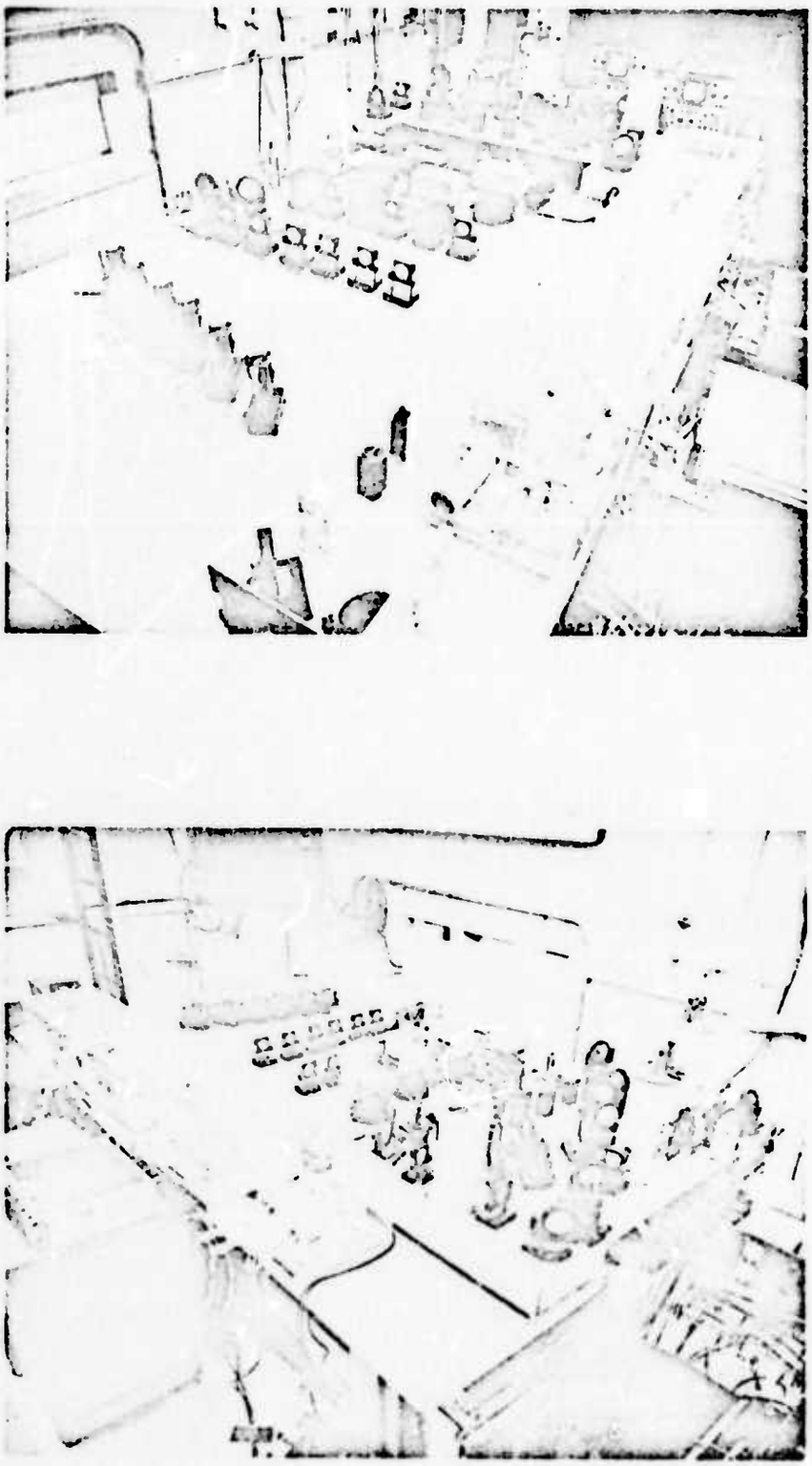

Figure II-3. Two Views of COAT Six-Element System

(The modulator for one arm can be used as a frequency shifter only, serving as a reference for the other arms.) After being frequency shifted by one-half the IF frequency, the wave passes through the telescope and a quarter wave plate. The purpose of the $\lambda/4$ plate is to rotate the polarization of the wave a total of 90° when it passes out through the plate and returns through the same plate or one in another arm. This provides a return signal of the same polarization as the LO which has been shifted 90° in polarization. The telescopes are used to provide less beam divergence and to increase the level of the received signal.

The return wave comes back through the same optics. This is done so that not only the effects of the atmosphere, but also the effects introduced by all the components in the path are compensated. Passage through the frequency shifter produces an additional frequency shift of one-half the IF. The received wave is then combined with the LO at the beamsplitter to provide an IF signal for phase comparison. If the phase of the IF from detector n does not agree with the phase of the IF from the reference detector, the difference is used to drive the phase modulator so that the phases are equal. This automatically sets the phase modulator so that the conjugate of the received signal is transmitted.

The same laser is used for the optical local oscillator and the transmitter. The wave passing through B_n is rotated in polarization by passing through the quarter wave plate and frequency shifter twice. The polarization-rotated wave is then partially reflected by the beam-splitters B_1, B_2 ....., B_n to provide a local oscillator (LO) signal

for the n detectors. (The polarization rotation is required to provide a heterodyne signal with the received radiation and prevents the laser signal used as a LO from feeding back into the laser and causing instabilities. (A side effect of the rotation of the polarization of the LO is that the reflectivity of the beamsplitters B_1 - B_n is different for the LO than for the transmitted waves.) In this way any scatter in the transmit path prior to the frequency modulator has an associated frequency which is at baseband. Since the return signal when detected generates an i-f of twice the phase-modulator frequency bandpass filtering isolates the effects of this scatter.

For these components in the transmit path between the modulator and the array apertures, any scatter directed back toward the receiver appears at the i-f frequency. The quarter wave plates serve to isolate this unwanted signal. Only that radiation which passes through the exit wave plate twice (the return signal) will be of the proper polarization to combine with the LO to generate a signal. Thus, effective discrimination is achieved.

Two additional benefits are derived from using only one laser to mechanize a frequency offset heterodyne system of this type. First, the short-term laser stability requirements can be relaxed considerably from those required of two lasers phase-locked to a predetermined offset. A frequency shift of as much as 1.5 MHz/msec can be tolerated with little deterioration of system performance. Second, this interferometric approach lends itself to a self-compensation feature which is deemed necessary for future operation at increased power levels. The following discussion describes this feature.

Since the function of the adaptive array is to conjugate the phase of the transmitted beams with respect to the received beams, reasonable care must be exercised to assure that errors within the system are minimized. It is possible (probable in most implementations) that the system will tolerate a certain amount of fixed or slowly varying phase error. However, a configuration which compensates for path length changes within the system is highly desirable. To better understand the nature of the problem, consider the effect of a change in path length between the beam splitters B_1 and B_2. This causes a change in the relative phase of the local oscillator to the detectors and, consequently, a change in the relative phase of the IF's. The system assumes a change in the atmosphere and incorrectly changes the phase shifter. The path change between B_1 and B_2 can be caused by local air turbulence, thermal expansion of the table or mount, or vibrations. Consequently, the system must be recalibrated. This was done manually in the original COAT experiments by peaking the received signal as the phase was varied, but as the number of elements increases, this becomes impractical. One approach which can be considered to eliminate the effects of such movements is to use a separate interferometer to control the positions of all the elements on the table. A preferable technique is to use a self-compensating system.

To obtain self-compensation for path changes internal to the system, all paths - after the transmitter and local oscillator beam are split for the n-elements - must be traversed by two waves. With the exceptions of the LO and received waves, they must be traveling in opposite directions. The configuration of Figure II-2 meets this requirement. In this case, if the separation between B_1 and B_2 changes, the system automatically

compensates. To analyze the operation, assume that the transmitted waves in arms 1 and 2 are properly phased and the beamsplitter separation ℓ increases. This causes the transmitted wave of arm No. 2 to be retarded by, say δ radians. The signal into detector No. 1 remains

$$S_1 = A_1 \cos \omega_r t + \cos \omega_o t \tag{1}$$

where A_1 is the amplitude and ω_r the angular frequency of the received wave in arm No. 1 and ω_o is the angular frequency of the LO. The signal into detector No. 2 becomes

$$A_2 \cos \omega_r t + \cos(\omega_o t + \delta) \tag{2}$$

The resulting intermediate frequencies (IF's) are described by

$$A_1 \cos(\omega_r - \omega_o)t \tag{3}$$

and

$$A_2 \cos[(\omega_r - \omega_o)t - \delta] \tag{4}$$

The system assumes that its LO is always true and therefore reacts as if the <u>received</u> wave at No. 2 were <u>retarded</u> δ degrees by atmospheric effects. The attempt to compensate by conjugating the transmitted wave then results in the phase of the transmitted wave from element No. 2 being advanced in phase. This compensates for the retardation caused by the increase in the distance ℓ.

If the path length from B_1 to the detector changes, it simply adds a phase α to both cosines of Eq. 2 resulting in its removal by sub-

traction in the IF or difference frequency Eq. 4. Similarly, any changes in the phase of the LO or transmitter before they pass through a beamsplitter affect all signals equally; the relative phase does not change.

This system has been assembled as shown in Figure II-3 and performs in the manner described. In summary, the system provides:

1. Offset heterodyne operation.
2. Phase control of unlimited dynamic range through frequency modulation.
3. A six-element linear array of variable width.
4. A self-compensating interferometer to eliminate the effects of component movement.
5. Isolation from component backscatter.
6. Optical isolation between receiver channels, and
7. Implementation of a conjugate control system.

Complete details of the design of each component of the system are presented in the first quarterly report of the present contract[3]. Only a brief description is presented here.

B. Theoretical Prediction of Performance

Before presenting the experimental results and technical description of the system, it is informative to mathematically determine what the performance of an array of this type should be. In practice, this type of prediction is done by a sophisticated computer program which

provides an exact solution. For purposes of discussion an analytical approach yields a means of assessing system performance in terms of array parameters.

Figure II-4 illustrates the approach to be described. The illumination of the array (aperture function) can be mathematically described by the convolution and multiplication of several independent functions. Let a circular aperture by illuminated by a Gaussian function

$$A(r) = K\, e^{-r^2/\sigma^2} \tag{5}$$

The basic aperture function is

$$\text{circ}(r) = \begin{cases} 1 & r < d/2 \\ 0 & r > d/2 \end{cases} \tag{6}$$

Thus, the generalized illumination for this aperture is given by

$$\begin{aligned} f_{\text{aperture}} &= A(r)\ \ \text{Circ}(r) \\ &= Ke^{-r^2/\sigma^2}\ \text{Circ}(r) \end{aligned} \tag{7}$$

Since d is fixed, to account for an aperture filling factor due to the Gaussian, let

$$d/2 = kT$$

or

$$\sigma = d/2k \tag{8}$$

for use in generalized evaluation after the analysis has been carried through for far field conditions.

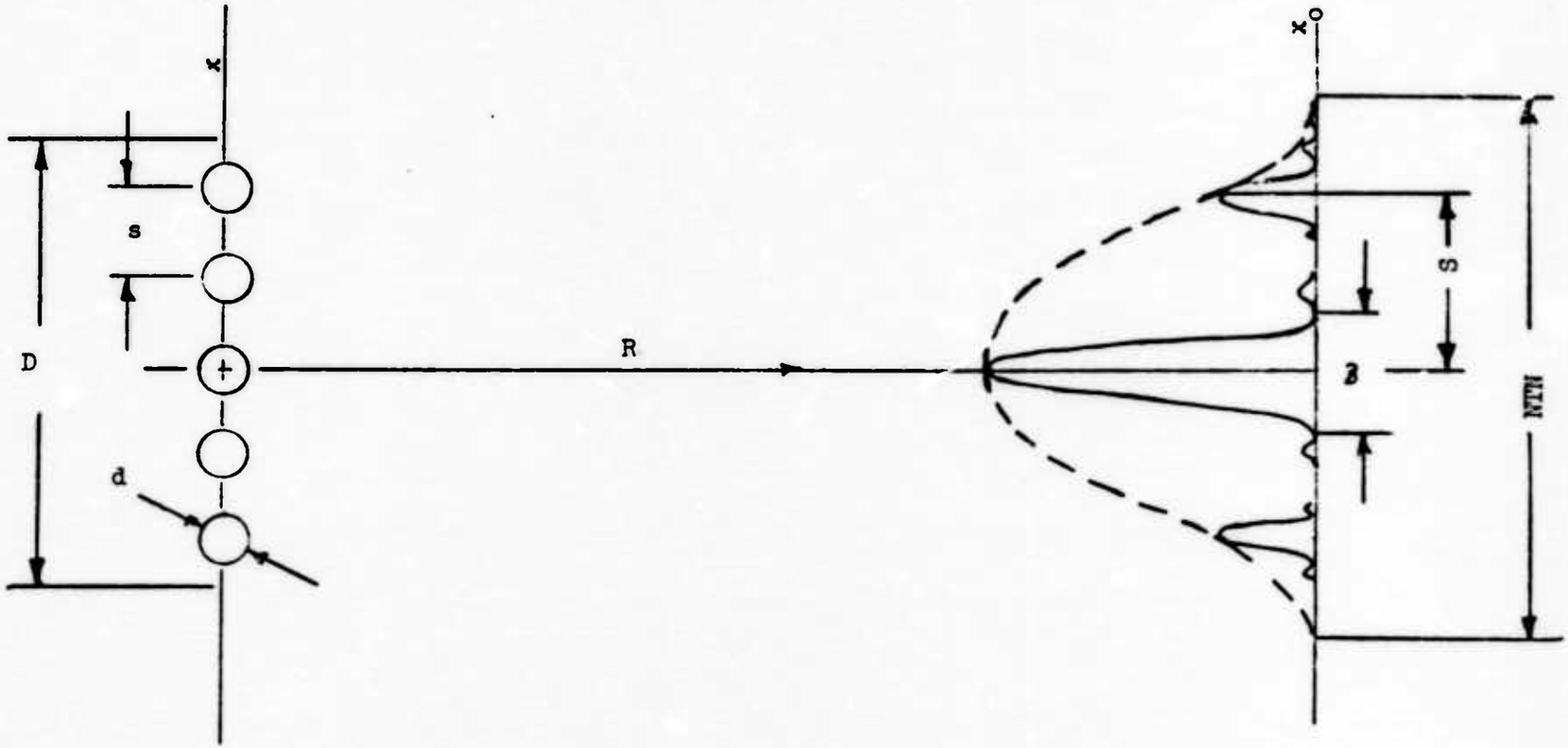

$$f_{array} = \left[A(r)\ \mathrm{Circ}(r) \circledast \mathrm{Comb}\left(\frac{x}{s}\right)\right] \mathrm{Rect}\left(\frac{x}{D}\right) \longrightarrow \omega = 2\,\frac{\lambda R}{D}$$

$$S = \frac{\lambda R}{s}$$

$$NTN_{min} = 2.44\,\frac{\lambda R}{d}$$

Figure II-4 Definition of Symbols for Calculation of Array Diffraction Patterns

To complete the description of the input function, the comb function is required, i.e.,

$$\text{comb}\left(\frac{x}{s}\right) = s \sum_{n=-\infty}^{\infty} \delta(x-ns) \tag{9}$$

along with the aperture limiting function

$$\text{rect}\left(\frac{x}{D}\right) = \begin{cases} 1 & |x| < D/2 \\ 0 & |x| > D/2 \end{cases} \tag{10}$$

The array function can now be written as

$$f_{array} = \left[A(r) \cdot \text{Circ}(r) \circledast \text{comb}\left(\frac{x}{s}\right)\right] \cdot \text{Rect}\left(\frac{x}{D}\right) \tag{11}$$

where $\circledast$ denotes a convolution operation.

Invoking the convolution theorem for far field conditions

$$\overline{f_{array}} = \left[\left[\overline{A(r)} \circledast \overline{\text{Circ}(r)}\right] \overline{\text{comb}\left(\frac{x}{s}\right)}\right] \circledast \overline{\text{Rect}\left(\frac{x}{D}\right)} \tag{12}$$

$$\text{or} \quad \left[\overline{A(r)} \circledast \overline{\text{Circ}(r)}\right]\left[\overline{\text{comb}\left(\frac{x}{s}\right)} \circledast \overline{\text{Rect}\left(\frac{x}{D}\right)}\right] \tag{13}$$

where $\overline{}$ indicates a Fourier transform operation. To evaluate this function requires that the individual transforms be completed and the appropriate convolution operation be performed.

To evaluate $\overline{A(r)}$ and $\overline{\text{Circ}(r)}$ use is made of the Hankel transform of zero order. That is,

$$F(\rho) = 2\pi \int_0^{\infty} f(r)\, r\, J_0(2\pi r\rho)\, dr \tag{14}$$

Thus,

$$\overline{A(r)} = 2\pi K \int_0^\infty e^{-r^2/\sigma^2} r J_o(2\pi r\rho) dr$$

$$= e^{-\pi^2\sigma^2\rho^2} \tag{15}$$

and

$$\overline{Circ(r)} = 2\pi \int_0^{d/2} r J_o(2\pi r\rho) dr$$

$$\propto \frac{J_1(\pi d\rho)}{\rho} \tag{16}$$

It is also known that

$$\overline{comb\ (\frac{x}{s})} = s\ comb\ (\frac{fx}{s}) = \sum_{n=-\infty}^{\infty} \delta(fx - \frac{n}{s})$$

where $fx = x_o/\lambda R$ and x_o is the transform plane coordinate. Of course, $\rho^2 = fx^2 + fy^2$ in the same plane for a system of cylindrical coordinates chosen.

The final transform is

$$\overline{Rect\ (\frac{x}{D})} = sinc\ \pi\ fx\ x_o$$

$$= sinc\ \frac{\pi D}{\lambda R} x_o \tag{17}$$

The far field distribtuion is from (13)

$$\overline{f_{array}} = \left[e^{-\pi^2\sigma^2\rho^2} \circledast \frac{J_1(\pi d\rho)}{\rho} \right] \left[\sum_{n=-\infty}^{\infty} \delta(fx - \frac{n}{s}) \circledast sinc\ \frac{\pi D}{\lambda R} x_o \right]$$

$$= \left[e^{-\frac{x_o^2}{(\frac{\lambda R}{\pi\sigma})^2}} e^{-\frac{y_o^2}{(\frac{\lambda R}{\pi\sigma})^2}} \circledast \frac{J_1\left(\frac{\pi d}{\lambda R}\sqrt{x_o^2+y_o^2}\right)}{\frac{1}{\lambda R}\sqrt{x_o^2+y_o^2}} \right] \left[\sum_{n=-\infty}^{\infty} \delta\left(\frac{x_o}{\lambda R} - \frac{n}{s}\right) \circledast sinc\ \frac{\pi D}{\lambda R} x_o \right] \tag{18}$$

This is a two-dimensional distribution which was scanned in the $y_o = 0$ plane. Thus, the field distribution at the detector becomes

$$\overline{f_{array}}\Big|_{y_o=0} = \left[e^{-\frac{x_o^2}{(\frac{\lambda R}{\pi\sigma})^2}} \circledast \frac{J_1(\frac{\pi d}{\lambda R} x_o)}{\frac{1}{\lambda R} \cdot x_o} \right] \left[\sum_{n=-\infty}^{\infty} \delta\left(\frac{x_o}{\lambda R} - \frac{n}{s}\right) \circledast \operatorname{sinc} \frac{\pi D}{\lambda R} x_o \right] \qquad (19)$$

The field of view of the array is determined by the first term in brackets. The second set of brackets contains all the information to describe the fringe spacing as well as the amplitude characteristics of each fringe. Of particular interest is the width associated with the field of view of the array and the impact of the extent of truncation of the illuminating Gaussian distributed radiation.

In terms of the fixed aperture diameter, the first bracket of (17) becomes

$$F(x_o) = e^{-\frac{x_o^2}{(2k\frac{\lambda R}{\pi d})^2}} \circledast \frac{J_1(\frac{\pi d}{\lambda R} x_o)}{\frac{x_o}{\lambda R}} \qquad (20)$$

Expressed as the standard deviation parameter in the far field

$$\sigma_o = \frac{2k}{\pi} \frac{\lambda R}{d} \qquad (21)$$

For an input function which is not truncated at the $1/e^2$ points ($k = 1$), the far field pattern width at the same points is $2\sigma_o = \frac{4}{\pi} \frac{\lambda R}{d}$ as is well known. Truncation, however, causes the far field pattern to become larger and the overall width is governed by the convolution distance associated with the intensity function obtained by squaring (20).

This is not easily evaluated analytically, but some general conclusions can be obtained.

First, if $k \to o$ $(\sigma \to \infty)$, or plane wave illumination the null to null spacing of the patterns is given from

$$\frac{J_1 \left(\frac{\pi d}{\lambda R} x_o\right)}{\left(\frac{x_o}{\lambda R}\right)} = 0.$$

That is

$$2x_o = \frac{2(3.83)}{\pi} \frac{\lambda R}{d}$$

$$= 2.44 \frac{\lambda R}{d} \qquad (22)$$

For this case, the field of view can be no narrower. If $k \to \infty$ $(\sigma \to o)$ the field of view is infinitely wide. For k generally, the field of view is bounded as

$$\text{Max}\left[\frac{2k}{\pi} \frac{\lambda R}{d}, \frac{2.44\ \lambda R}{d}\right] < W < \frac{2.44\ \lambda R}{d} + \frac{2k}{\pi} \frac{\lambda R}{d} = \left(2.44 + \frac{2k}{\pi}\right) \frac{\lambda R}{d} \qquad (23)$$

using the nulls of one distribution and $1/e^2$ points of the other. A general conclusion from this analysis would be that the illuminating function for each element should be such to fill the aperture as much as possible without sacrificing an exorbitant amount of power. Experimental results show this to be true and the filling factor for the present system can be readily calculated.

In summary, to achieve optimum array performance in terms of resolution or delivery of energy to the target, a closely packed array with small array

elements should be constructed. The larger the overall dimensions of the array, the better the system resolution can be at the expense of constructing a large number of elements. System performance of the linear array constructed and tested for this program will be made in terms of this analysis.

III. DESCRIPTION OF EQUIPMENT

A. Array Components

In this section, a brief description of each of the components used to mechanize the system is presented. The first quarterly technical progress report[3] gives a more detailed presentation of each device.

From Figure II-2, the first components in the transmission path are the beamsplitters $B_1 \ldots B_n$. Their basic function is to provide the proper power distribution of the laser output to the various channels of the array. This includes not only the transmit power, but also the LO power distribution required for heterodyne operation as part of the self-compensation feature of this system. In addition, they also provide interchannel isolation.

To achieve the best performance, the material must exhibit a low loss, introduce little depolarization of the beam, and provide relatively scatterfree surfaces. The alkali halide salts, in general, adequately meet these requirements. The optical absorption at 10.6 micron is usually too small to measure, and the fact that they are hygroscopic is immaterial since all experiments are performed in a controlled environment. Other materials, semiconductors, are available but are not used for COAT as a matter of economy.

The key element in the implementation of the COAT system is the phase modulator. This device provides the means for achieving phase conjugate operation of the array. Ideally, this modulation function should have unlimited dynamic range, wide bandwidth, and introduce no insertion loss. Consideration was given to electromechanical, electromagnetic, electro-optical, and acousto-optical concepts for implementing this function. It was found that the acousto-optic Bragg cell functioning as a frequency modulator can meet the unlimited dynamic range and bandwidth requirements with some penalty being paid in the area of insertion loss.

A complete description of this device is found in Reference 4. Briefly, the modulator is composed of a germanium substrate with a $LiNbO_3$ transducer bonded to one end of the substrate and an acoustic absorber at the other end. The acoustic frequency used to drive the cell is centered at 18 MHz for the transmitting channels and at 15.75 MHz for the local oscillator beam. This results, upon detection, in an intermediate frequency of 4.5 MHz which is used for the electronic processing controls. Class C amplifiers driven by voltage controlled oscillators provide the acoustic power to achieve the frequency conversion of the optical beam.

Since germanium is transparent to the 10.6 micron radiation only if the crystal temperature is not too far above room temperature a simple, effective cooling system has been provided. Figure III-1 shows the

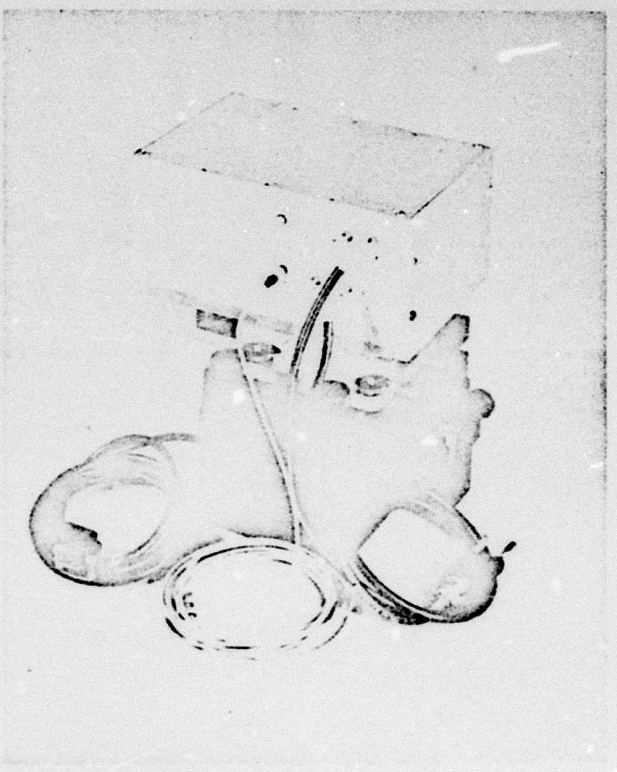

Figure III-1: Acousto-Optic Frequency Modulator

modulator as constructed, complete with cooling jacket, power driver, and positioning mount.

Upon exiting from the frequency shifters as a 1 cm beam, beam expanders are inserted in order to meet the exit aperture design of 2.5 cm. This has been accomplished by the fabrication of simple 2.5X telescopes having NaCl lenses. Sufficient space was provided in the optical layout to accommodate a high f number design so that spherical aberration is negligible. NaFlcoatings were provided to minimize surface reflection.

The final elements in the optical paths (6 channels) are mounts for implementing the linear array. They consist of a turning mirror and quarter-wave plate assembly as illustrated by Figure III-2. The pointing sensitivity is 2/3 milliradian per 360° rotation of the adjustment micrometer for both elevation and azimuth. A minimum spacing of 4 mm can be achieved from a 6-inch incident spacing for the six beams.

The quarter-wave plates have been fabricated from single crystal cadmium sulfide having a clear aperture of 25 mm. The retardation error of these units is less than ± 1% of the total 5/4 λ retardation. Antireflection coatings yield less than 1% reflection per surface. Absorption is about 0.5% cm^{-1} for the approximate 3 mm thickness. Crystal orientation has been determined and marked to within 0.5°.

The detector-receiver assembly uses a $Pb_{1-x}Sn_xTe$ (photovoltaic) detector as the initial element in the processing chain. These devices have been made available through the cooperation of the North American Rockwell Science Center and are characterized by wide bandwidth and quantum

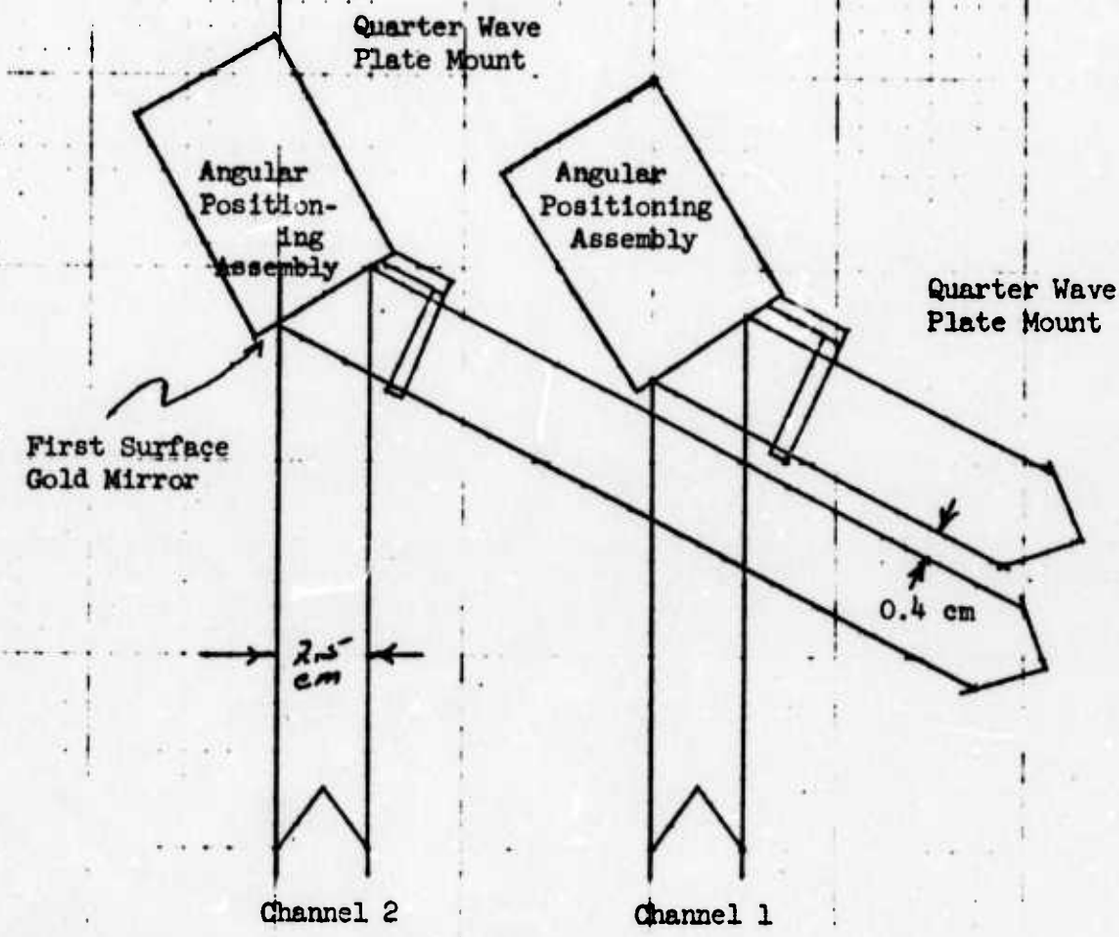

Figure III-2. Final Turning Mirror and Quarter Wave Plate Mount

efficiencies of up to 80%. Their operation at 77°K (liquid N_2) provides a distinct advantage over other detectors. Two detectors are mounted in each dewar used in the system as shown in Figure III-3.

The outputs of these detectors at 4.5 MHz are used to achieve adaptive compensation. The electronics function within a closed loop to generate a transmitted wavefront which is the conjugate of the received wave. At the same time isolation from noise sources and phase perturbations must be provided. FigureIII-4 illustrates a simplified configuration which accomplishes these tasks. The detector, i-f, phase demodulation, VCO, and frequency modulator combination forms the "nulling" servo which controls adaption. This is done by sampling the relative phase difference between each channel and a reference and using this signal to control the frequency modulator which then provides automatic compensation of the transmitted wave.

Frequency modulation techniques as a form of angle modulation are attractive for two reasons and have been implemented in this system. First, frequency modulation provides the means for a phase shifter of unlimited dynamic range. Second, it provides the necessary frequency offset to attain heterodyne detection at a predetermined IF value. As discussed previously, a device well-suited to this task is an acousto-optic modulator operating in the Bragg angle mode. An acoustic wave propagating in the medium (e.g., Ge) interacts with the laser radiation to impose on it a Doppler shift corresponding to the driving frequency. Transmission efficiency depends upon the electronic power input as well as optical path length. By varying the driving power, amplitude modulation

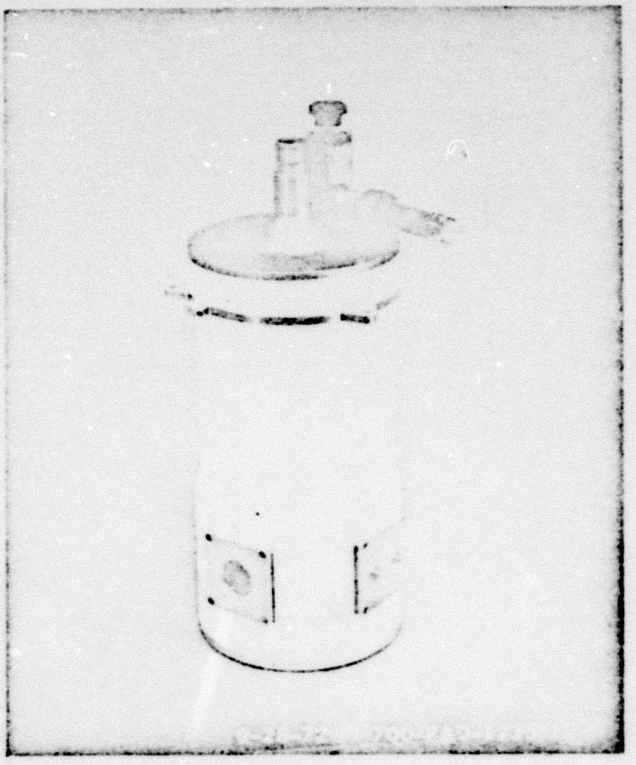

Figure III-3. Dewar Assembly Containing Two PbSnTe Detectors

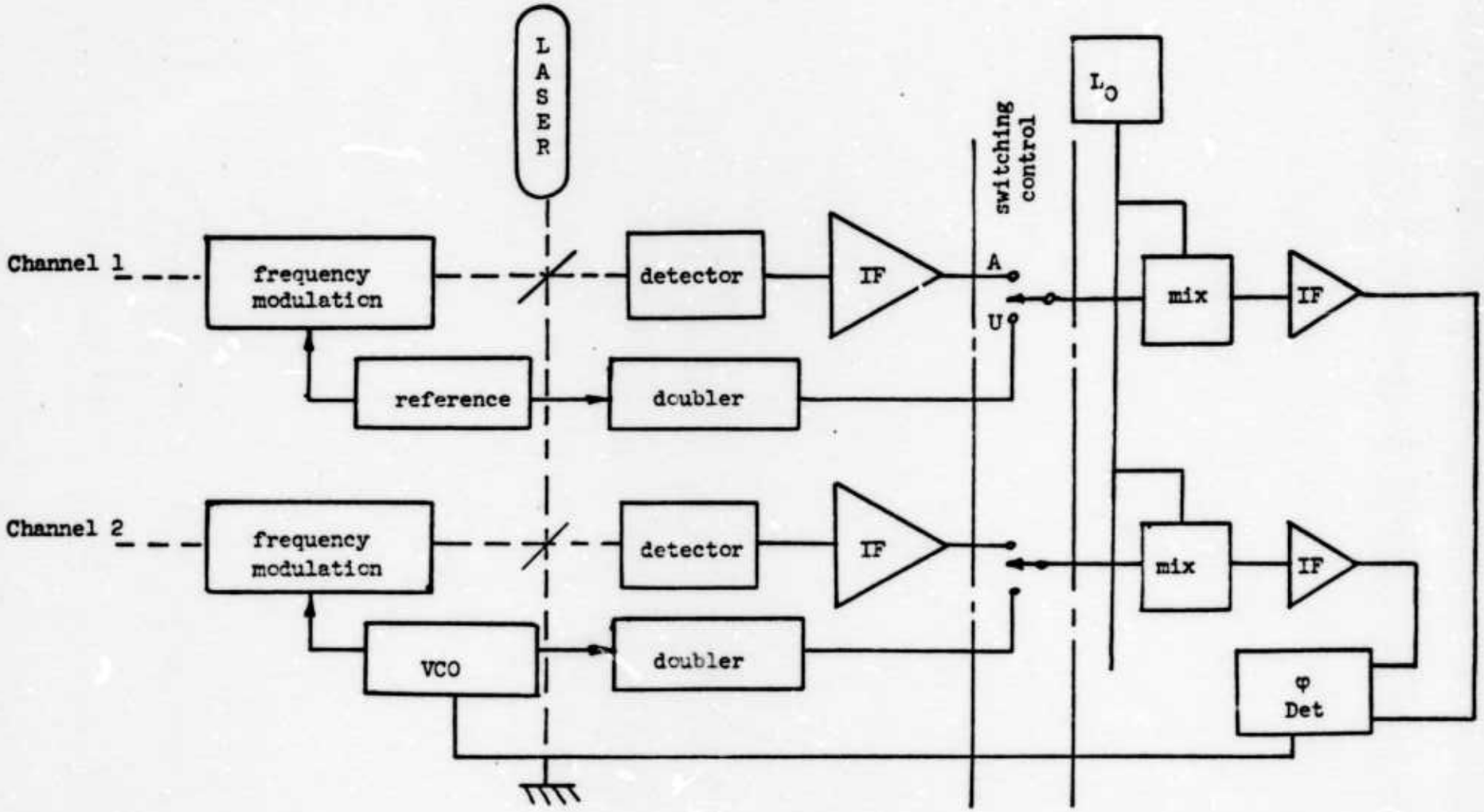

Figure III-4. COAT Control Electronics (U)

can be realized; by varying the frequency of the driver, phase modulation results. The frequency deviation required can be determined in the following manner.

The equation of an a-c wave in generalized form is

$$S = A \sin \psi(t)$$

where

S = instantaneous amplitude

A = peak amplitude

$\psi(t)$ = total angular displacement at time t.

The instnataneous angular velocity ω_i is by definition

$$\omega_i = \frac{d\,\omega(t)}{dt} .$$

A frequency modulated wave is by definition a wave in which the instantaneous angular velocity is varied as

$$\omega_i = \omega_o + \Delta\omega(t)$$

Thus,

$$\omega_i = \frac{d\,\psi(t)}{dt} = \omega_o + \Delta\omega(t)$$

Therefore,

$$\psi(t) = \int \omega_o dt + \int \Delta\omega(t)dt$$

$$= \omega_o t + \int \Delta\omega(t)dt .$$

Since the compensation required in the COAT system must follow the form

$$S = A \sin (\omega_o t + \varphi(t) + \varphi_o)$$

it follows that the change in frequency required to match the time varying phase is

$$\varphi(t) + \varphi_o = \int \Delta\omega(t)dt \quad .$$

The error detection portion of the control loop is mechanized with a synchronous detector using a reference frequency of 0.5 MHz. This is done by mixing a 5.0 MHz reference with the 4.5 MHz i-f's which is the heterodyne offset. (Twice the difference frequency of the frequency shifters.) Phase information is transferred directly from one carrier to another and processing of the information at a lower frequency is done to provide better accuracy of the measurement. The detector being used is fabricated from TTL devices. The main features of this circuit is its ability to furnish an error signal over $\pm 360^{\circ}$ before becoming cyclical. In closed loop operation, the error signal is a very small quantity in the neighborhood of 0° and the full range of detection is not necessary. However, in order to assess the amount of phase shift between any two elements during unadapted operation, such a device is required.

An additional feature not previously discussed but indicated in Figure III-4 is the two modes of operation for this system - adapted and unadapted. In the "unadapted" mode, the switching control bypasses

the I-F outputs and"locks" all channels to the reference oscillator. Thus, the phase differences between channels remain a constant. If such a feature was not provided, the phases between channels would vary randomly due to frequency instabilities inherent in VCO operation (residual f-m, temperature effects, etc.). This is tantamount to an induced "moving" fringe pattern at the target and measurements to be taken of atmospheric effects would be totally masked.

The switching control section (r-f switch) also provides the means for testing the transient behavior of the system. By monitoring the rate of power build-up at the target when changing from unadapted to the adapted mode an evaluation of system bandwidth can be made. Of course, the switching control must also provide synchronization signals to the detector at the target to provide a time base for the data. This has been mechanized through a laser communication link.

In summary, the processing control described provides closed loop operation for each channel during the unadapted and adapted modes with compensation for atmospheric effects occuring during the latter. Phase control over an unlimited dynamic range is provided. Data outputs from the I-F's(amplitude demodulated) and the phase detectors are the information from which an assessment of system operation have been made.

Table III-1 summarizes how the present system is fabricated. Operational data indicates that the system performs as designed as evidenced by the results to be presented later.

TABLE III-1

CONDENSED TABLE OF COAT PARAMETERS

OPTICS	
Number of Apertures	6
Power per Channel	0.3 watts
Size of Apertures	2.5 cm
Array Geometry	Linear (1 x 6) Variable Width (Nominally 3 cm)
Scatter Suppression	Polarization Discrimination Transmitter - Vertical Receiver - Horizontal
Optical Material for Lenses and Beamsplitters	NaCl
Phase Modulator	Acousto-Optic Bragg Cell Center Frequency - 18 MHz
Quarter Wave Plates	5/4 λ Cadmium Sulfide
LASER	
10.6 μm CO_2 - Single Mode	60 watts (max)
DETECTORS	
PbSnTe (77°K)	Heterodyne Mode Receiver
ELECTRONICS	
Post Detection Amplifier	Current Mode Operation
Processing I-F	4.5 MHz
Servo Control	Phase Lock
Phase Detector Range	$\pm$ 2π radians
Tracking & Acquisition Bandwidth for a Transit Time of 7.0 μ	50 KHz

B. Test Range Facilities

In order to establish conclusively the ability of the COAT system to compensate for atmospheric effects, testing facilities at two different ranges (nominally 1 Km and 10 Km) have been constructed. Figure III-5 illustrates the elevation profile for each site. Power and instrumentation at each receiving site is provided by a mobile van especially equipped for this purpose. Figure III-6 shows this unit with a diesel-powered generator and some of the instrumentation. Figure III-7 illustrates the permanent type facility at the 10 Km range which is used to house the target plane scanner, C_N^2 measurement instrumentation, weather instruments, and ancillary equipment.

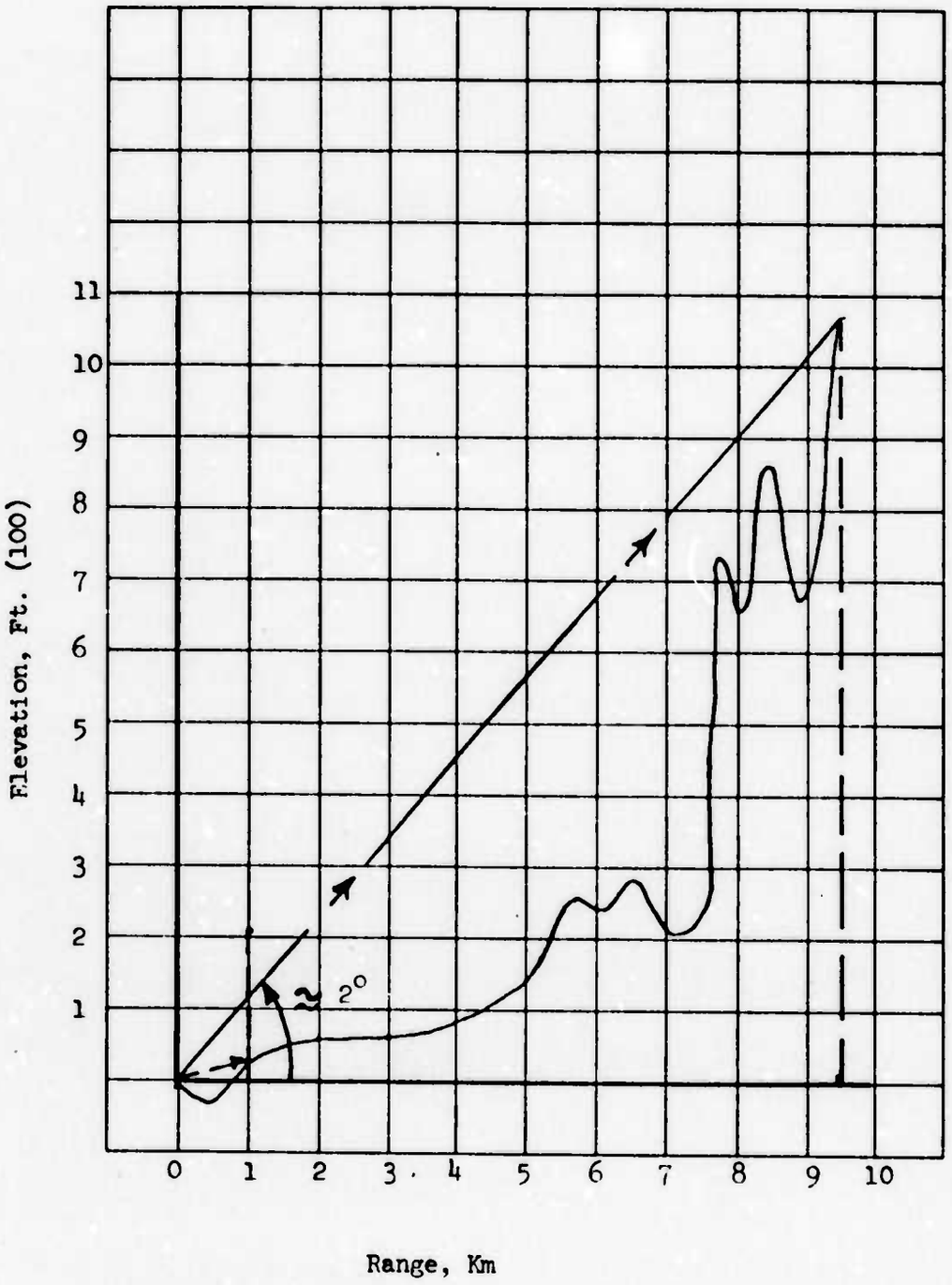

Figure III-5. Range Profile

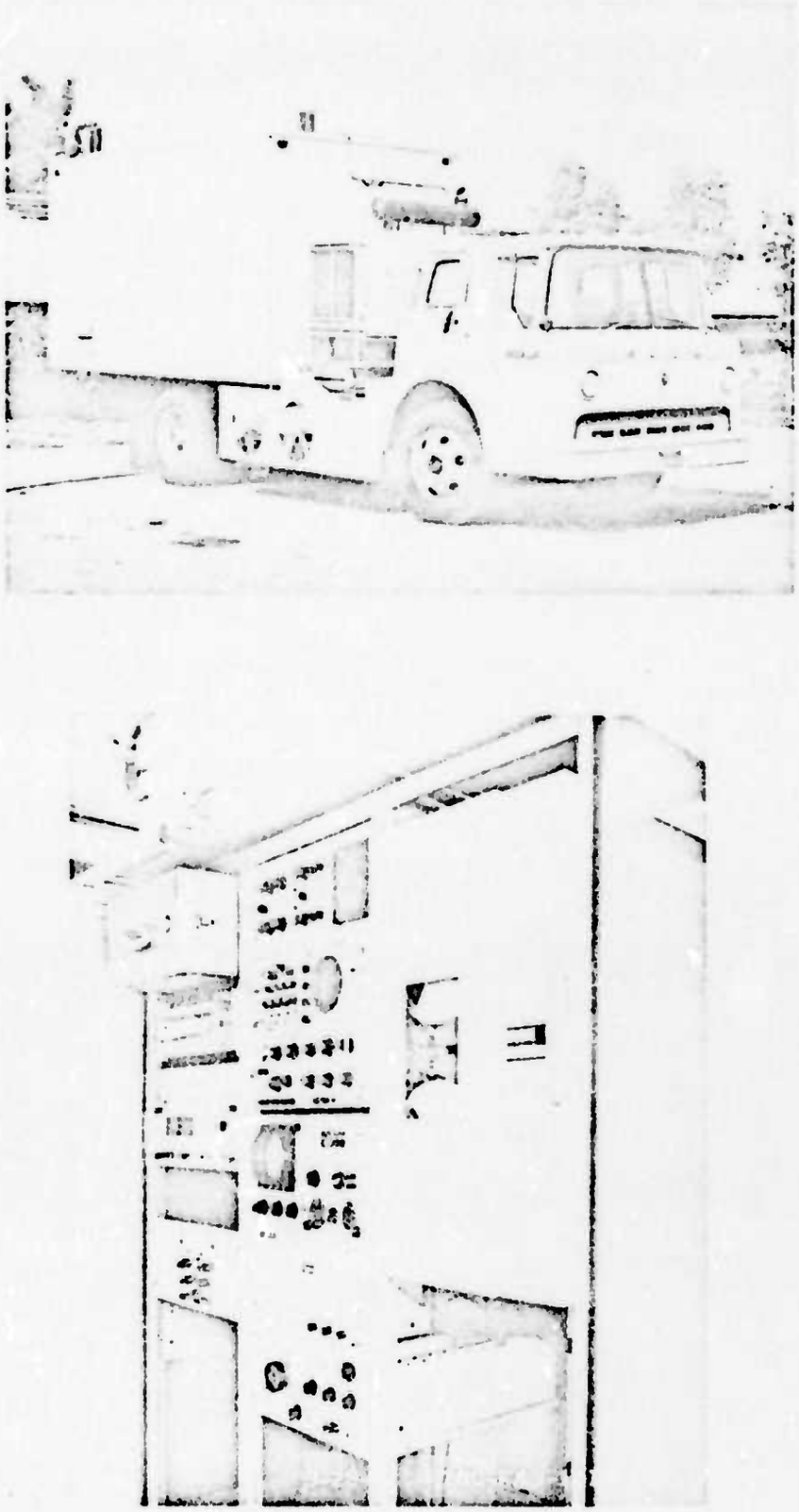

Figure III-6. Mobile Power and Instrumentation Van for Use at Remote Sites

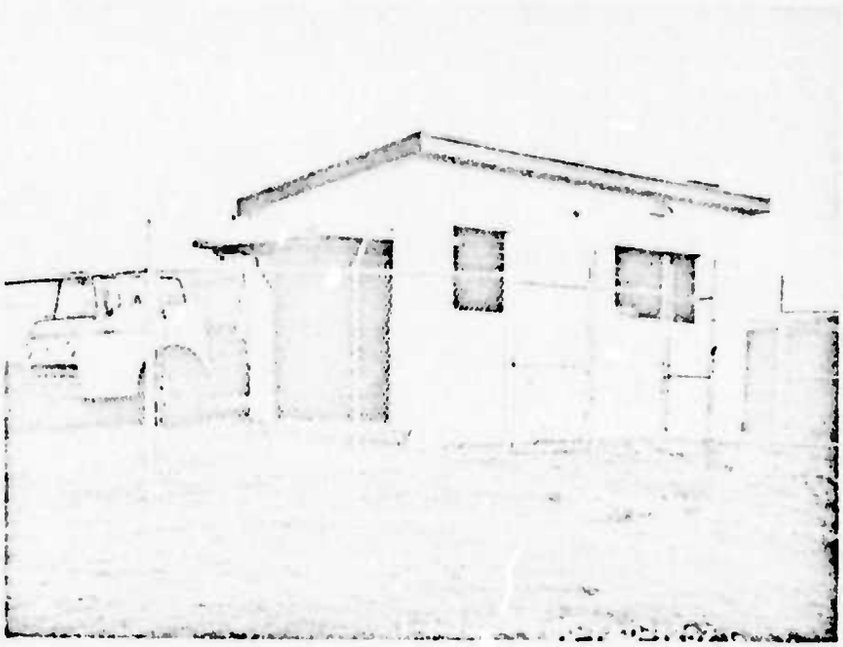

10 Km Facility

10 Km Transmission Path

Figure III-7. 10 Km Test Range

C. Target Diagnostic Equipment

For adequate assessment of system performance, both temporal and spatial measurements of the target plane intensity distribution are required.

The measurement of the COAT transmitted intensity distribution in the target plane before and after adaption is made by moving a Hg-Cd-Te detector across the field and monitoring the position and output of the detector. This task is accomplished by using a standard laboratory optical bench, slightly greater than 1.6 meters in length, as a base for two precision ground guide rails which carry a carriage for mounting the detector package. This detector carriage can be driven, at speeds up to 3 cm per second, over a distance of 1.5 meters by means of a drive motor and circulating ball lead screw. The field-of-view of the detector package is 2 milliradians and since the 1.5 meter carriage travel at the 1 km range produces a 1.5 milliradian azimuth change in the direction of incident radiation at the detector, the allowed pointing error of the detector package, plus the angular tolerance in the carriage, is less than 0.5 milliradians. An electrical pick-off provides a single voltage proportional to the carriage position in the 1.5 meter travel distance. A pair of limit switches mechanically adjustable in position and located one on each side of the carriage are wired to reverse the drive motor direction when tripped. By adjusting the position of the limit switches, a field width up to a maximum of 1.5 meters can be scanned by the detector. Figure III-8 shows this scanner in operation.

The detectivity (D^*) of this detector is 2×10^{10} cm $Hz^{\frac{1}{2}}$ watt^{-1} which permits operation at a SNR of 100 db with an aperture of 1 cm at 1 Km.

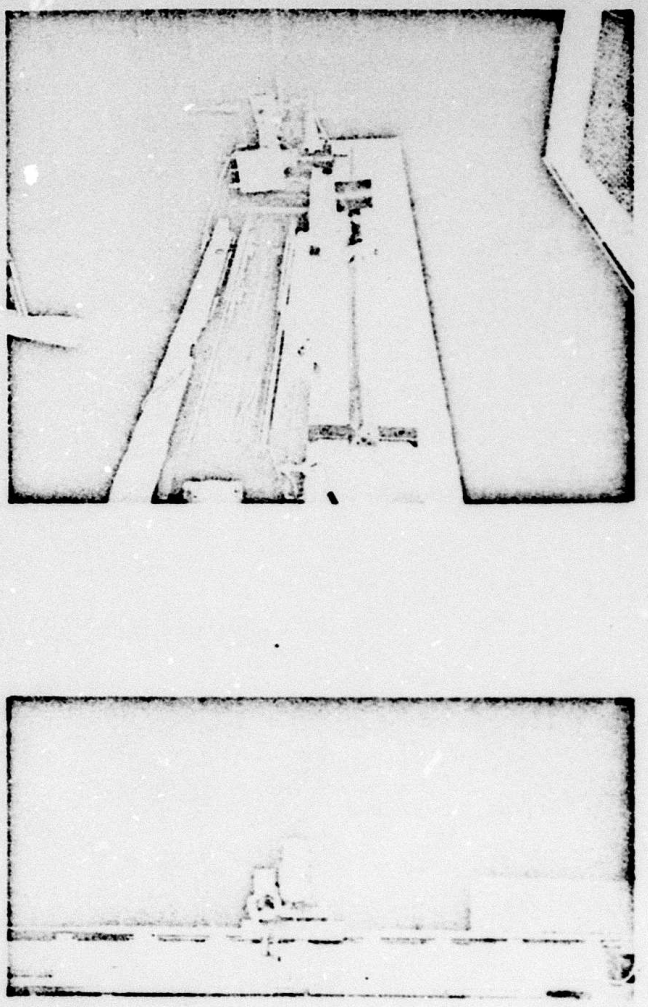

Figure III-8. HgGdTe Detector and Target Plane Scanner

With this signal margin available, test results have been taken with the aperture reduced to a 1 mm vertical slit. Thus, in all scanned results that are presented a resolution of 1 mm is assured. Post detection electronics are designed to have a bandwidth of 100 KHz so that sufficient response is available to assess the COAT adaptive power build-up response within one transit time.

D. Atmospheric Diagnostic Equipment

In order to adequately assess the COAT system's ability to compensate for atmospheric effects, diagnostic equipment to define the refractive index structure constant, C_N^2, is required. Two related types of C_N^2 measurements have been made for this program based upon an optical measurement and using thermal probe data which can be simply related to C_N^2 through C_T^2. Simultaneous readings of air temperature, barometric pressure, relative humidity, and wind velocity have been made.

The optical measurement of the refractive index structure constant was made with a small-bore 10.6 micron laser ($\approx$ 5 watts output) located at the transceiver end of the COAT range and propagating over nearly the same path* as used for the COAT system tests. The laser (Sylvania, Model 948) was mounted on a platform which is stable and can be pointed in azimuth and elevation to an accuracy of 1 arc minute using a telescope mounted on the platform and bore-sighted to the laser. In addition, the laser meets

* This laser beam and the COAT beams travel at the same height above the ground, but are made to diverge a maximum of 3 meters as they approach the target field to prevent interference of the two measurements.

the following operating requirements:

1. Operation - CW
2. Spatial mode structure - TEM_{00}
3. Beam diameter - 1.0×10^{-2} m*
4. Intensity fluctuation** - 3×10^{-3}.***

At the target end of the propagation range the atmospheric-produced scintillation of the laser source was observed with a 10.6 micron "point" collector.**** This receiver (Figure III-9) used a liquid neon-cooled Hg:Ge detector and was designed to the following specifications:

1. Collection aperture - $\leq 1 \times 10^{-2}$ meters

   The objective lens of the receiver is actually 2.5 cm diameter, f/5 lens, but uses a 1 cm mechanical stop to meet the requirements of propagation theory.
2. Electrical bandwidth - DC to 2 kHz
3. Linear dynamic range - 1000:1
4. Operating signal-to-noise ratio of > 40 db for a propagation range of 10 km and an atmospheric attenuation of 1 db/km.

---

* This value is based on a minimum measurement range of 1.0 km and assumes a Gaussian distributed laser exit pupil - - provides the necessary conditions to apply spherical-wave propagation theory.

** The ratio of the rms intensity fluctuation, as measured over the bandwidth of DC to 2 kHz, to the mean intensity.

*** This intensity fluctuation is one-tenth the scintillation produced by a value of $C_N^2 = 1.0 \times 10^{-15}$ $m^{-2/3}$ for operation at 10.6 microns over a minimum range of 1.0 km.

**** An aperture small enough so that the intensity distribution across the aperture is well correlated. Theory predicts this dimension to be the square root of the wavelength propagation range product, but experience has shown that a dimension of about one-tenth of this value produces more usable results.

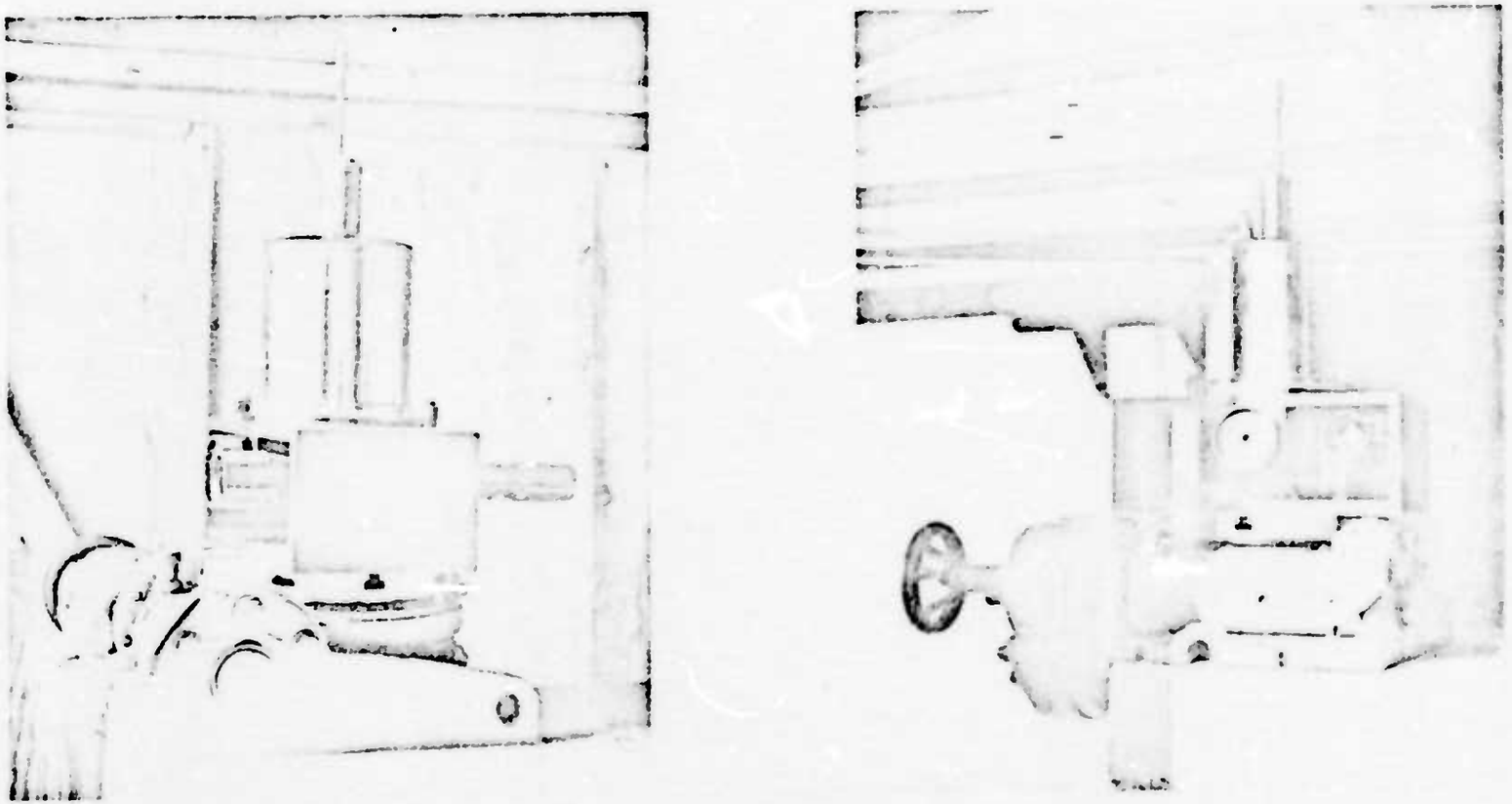

Figure III-13. Hg:Ge Detector/Receiver for C_N^2 Tests

In addition, the receiver pre-amp was designed such that the bias voltage of the detector could be "bucked-out" of the output signal. This permitted maximum utilization of the magnetic data recorder dynamic range used for data storage. For alignment this receiver was mounted on a platform that could be pointed in azimuth and elevation to an accuracy of five arc minutes.

The refractive index structure constant was also determined by measuring the temperature structure constant, C_T^2, which is simply relatable to C_N^2 when the mean air temperature and barometric pressure are known. This measurement was made with a pair of small (about 10 micron diameter) platinum wire thermal probes spatially separated by a small distance (10 to 15 cm) and connected in a bridge configuration so that the temperature differences between probes could be measured (Figure III-10). The actual response time required with these thermal probes is a function of the wind speed, but past operation has shown that a 300 Hz bandwidth is sufficient for good measurements.

Unlike the optical technique, there are no problems with careful control of angular alignment associated with use of the thermal technique. This fact and the lack of large measurement space and elaborate equipment has led many workers to use the thermal technique for measurement of the refractive index structure constant. This technique, however, is not without its problems. Basically, the thermal probe measurement is more noisy than the optical measurement, its accuracy in measuring C_N^2 is somewhat dependent on wind speed, and it can be adversely affected by airborne solid matter (both by erosion of the thermal probes and anomalous

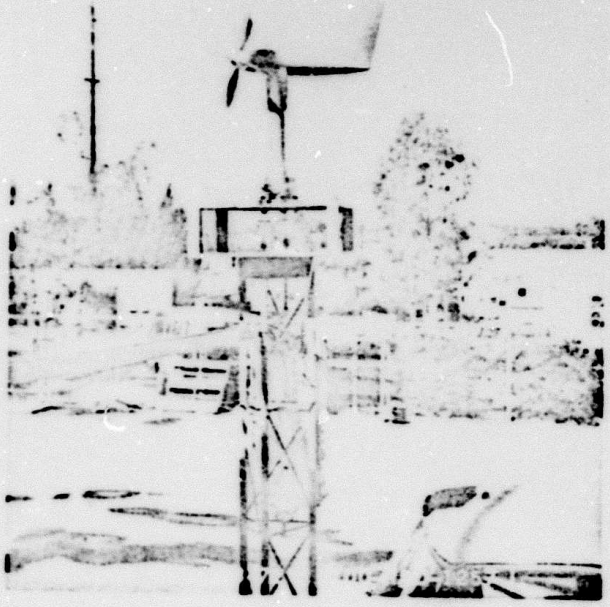

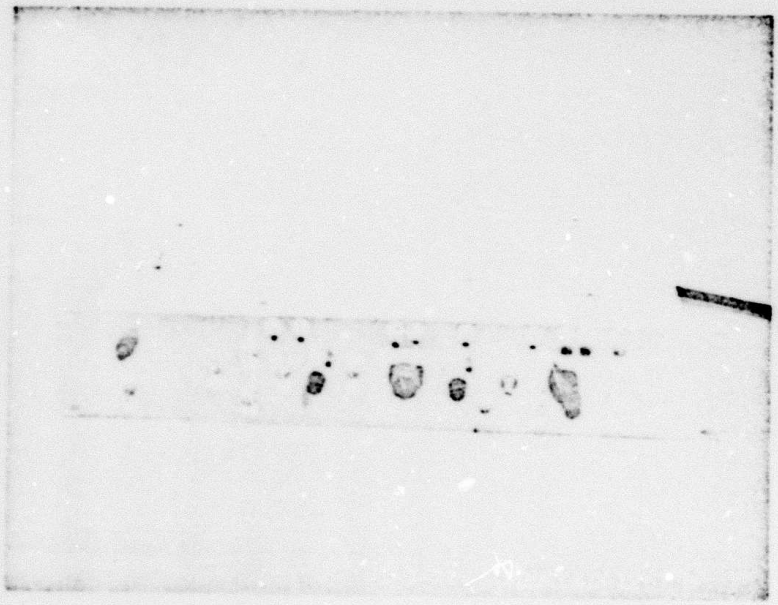

Figure III-10. Thermal Probes and Temperature Bridge for C_T^2 Measurements.

thermal impulses). In addition, when using the thermal bridge the probes must be protected from solar loading that may cause an imbalance of the bridge. Consequently, consideration must be given to the wind speed (especially if it is strong enough to kick up dust) and solar loading for collecting thermal probe data. This latter problem, however, was remedied by mounting the thermal transducers at laser-beam height above the ground between two wooden plates (plywood, 0.5-m square) that are separated by approximately 15 cm. In this manner the probes were protected from direct solar loading, for the most part, but were open to the free passage of air.

In addition to the strength of optical turbulence measurements, the temperature and barometric pressure were measured so that the temperature structure constant data could be converted to values of the refractive index structure constant. The wind speed and direction were monitored so that we would have a measure of the frequency range of the atmospheric-produced scintillation. These wind velocity data permitted us a measure of the Doppler shift associated with atmospheric backscatter into the COAT receivers. The temperature and relative humidity data were collected to provide a measure of the strength of atmospheric attenuation of the COAT transmitted beam. These data were collected at each end of the propagation link during each COAT test by means of a multi-channel digital recording voltmeter. Instrumentation was selected to provide the following weather measurement accuracy.

1. Air temperature - $\pm 0.5^{\circ}C$ over a range of $10^{\circ}C$ to $43^{\circ}C$.
2. Relative humidity - $\pm 5\%$ over the range of 5% to 95%.
3. Barometric pressure - ± 1 millibar over the range of 945 to 1045 millibars.

4. Wind velocity - 0.5 m/sec over the range of 0 to 30 m/sec
   ± 5 degrees over the range of 0 to 350 degrees.

The equipment used in gathering and recording this data is shown in Figure III-11.

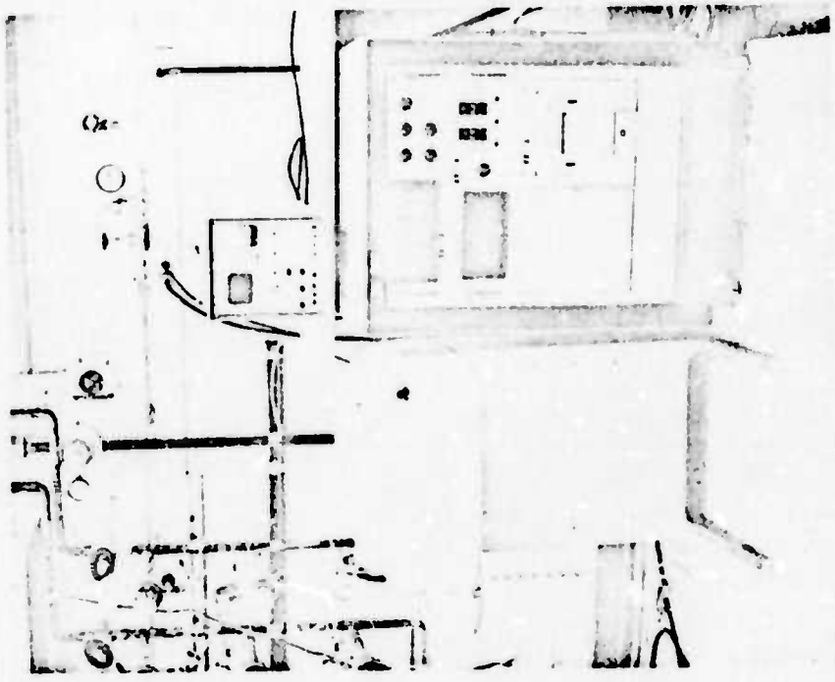

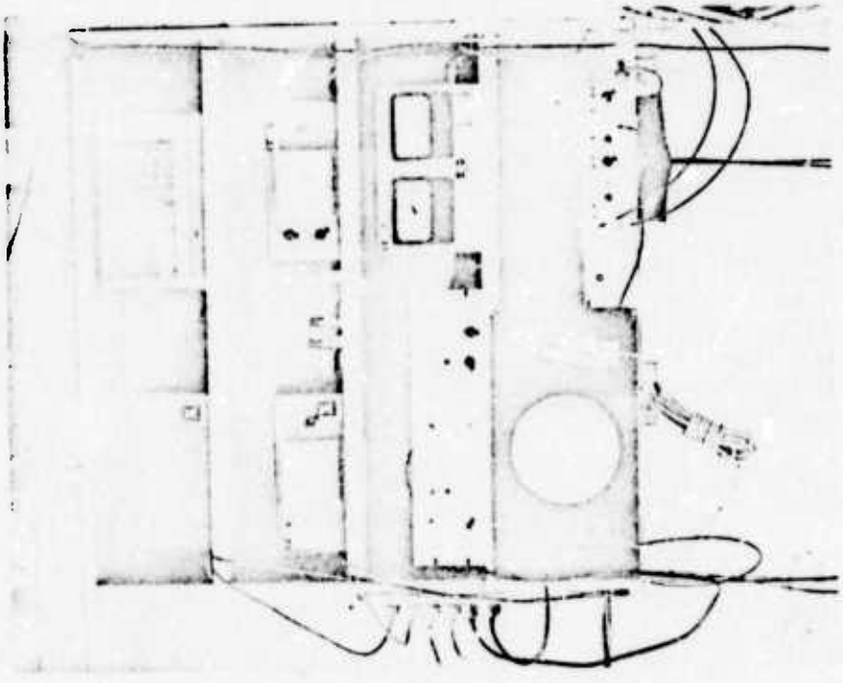

Figure III-11. Weather Data Measuring Instrumentation

IV. TEST RESULTS

The experimental tests were structured to obtain data which would prove conclusively the ability of the COAT array to compensate for atmospheric effects, focus energy at the target, provide automatic acquisition and tracking, and reach optimum performance within several round-trip transit times. The manner in which the data was taken was dictated in part by the availability of material for frequency modulator construction. As frequency shifters became available more channels were added until the full complement of six was complete. The chronological sequence of the data reflects this fact.

A. Three-Element Array

Initially, performance tests were conducted at a range of 1 Km with three channels being operational. A minimum of three was used since previous experiments in 1968 had already shown the validity of the concept and little additional information was to be gained by using two apertures. Preliminary system alignment and evaluation of signal-to-noise ratio, channel isolation, scattering introduced by table components, electronic checkout, etc, was, of course, conducted with each channel as hardware was fabricated.

Figures IV-1 through IV-13 illustrate conclusively some of the objectives of this program. Using the target plane scanner previously described, the intensity of the array pattern was recorded on an x-y plotter as function of the detector position in the field. Figure IV-1 shows the Gaussian intensities exhibited by each of the individual channels (transmitters). No attempt was made to equalize the transmitted power for each channel at the time of these tests. However, subsequent testing when six channels were operational was conducted with all intensities approximately the same. The system, then, was locked to a target of unit reflectivity at the center of the field. The intensity pattern in this adaptive mode of operation is also shown. Of particular interest is the qualitative nature of this distribution which is predicted analytically in section II-B. Figure IV-2 is the corresponding distribution when the system is not compensating for atmospheric effects or holding the pattern on target. While the atmospheric effects at this range and wavelength are mild, the scintillation is evident in the recording and the main lobe has drifted off of the target.

Having established the fact that the system was operating as designed, a series of recordings was done to establish the successful operation of the array for the major program goals. Figures IV-3 through IV-11 are the results of these tests recorded at time intervals of approximately five minutes. These data are somewhat repetitious in nature, but serve to reinforce and substantiate successful system operation. Figure IV-3 again shows the target plane distribution for the system when locked to the target in the center of the field. The same target was then transferred 10 cm to the left of center and the corresponding distribution is

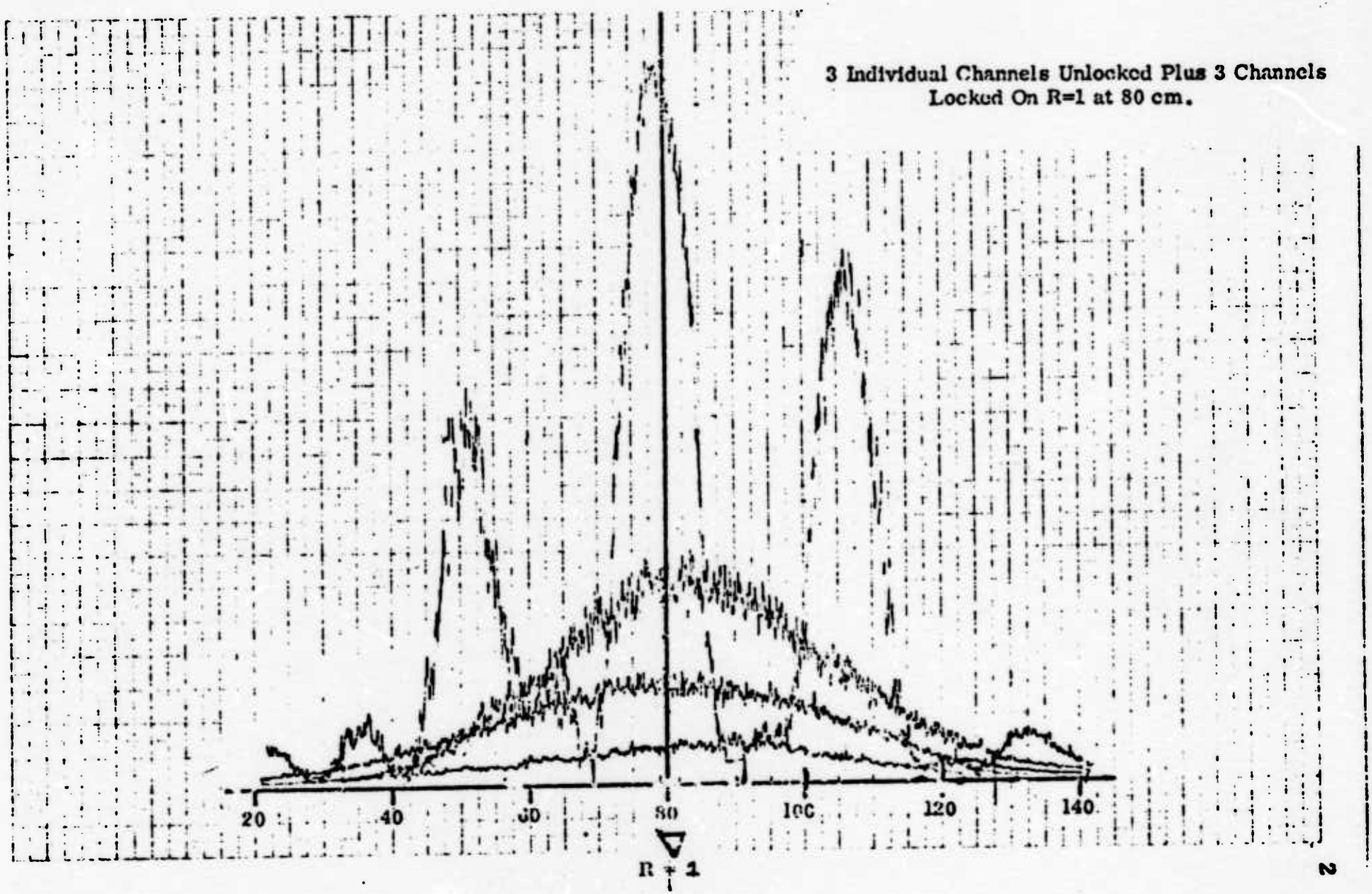

Figure IV-1. Initial Individual Intensities and Adapted Intensity Pattern

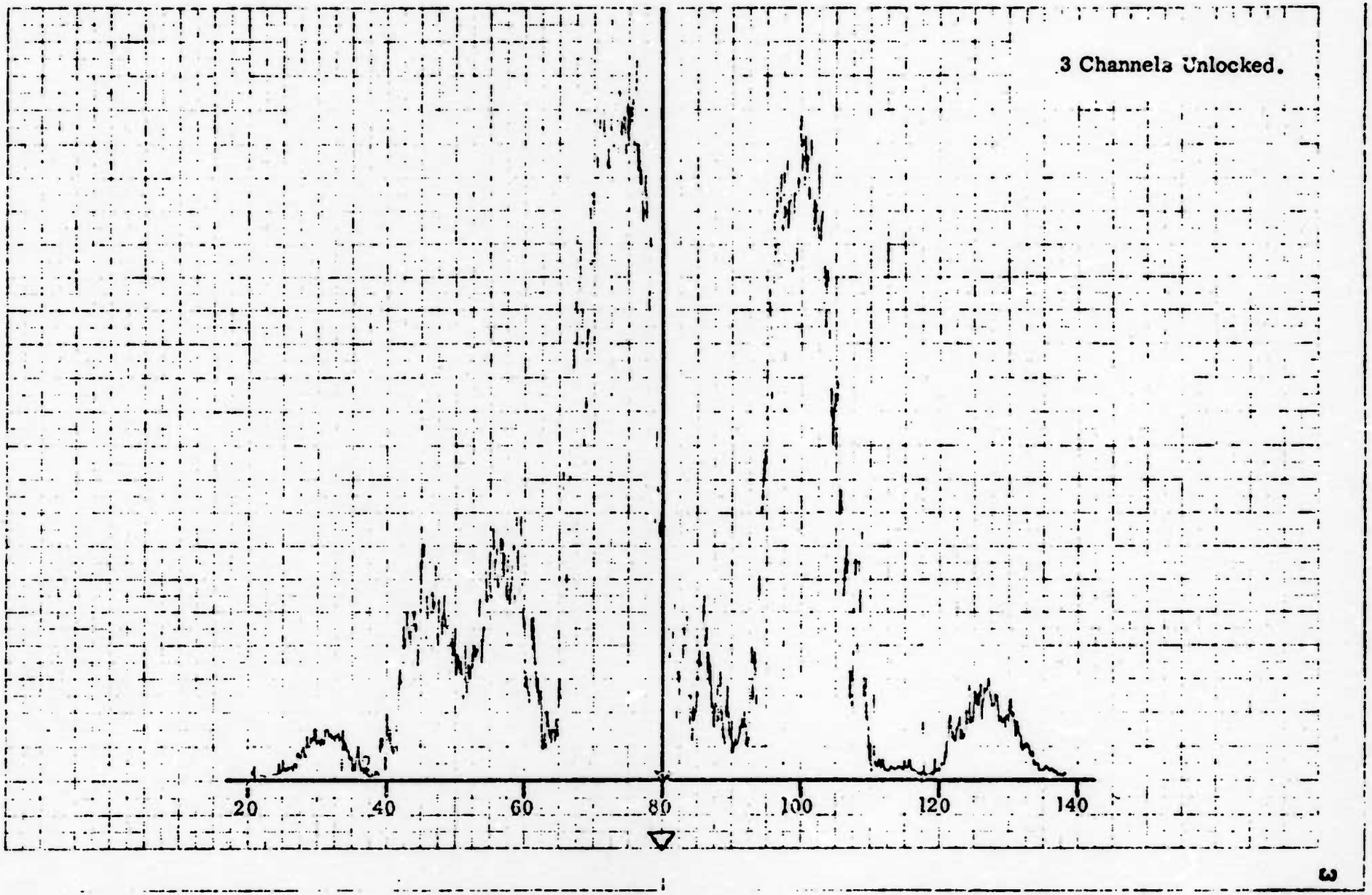

Figure IV-2. Unadapted Intensity Distribution

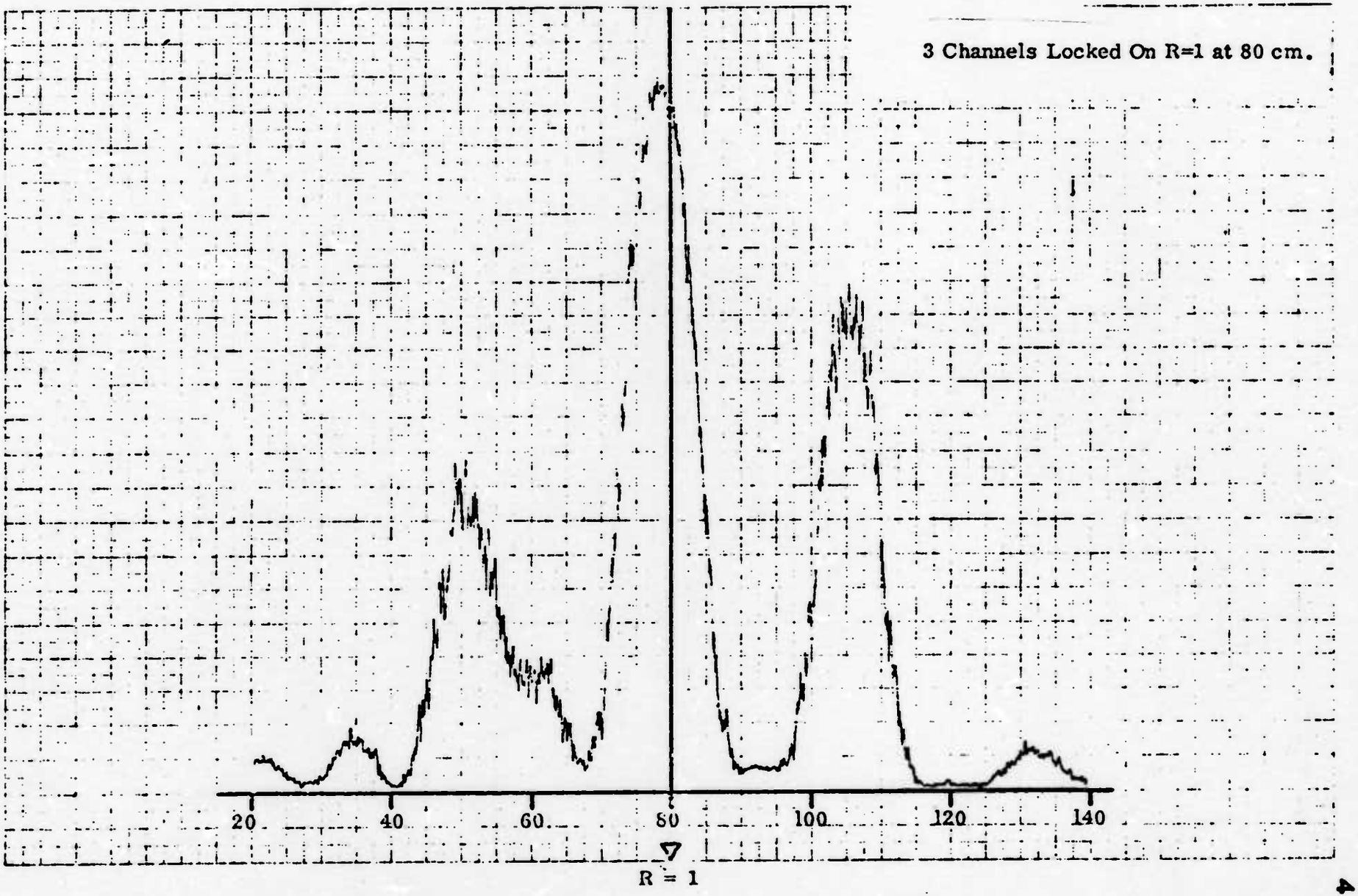

Figure IV-3. Adapted Intensity Distribution in Center of Field

as predicted (Figure IV-4). This sequence was again repeated (Figures IV-5 and IV-6) with no substantial changes in the pattern.

Two targets of different reflectivities (1.0 and 0.5) were then introduced into the field simultaneously. The dim target was placed at the center of the field to insure maximum illumination. The bright reflector was situated where a null of the system was contemplated. Under adaptive control, the dim target was ignored and lock was maintained on the bright target (Figure IV-7). This occurs even though the product of target reflectivity and initial illumination is much greater for the dim target. This is not an unexpected result and was predicted for system operation.

To insure that the system was capable of locking to the dim target, the bright reflector was covered. Figure IV-8 shows that the system self-adjusted to lock to the dim target located at field center. Upon uncovering the bright target, the pattern shifted to that shown in Figure IV-9 and establishes the repeatability of the previous results. The dim target was then covered and the pattern of Figure IV-10 is unchanged from the previous distribution and indicates that the system did ignore this reflector when both were within the field of view.

To determine over what field of view the array could perform its adaptive function, the target was moved through a distance in the target plane which exceeded the expected field of view. The detector was simultaneously moved with the target and Figure IV-11 displays the results.

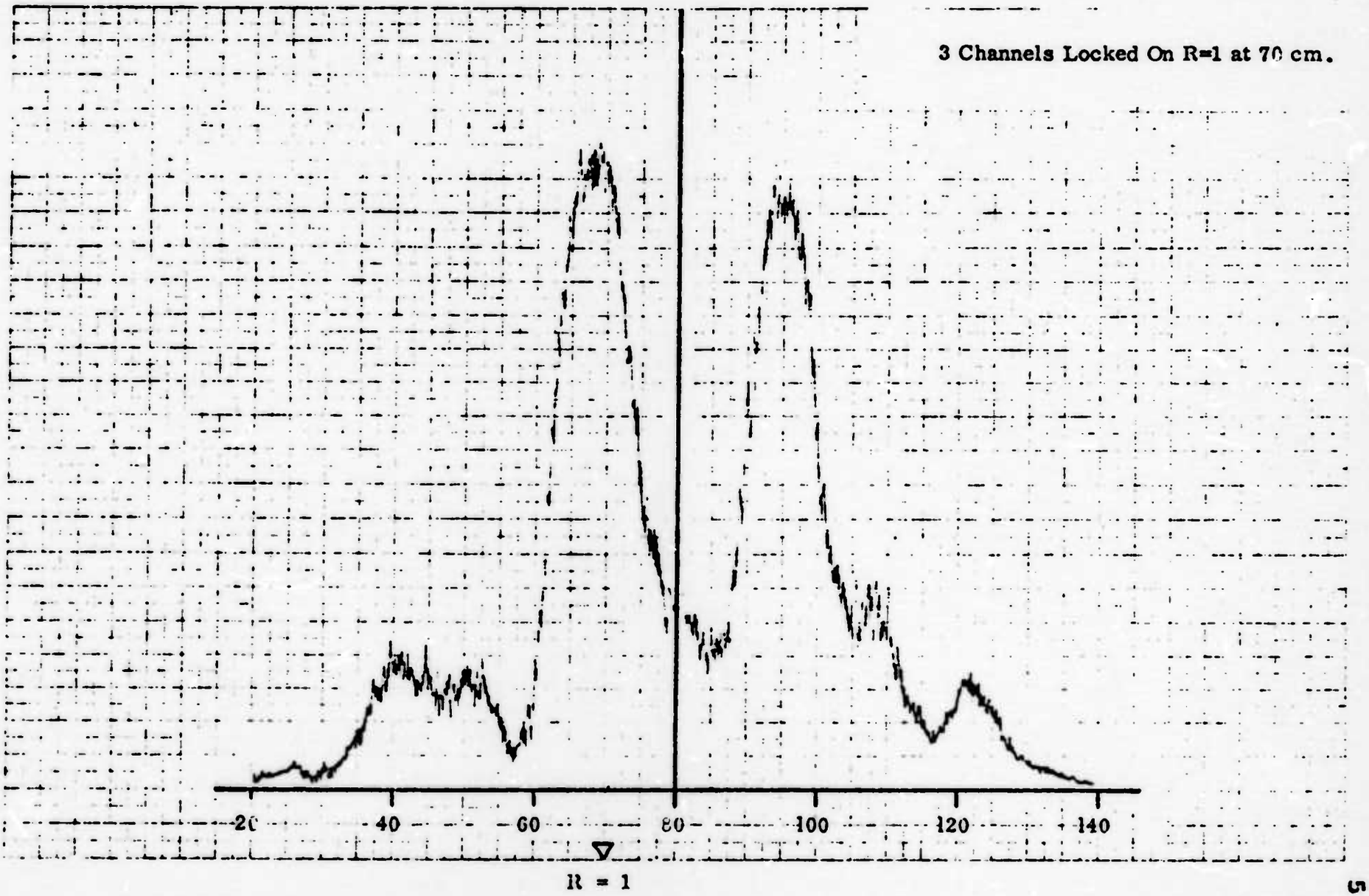

Figure IV-4. Adapted Distribution with Target Not In the Center of Field

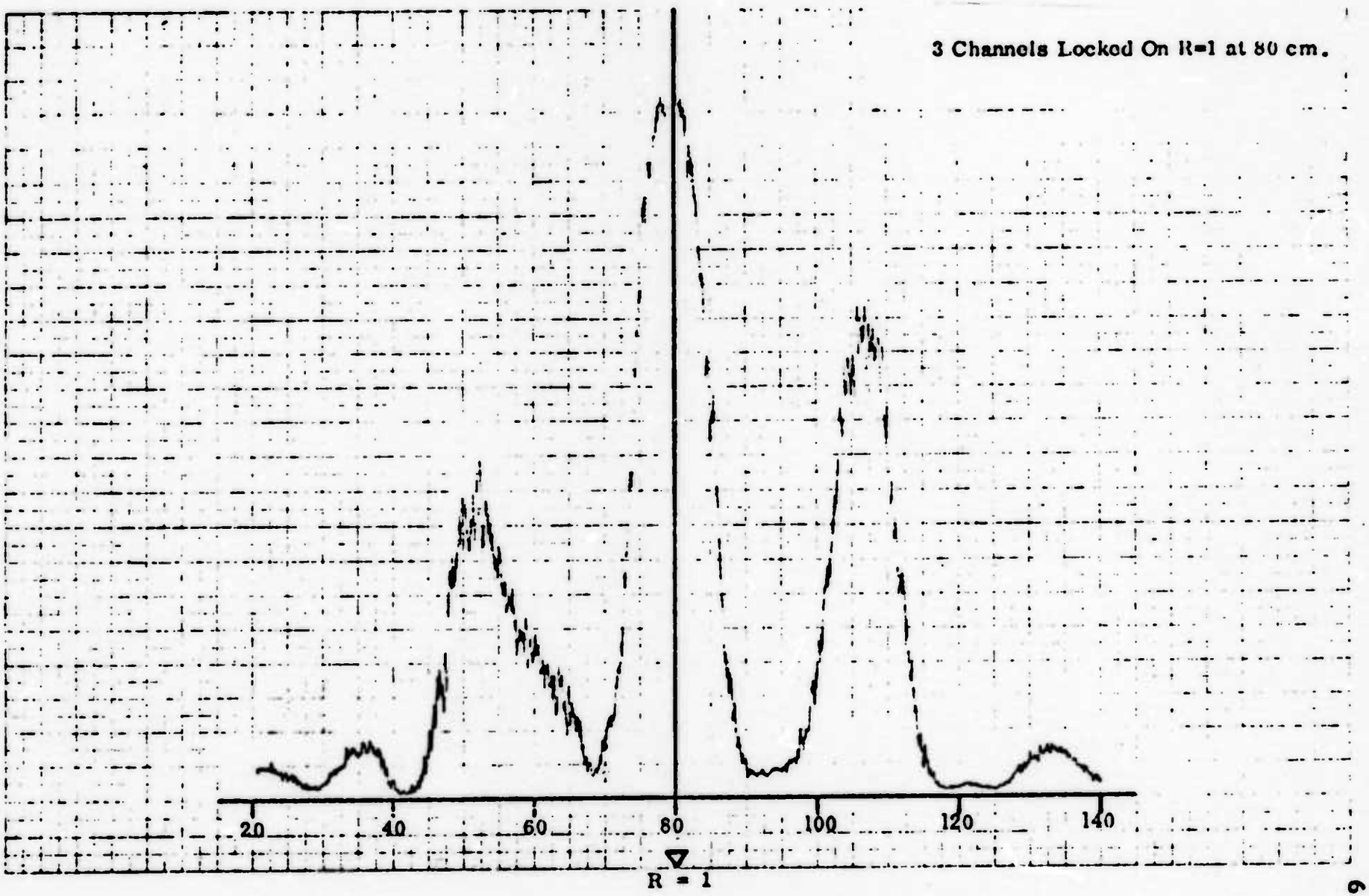

Figure IV-5. Adapted Intensity Distribution in Center of Field

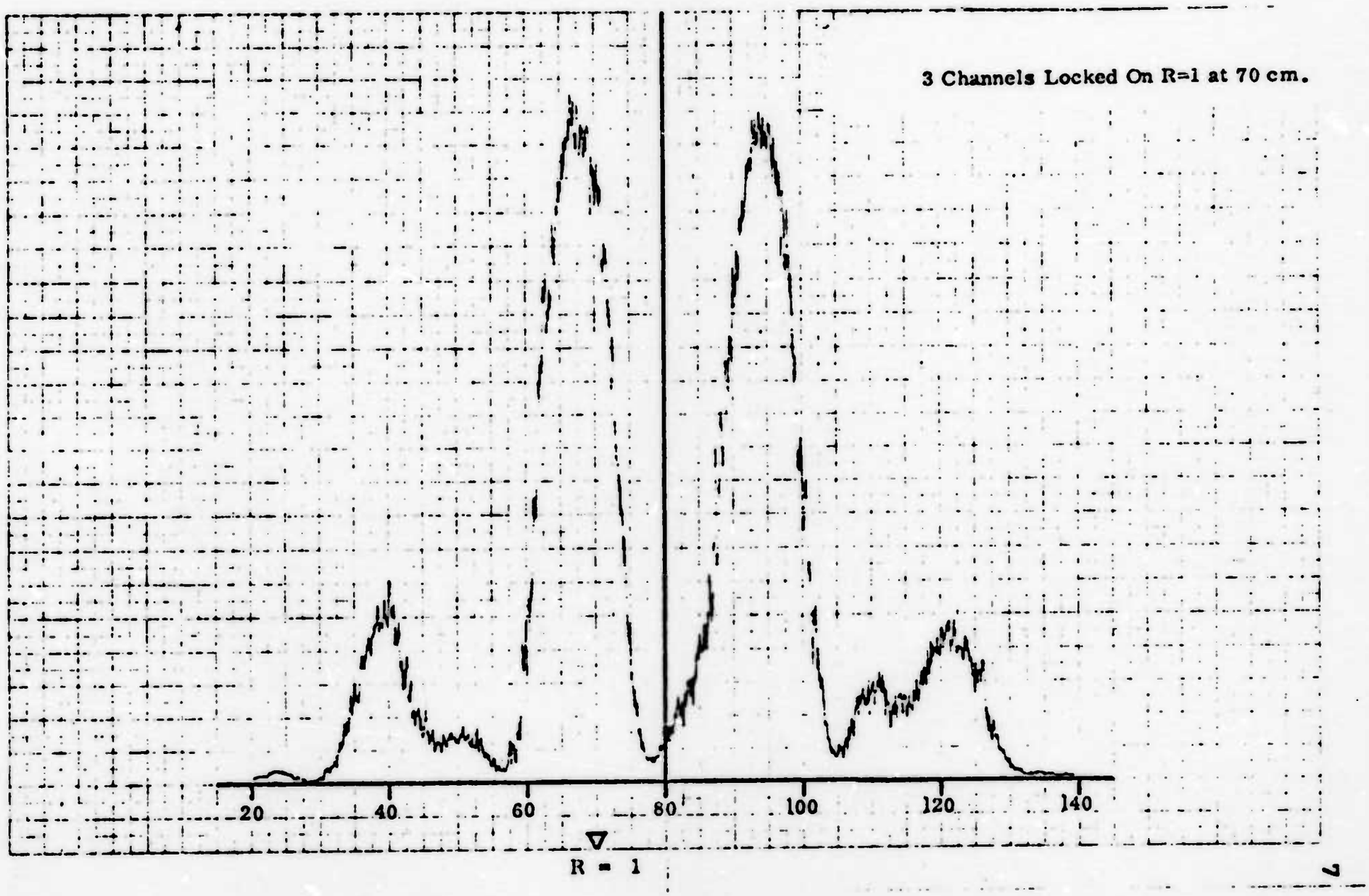

Figure IV-6. Adapted Distribution with Target Not in the Center of the Field

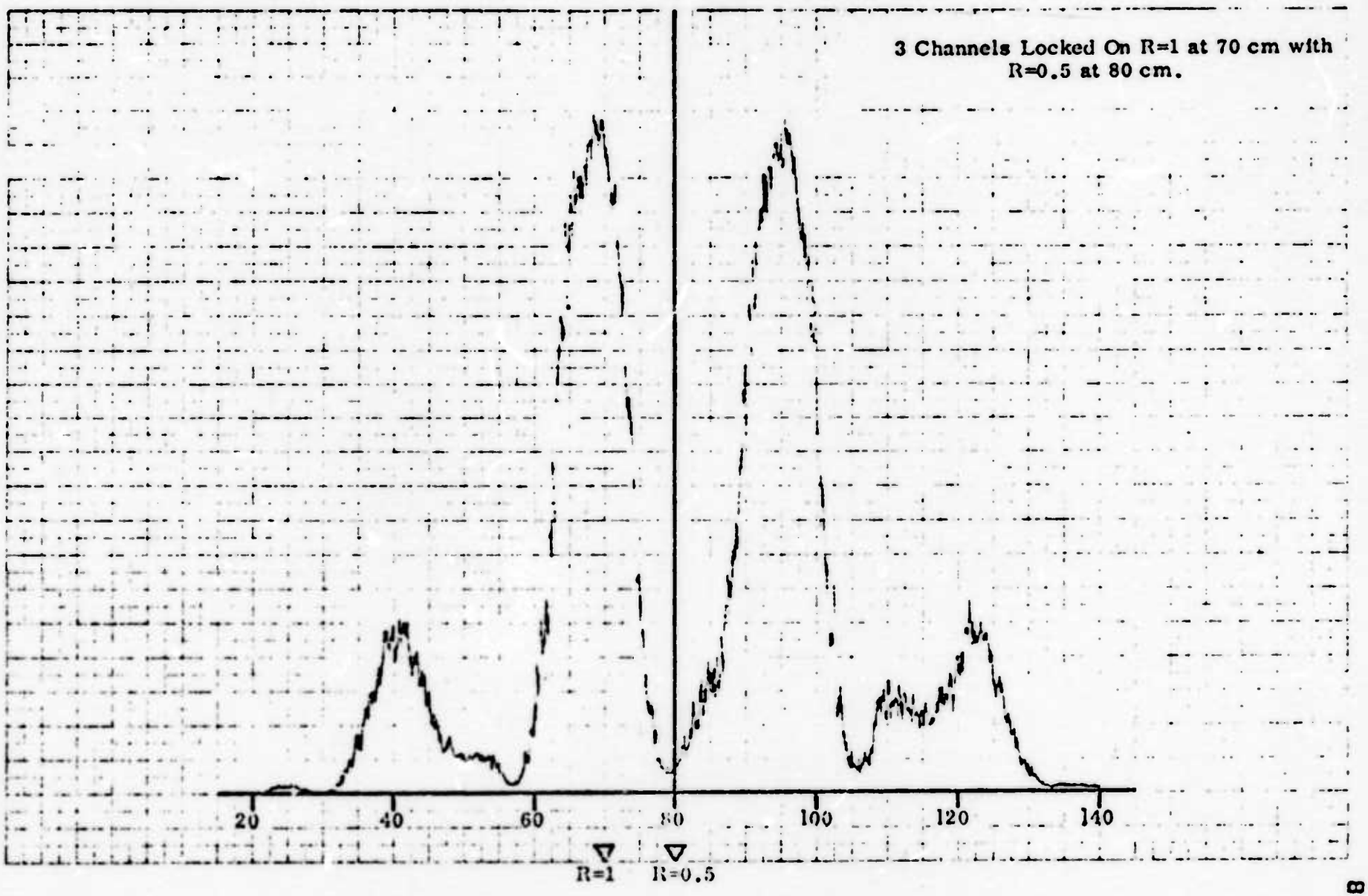

Figure IV-7. Intensity Distribution Showing System Preference for Bright Target

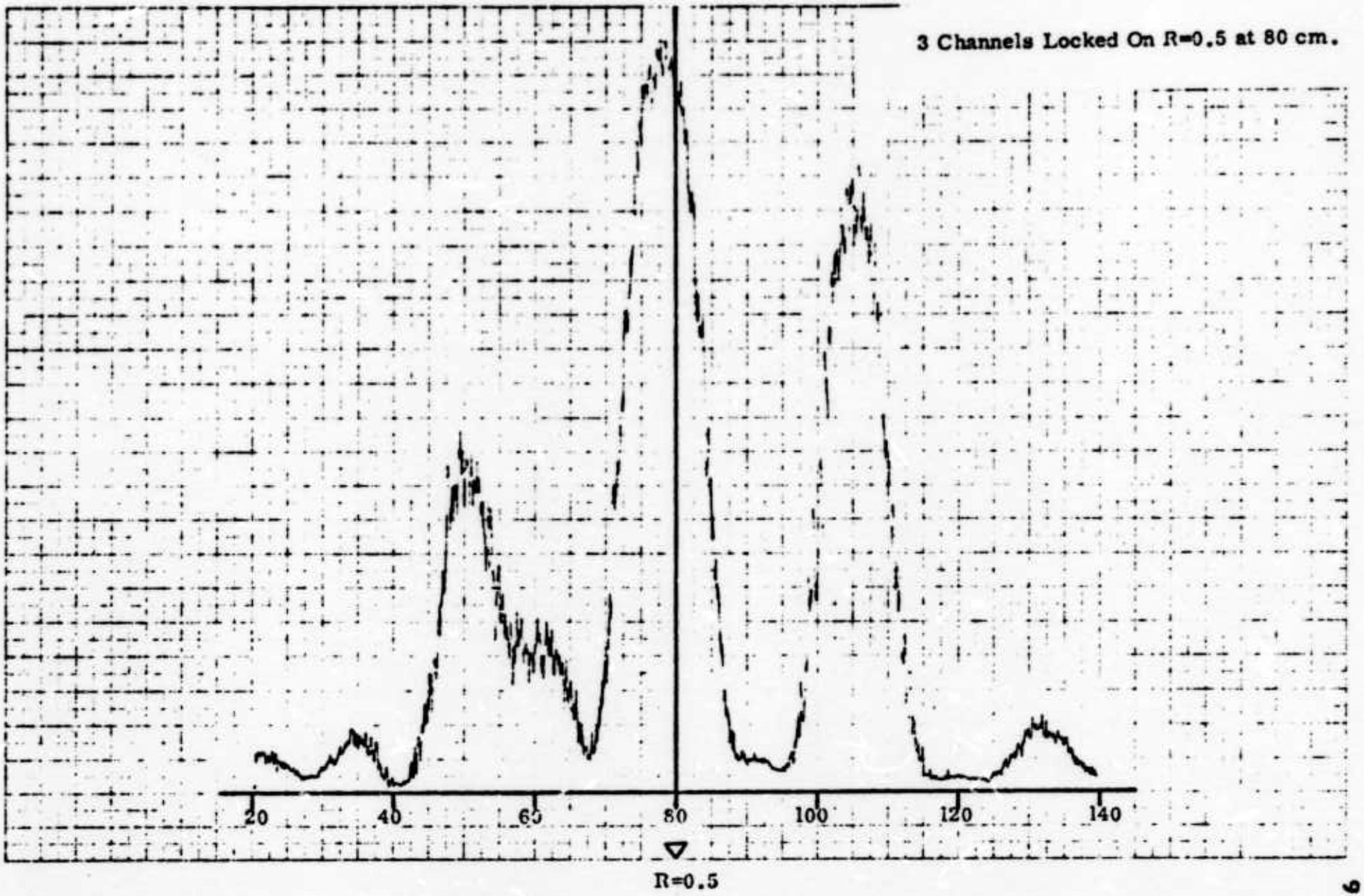

Figure IV-8. System Locked to Dim Target at Center of Field

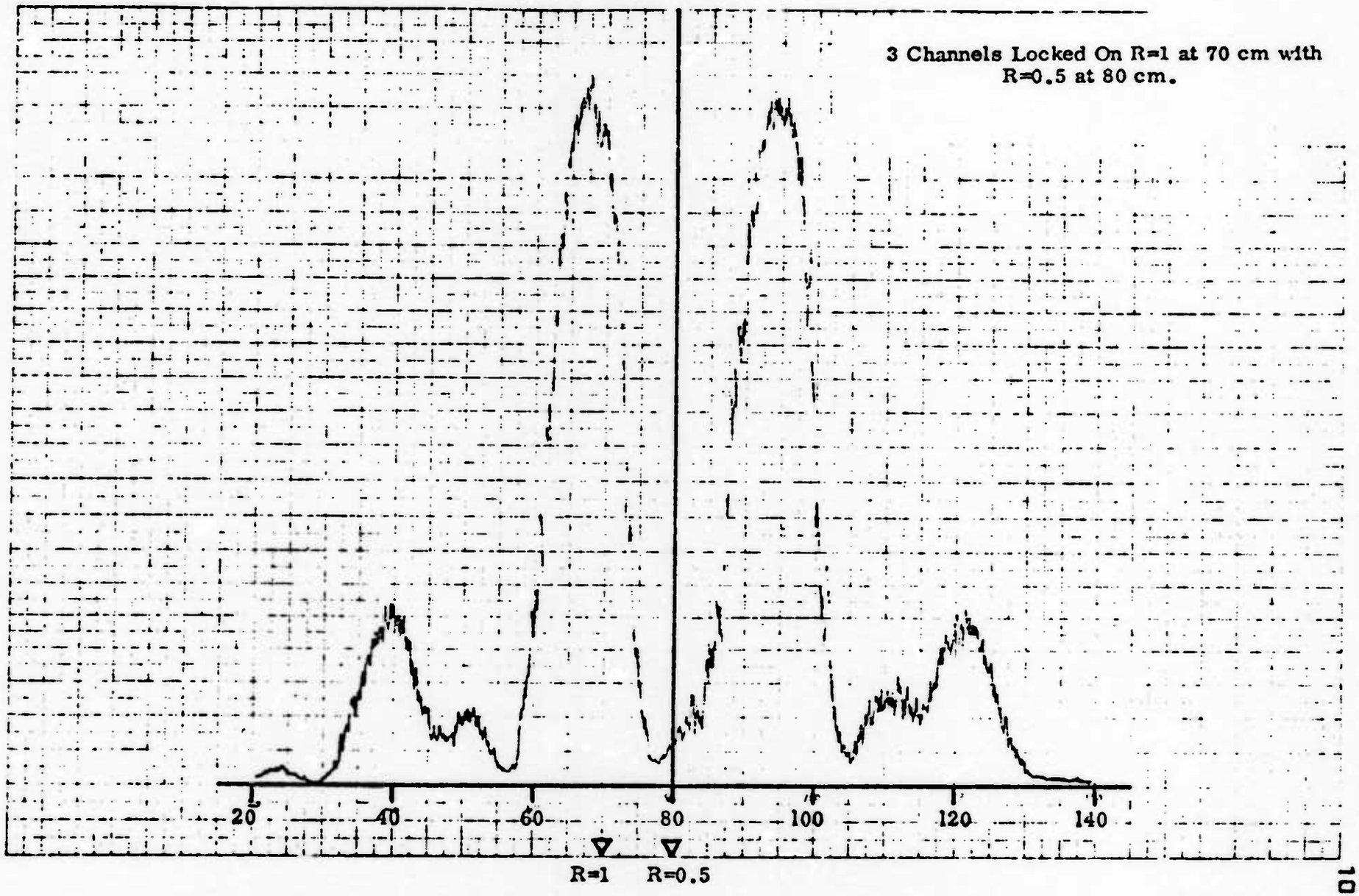

Figure IV-9. System Locked to Preferred Bright Target not in Center of Field

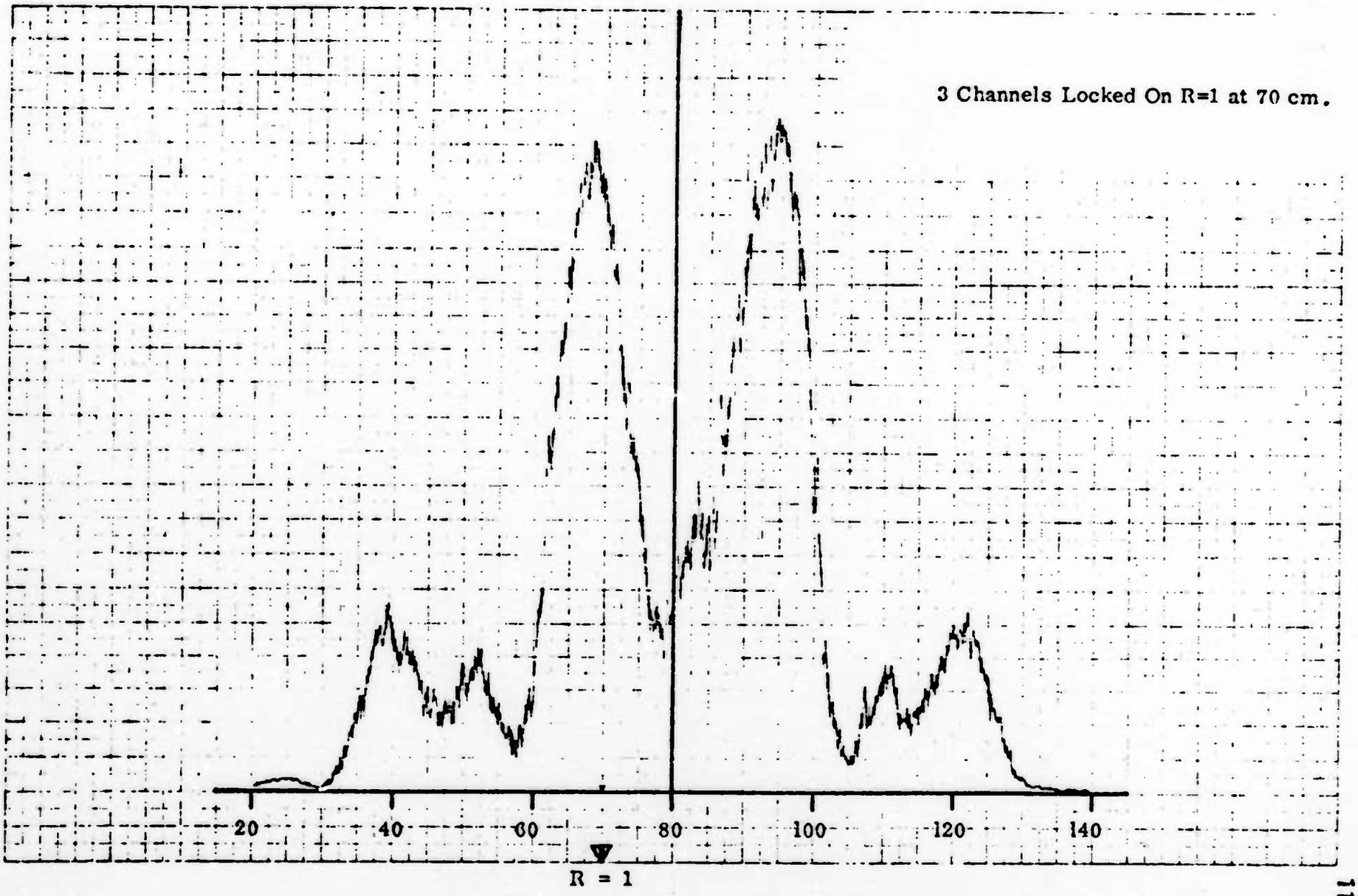

Figure IV-10. System Locked to Bright Target Not in Center of Field

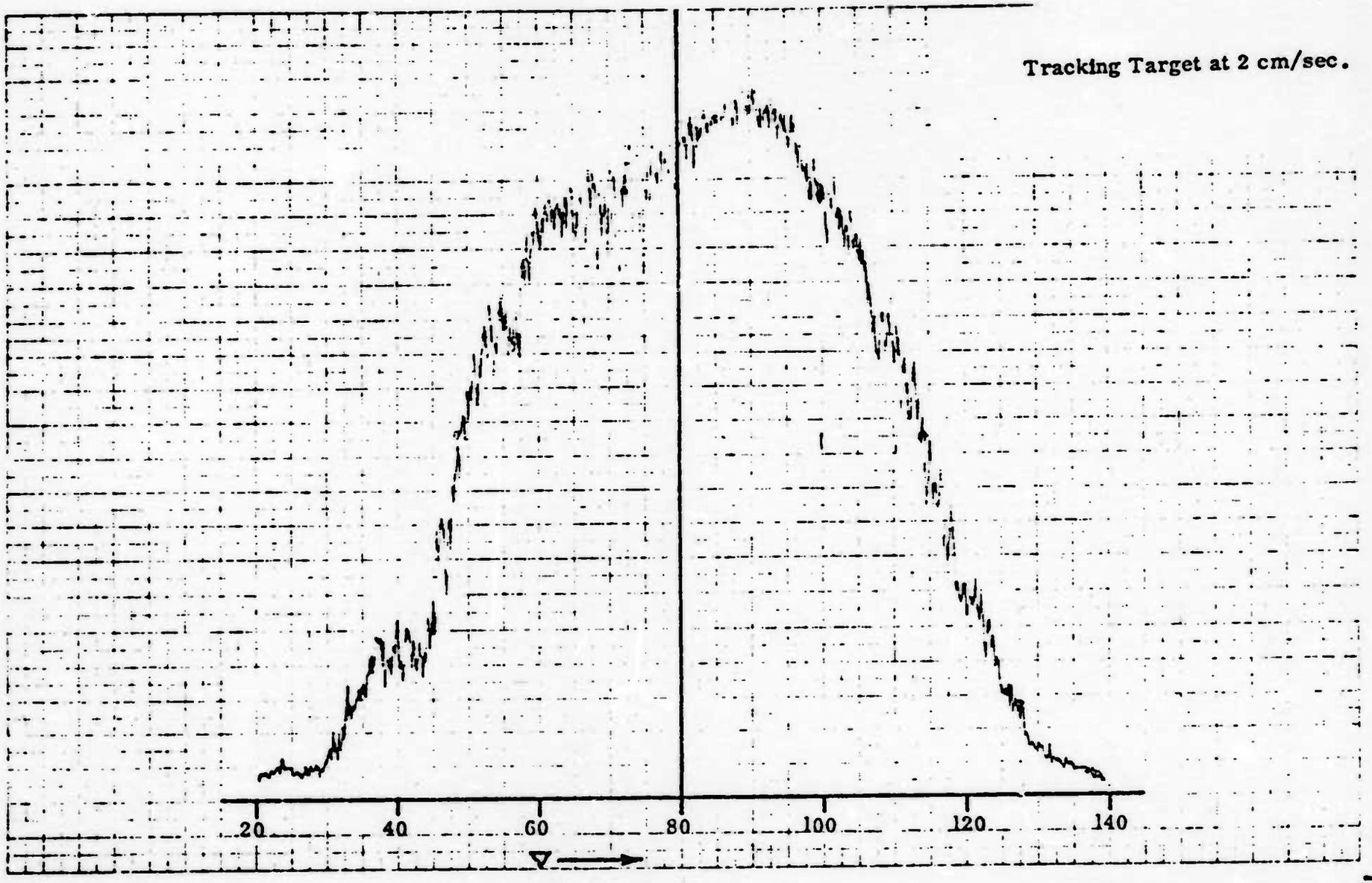

Figure IV-11. Intensity Envelope Defined by Moving Target Test

Maintaining lock through the scan interval kept a lobe located at the target which also kept the detector optimally illuminated. The resulting pattern defines the operational field of view of the array. The nulls of the distribution appear to be very close to the limits of the scan - approximately 120 cm. This is in general agreement with the theoretical prediction of section II-B in that the minimum separation possible is approximately 100 cm. Taking into account the Gaussian illumination of the transmitters, the 120 cm result is very close to the to the expected value.

Of further interest are the fringe spacing and fringe width. For the element-to-element separation of 3 cm used in the array a fringe separation of 33 cm and a fringe width of 22 cm are expected. The latter parameter is met very closely. Examination of the recordings shows some discrepancy in the fringe spacing. This anomaly was traced to an uneven spacing in the transmitter array and upon correcting the spacing for the six element tests all aspects of the theoretical predictions were met.

The final test conducted with three elements was an evaluation of the speed of response. Initially, this was done by monitoring the build-up of the return signal to one channel of the receiver as shown in Figure IV-12. A command pulse used to execute the adaptive mode was used as a timing mark. As is evident, the adaptive cycle was complete after 50 μsec. The actual rise time associated with energy build-up is approximately 20 μsec or 3 transit times for the 1 Km range. This rate of adaption is in complete agreement with computer simulated results.

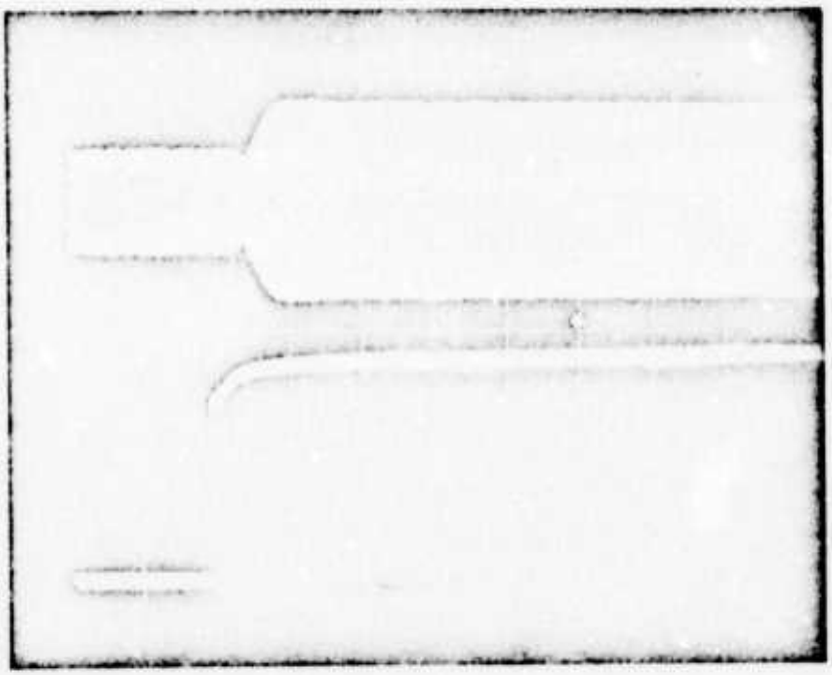

50 μs/cm

Figure IV-12. Speed of Adaptive Response Measured at the Receiver. Lower Trace is the Execute Command Pulse.

The fact that compensation is being achieved for what atmospheric perturbations are present at this range is evident upon examining the frequency content of the return signals in each channel. Phase fluctuations due to the atmosphere appear as a frequency modulation at the output of the optical detector. Without adaptive control the 4.5 MHz i-f for this system has the frequency content displayed in Figure IV-13(a). Upon compensating for the phase flucutations, the output spectrum is as shown in Figure IV-13(b). Clearly, the frequency broadening has been removed and the spectrum displayed is that of the reference to which the system is locked.

It should be clearly noted that the display shown is for an amplitude response of 10 db/cm. Thus, at signal levels down to -50 db of the peak, in excess of 20 db and as much as 40 db of the fluctuation due to phase perturbation of the atmosphere have been totally compensated. Also, the peak signal level has increased as a result by about 9 db. Properly interpreted, the adaption process has placed maximum energy on the target and maintained it there in the presence of atmospheric turbulence.

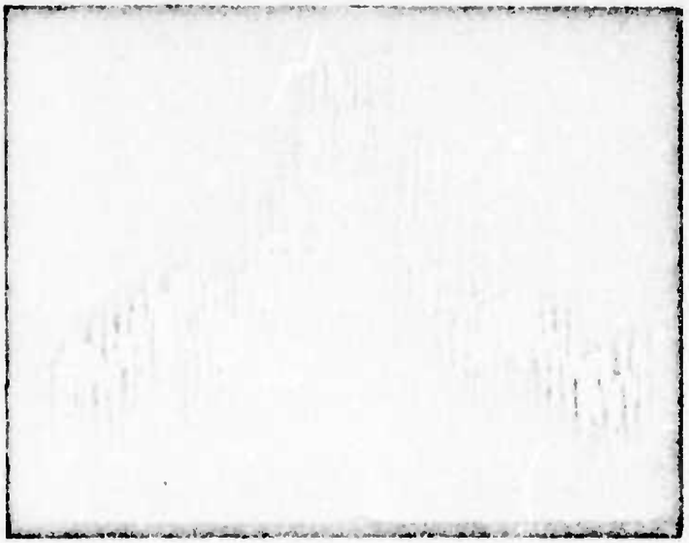

(a) Unadapted

(b) Adapted

Vertical - 10 db/cm Horizontal - 2 KHz/cm

Figure IV-13. Frequency Spectrum of 4.5 MHz Received Signal

B. Six-Element Array

The foregoing data are a complete demonstration that the system can and will perform as predicted. Further substantiation is evident in the data to follow where the same basic information was obtained with the full array (6 elements). Figure IV-14 is the field intensity with 6 channels transmitting with no adaptive compensation. It will be noted that the pattern has some fringe structure which indicates a degree of coherence exists among the beams. However, the fringes are spread out and scintillation is evident. Upon performing an adaptive lock, the distribution of Figure IV-15 resulted. The degree of coherence among the beams has been increased in that the fringe width (15 cm null to null) is close to the predicted value of 14 cm. The fringe spacing is now 34 cm and is within measurement error of the theoretical 33.3 cm. Also, clearly shown is the field envelope which governs the amplitude of the side fringe intensity. This result again clearly shows that COAT can correct for atmospherically induced beam broadening.

Numerous tests were conducted to ascertain if the six element array performed in the same manner as the three element system. The following data is representative of these tests and clearly establishes that operation is the same, but the larger array has produced an attendant improvement in the field distribution. The ability to lock onto a target not centered in the field is shown in Figure IV-16 in which a target of high reflectivity is situated 15 cm off center.

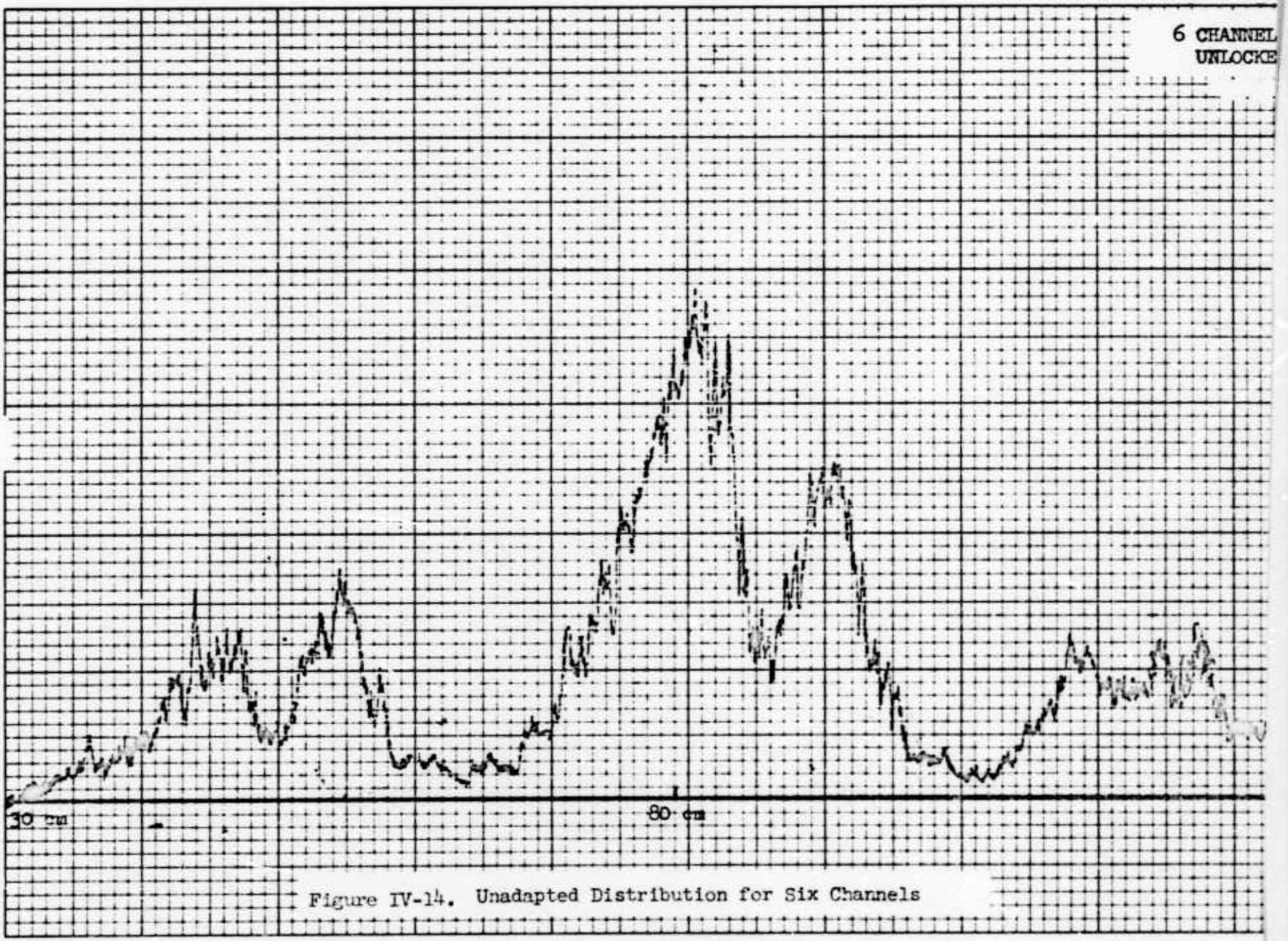

Figure IV-14. Unadapted Distribution for Six Channels

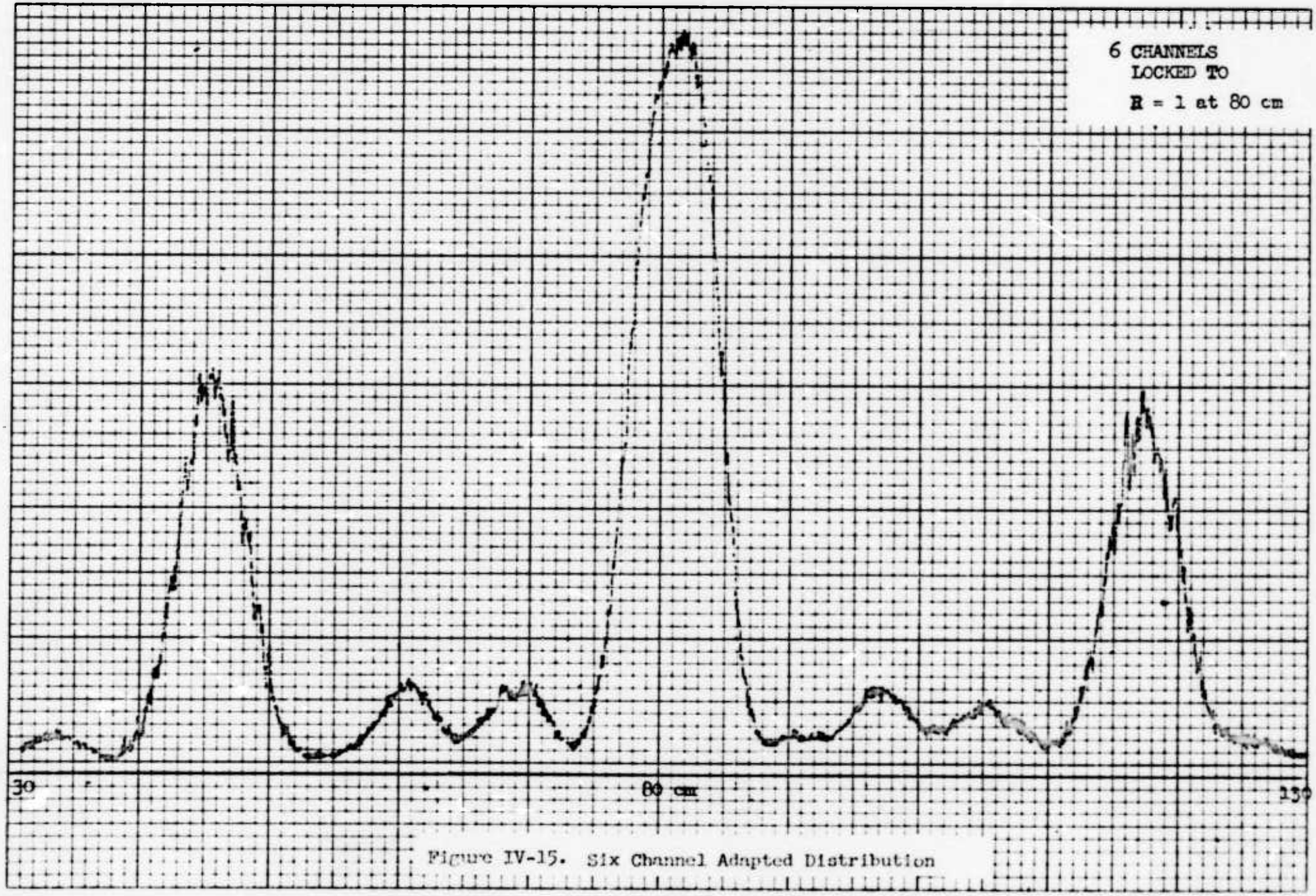

Figure IV-15. Six Channel Adapted Distribution

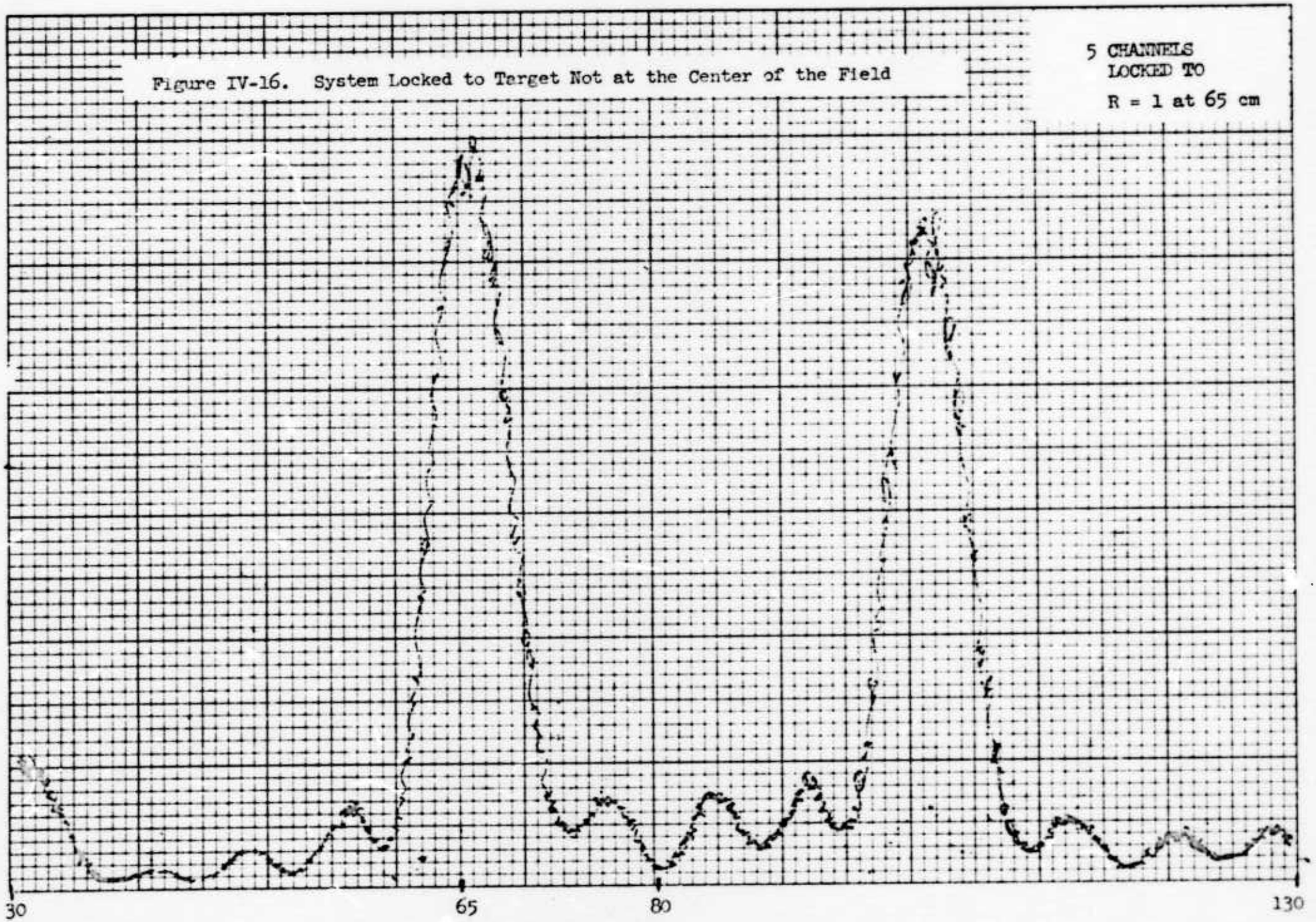

Figure IV-16. System Locked to Target Not at the Center of the Field

The next data were taken in the process of testing the system ability to lock onto the target of highest reflectivity. Locking to a dim target at field center is shown in Figure IV-17. Upon uncovering the bright target, automatic acquisition of the bright target was noted as before even though its initial illumination can be seen to be quite low (Figure IV-18). Changing the dim target at field center to one having the same reflectivity as the one 15 cm off center had the predicted effect as shown in Figure IV-19. That is, given two targets of the same reflectivity the system locks to the one having the higher initial illumination and appears to ignore the other one.

One additional result was taken in this series of experiments which was not presented in the three element data. Figure IV-20 is a recording of the field intensity at the target as a function of time when changing from the unadapted to adapted mode. The scintillation present during the unadapted portion is evident. Upon locking the system, two factors of system operation are shown. First, the power on target is increased since the main lobe is positioned at this point. Second, the scintillation of the beam on the target has been effectively reduced through compensation of the atmospheric perturbation.

The transient response of the system - adaptive compensation time - was evaluated at the target for the six element tests. A synchronization pulse delivered to the 1 Km site via a laser communication system triggered the scope trace shown in Figure IV-21. The compensation action is complete after about 150 μsec. The apparent rise time of power buildup is approximately 20 μsec as for the three element case, but a longer "hunt-time"

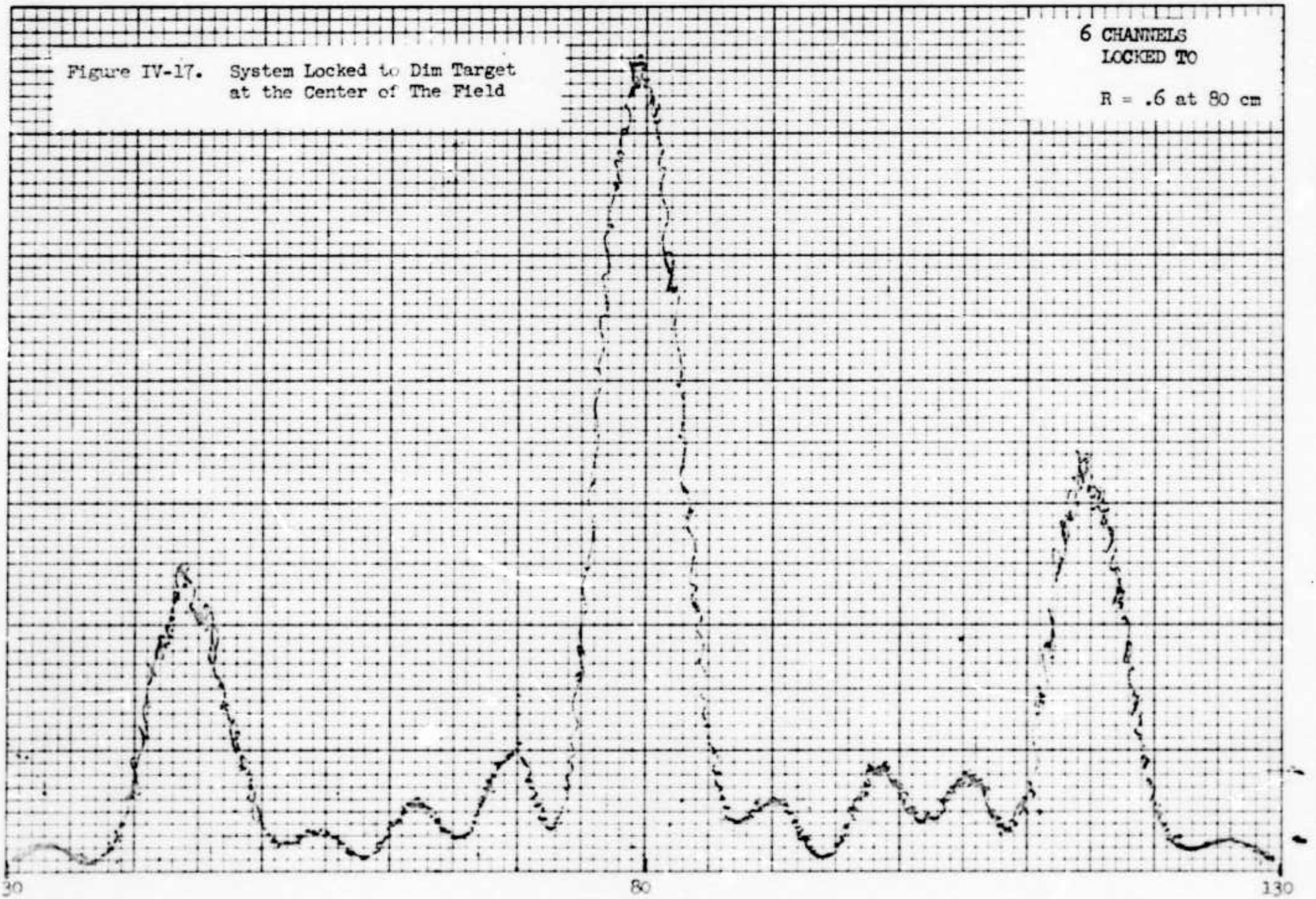

Figure IV-17. System Locked to Dim Target at the Center of The Field

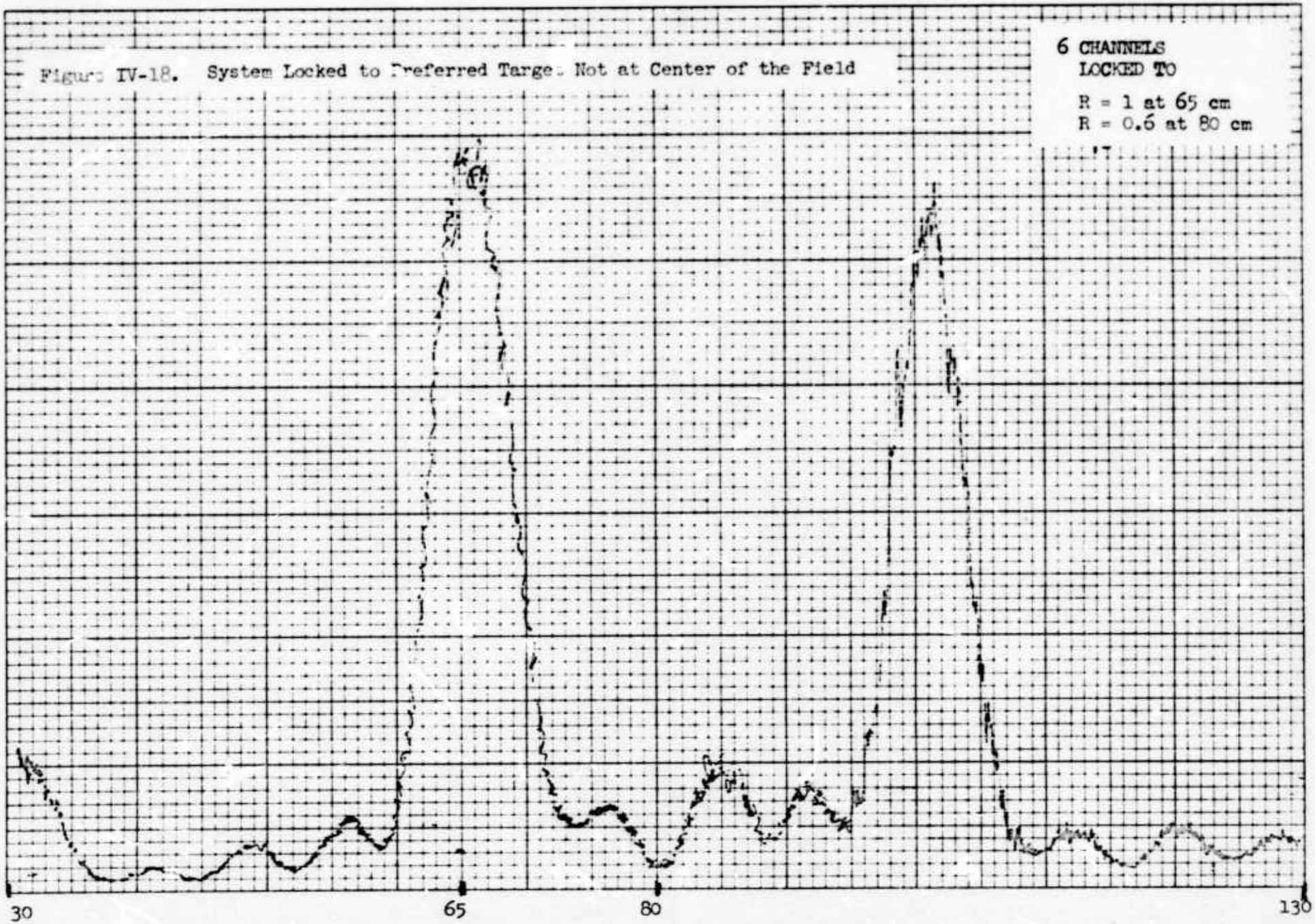

Figure IV-18. System Locked to Preferred Target Not at Center of the Field

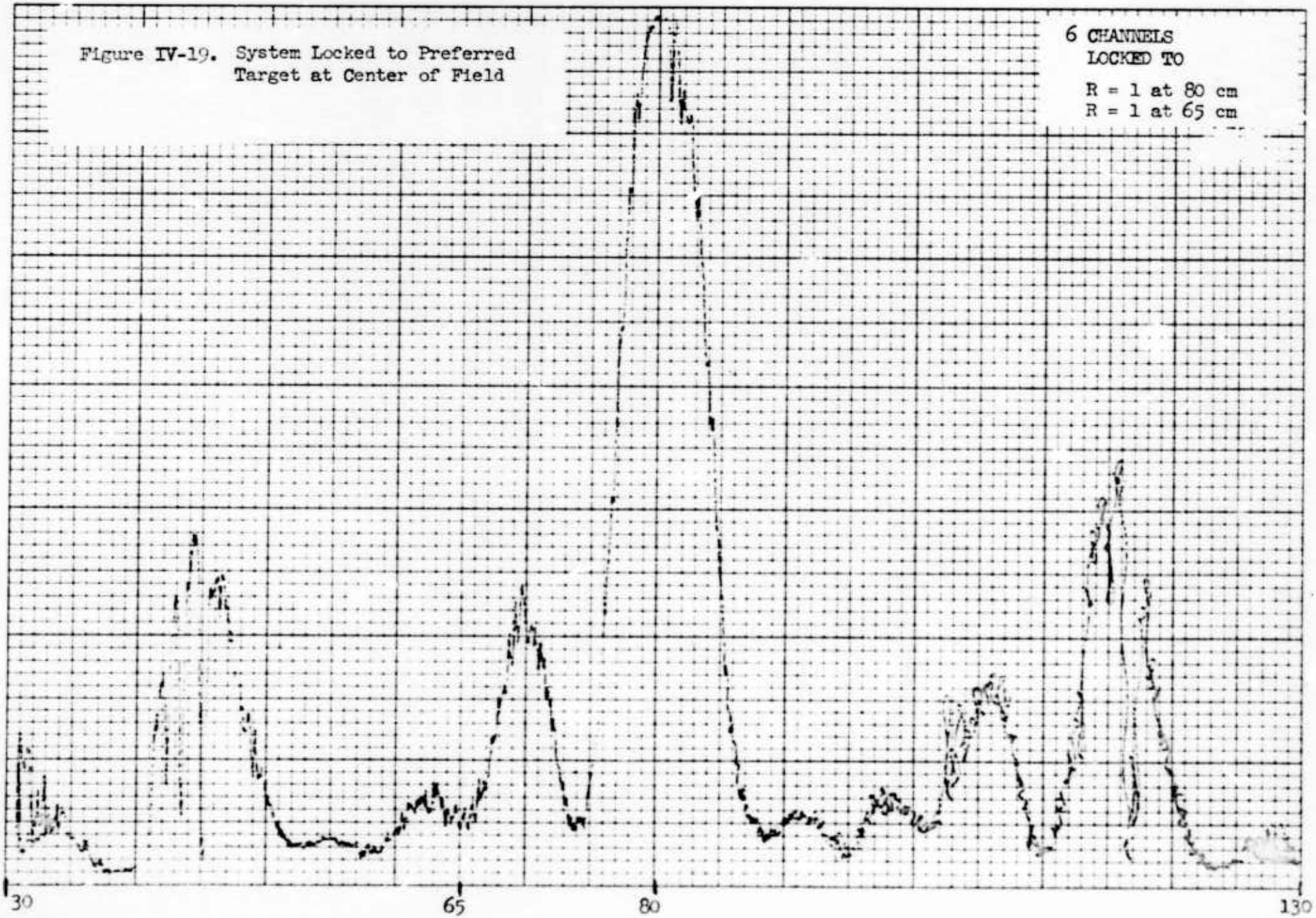

Figure IV-19. System Locked to Preferred Target at Center of Field

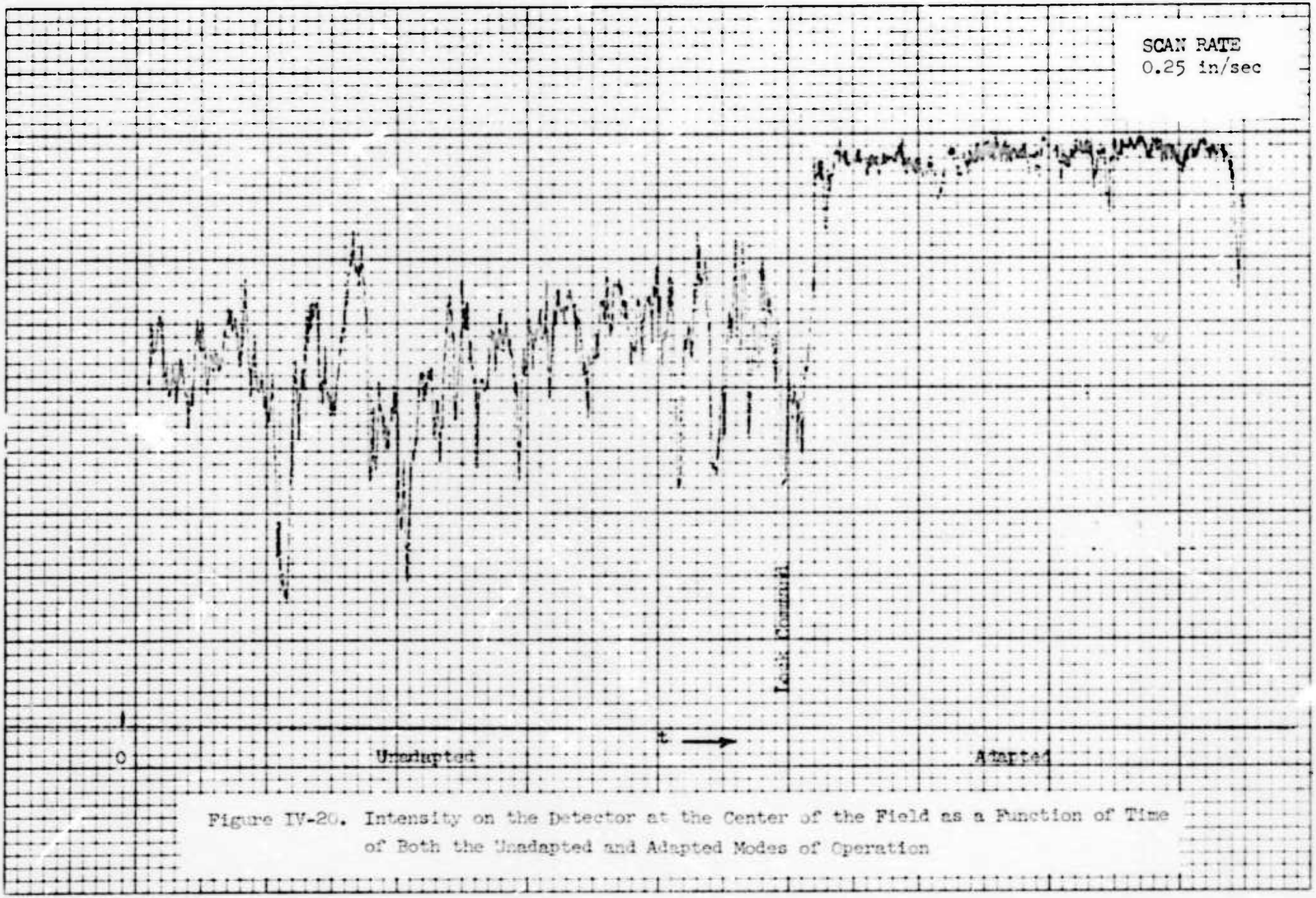

Figure IV-20. Intensity on the Detector at the Center of the Field as a Function of Time of Both the Unadapted and Adapted Modes of Operation

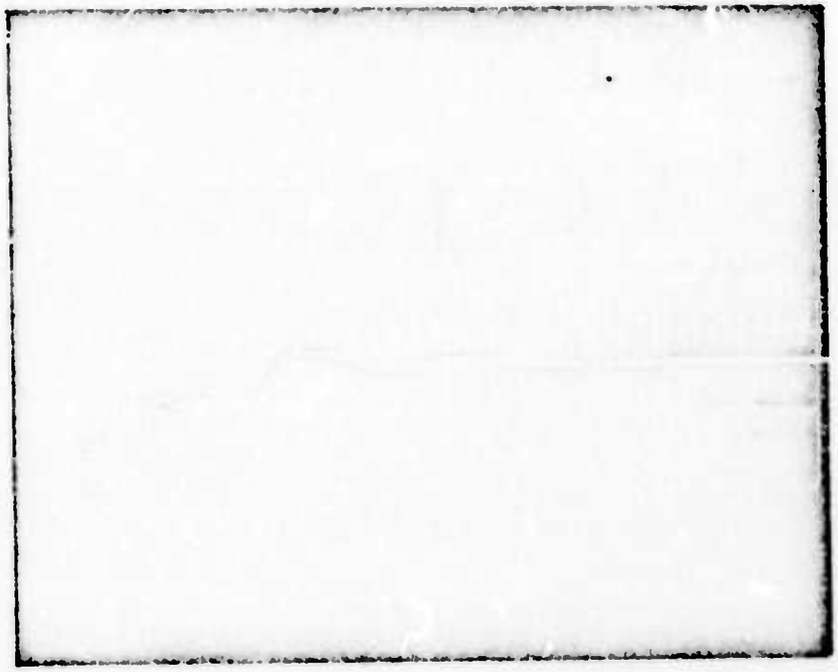

50 μs/cm

Figure IV-21. System Response Time Measured at the Target Over the 1 Km Range with Six Channels Operating

seems to be indicated. This factor probably depends in large part on the initial conditions at the transmitter, i.e., initial relative phases of the transmitted beams. The rise time, equivalent to about 3 transmit times to the target, is the same as before and is consistent with computer simulation.

C. Channel Sequencing for Power Buildup

An important aspect of this program has been to not only compensate for propagation path perturbations but also to demonstrate the increase in energy per unit area delivered to the target plane as the number of array elements are increased. To this end, a series of tests were conducted in which the peak intensity at the target was monitored as the number of adaptive elements was increased up to six. Figure IV-22 illustrates what is to be expected for both the incoherent and coherent (phased) conditions. For the incoherent case, the beam intensities add directly and the power is directly proportional to the number of array elements. When operating in the phased mode, a slightly different approach is required. Coherent addition of the field quantities result upon adaption (as opposed to intensity), and the improvement in field intensity is then proportional to the square of the number of elements. Mathematically:

Incoherent Case:

$$P = \sum_{R=1}^{N} E_R^2 = NI_R$$

where E_R is the same for all apertures.

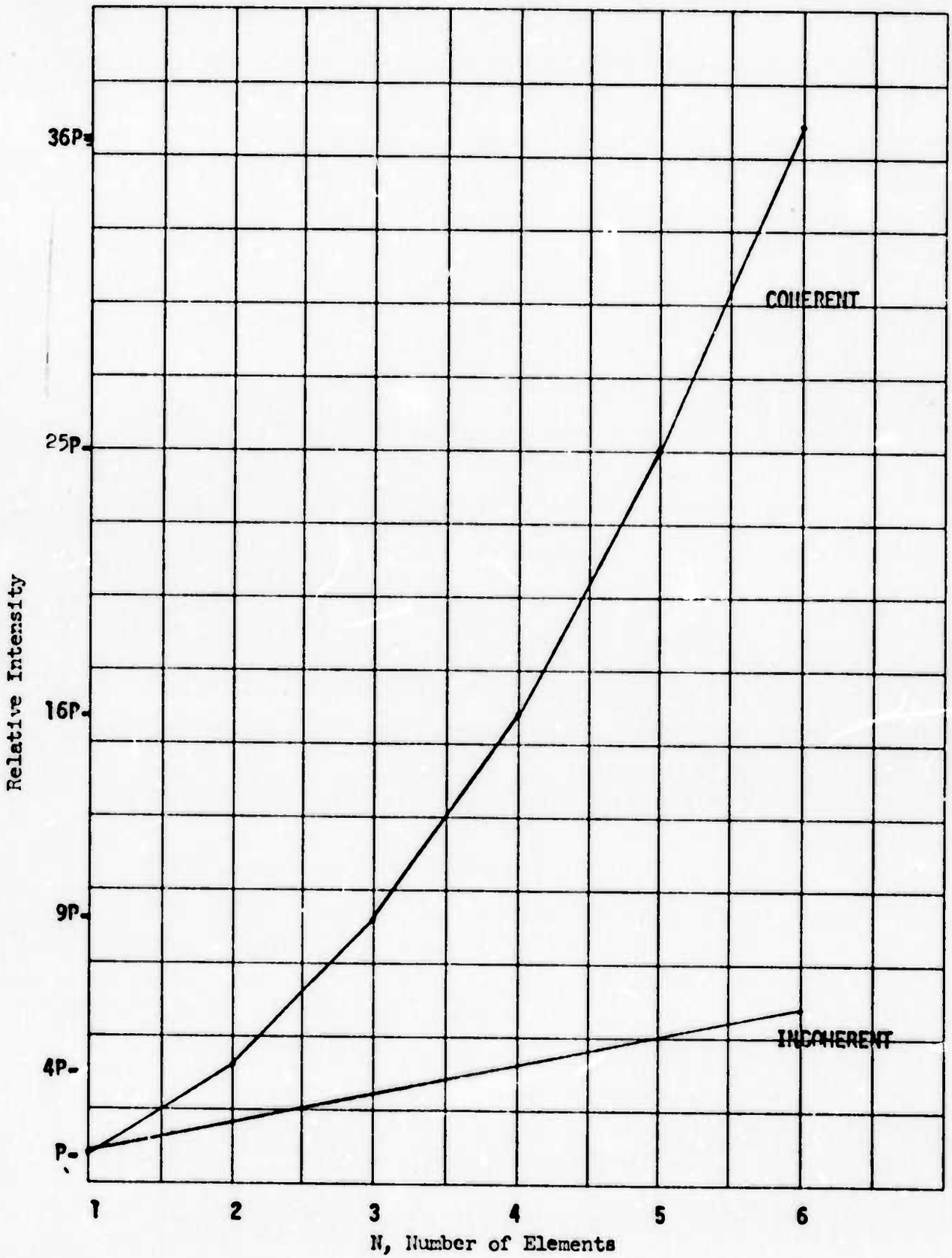

Figure IV-22. Relative Intensity at Target for Incoherent and Coherent Modes of Operation

Coherent Case:

$$P = \left[\sum_{R=1}^{N} E_R\right]^2 = \left[NE_R\right]^2 = N^2 I_R$$

Thus, for a six element system, an improvement factor of 36 relative to a single aperture is indicated. That is, the peak intensity of the intensity distribution at the target should increase by 36. The following data substantiates this point.

The tests were conducted by monitoring the intensity at the target as array elements were sequentially locked to the target. (1-2, 1-2-3, 1-2-3-4, etc.) With all elements transmitting approximately the same power, the scanned distributions for each condition are shown in Figures IV-23 through IV-27. Since the element spacing was the same for each test, the fringe spacing in the field pattern remains a constant. However, the array width is widened as more elements are added, and the fringe width must decrease. This fact is evident. The fringe width is approximately 39 cm when two elements are transmitting. This reduces to 13 cm for the six element case; the factor of three which is expected.

To evaluate the power buildup, it is first necessary to know the linearity of the field detector. A laboratory calibration of this device yielded the results shown in Figure IV-28. For the power levels at which the tests were run, the output is quite non-linear. This has been taken into account for the comparison of experiment to theoretical prediction illustrated in Figure IV-29.. As shown, the peak intensity increase is as expected.

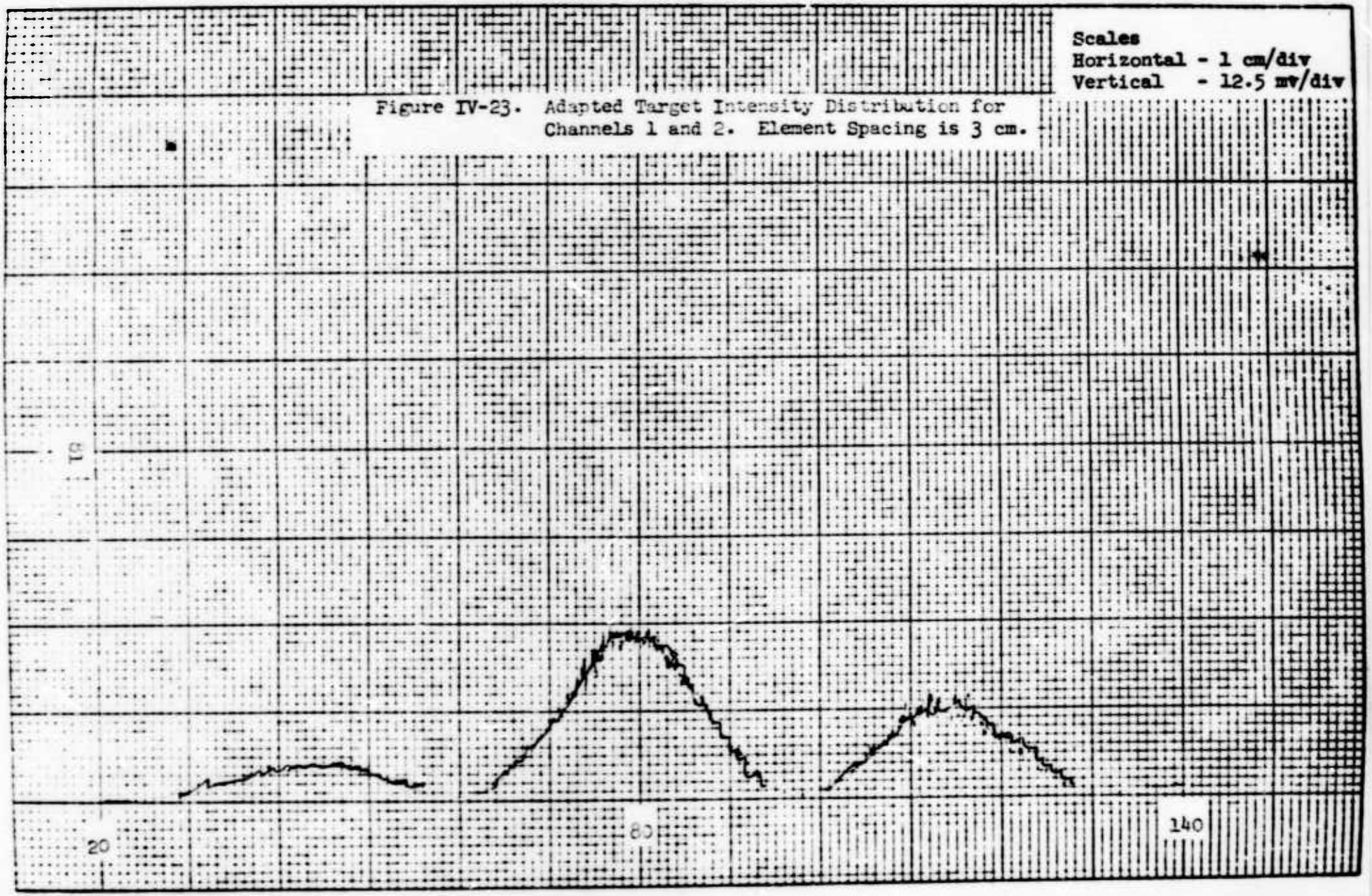

Figure IV-23. Adapted Target Intensity Distribution for Channels 1 and 2. Element Spacing is 3 cm.

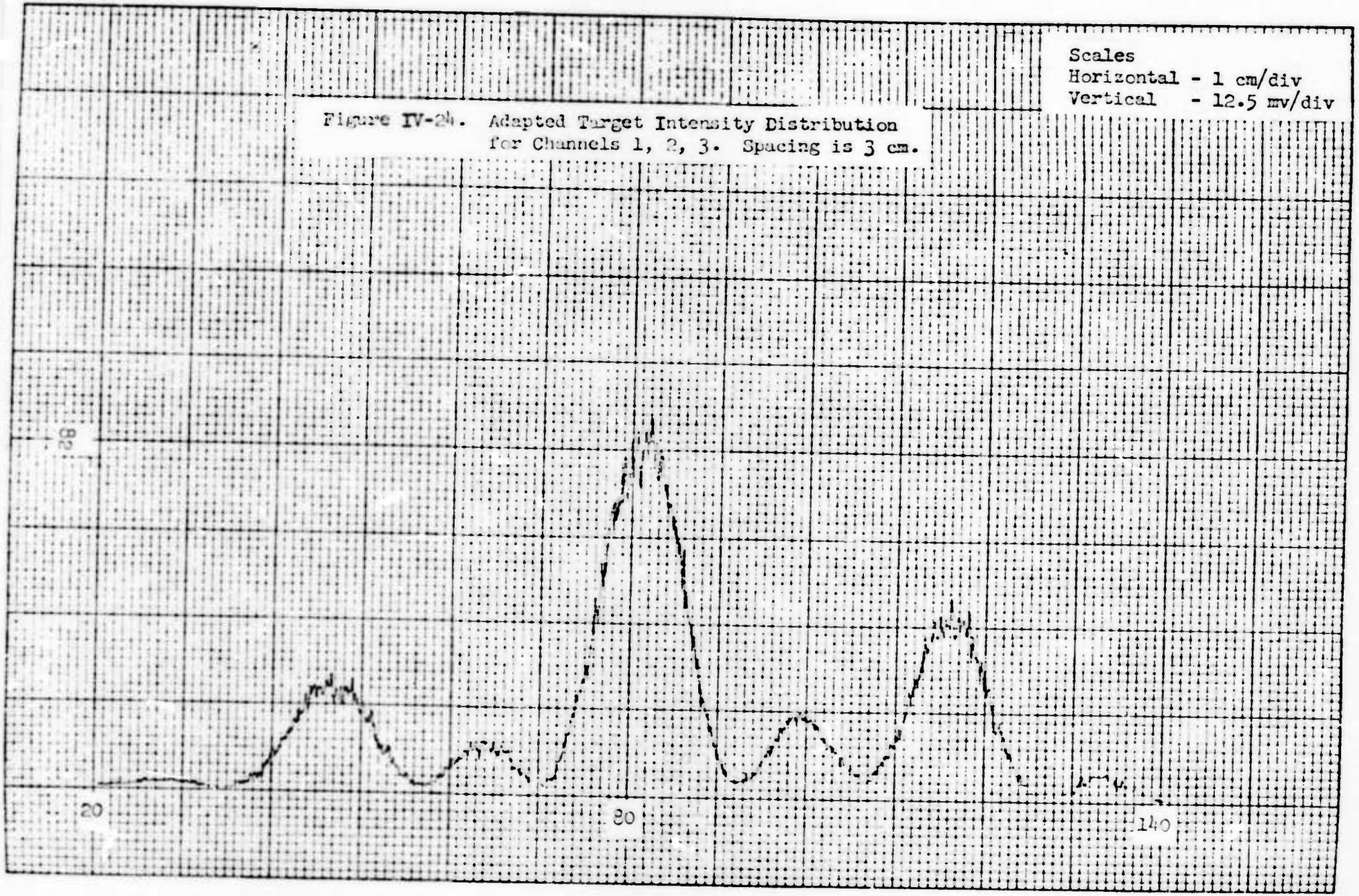

Figure IV-24. Adapted Target Intensity Distribution for Channels 1, 2, 3. Spacing is 3 cm.

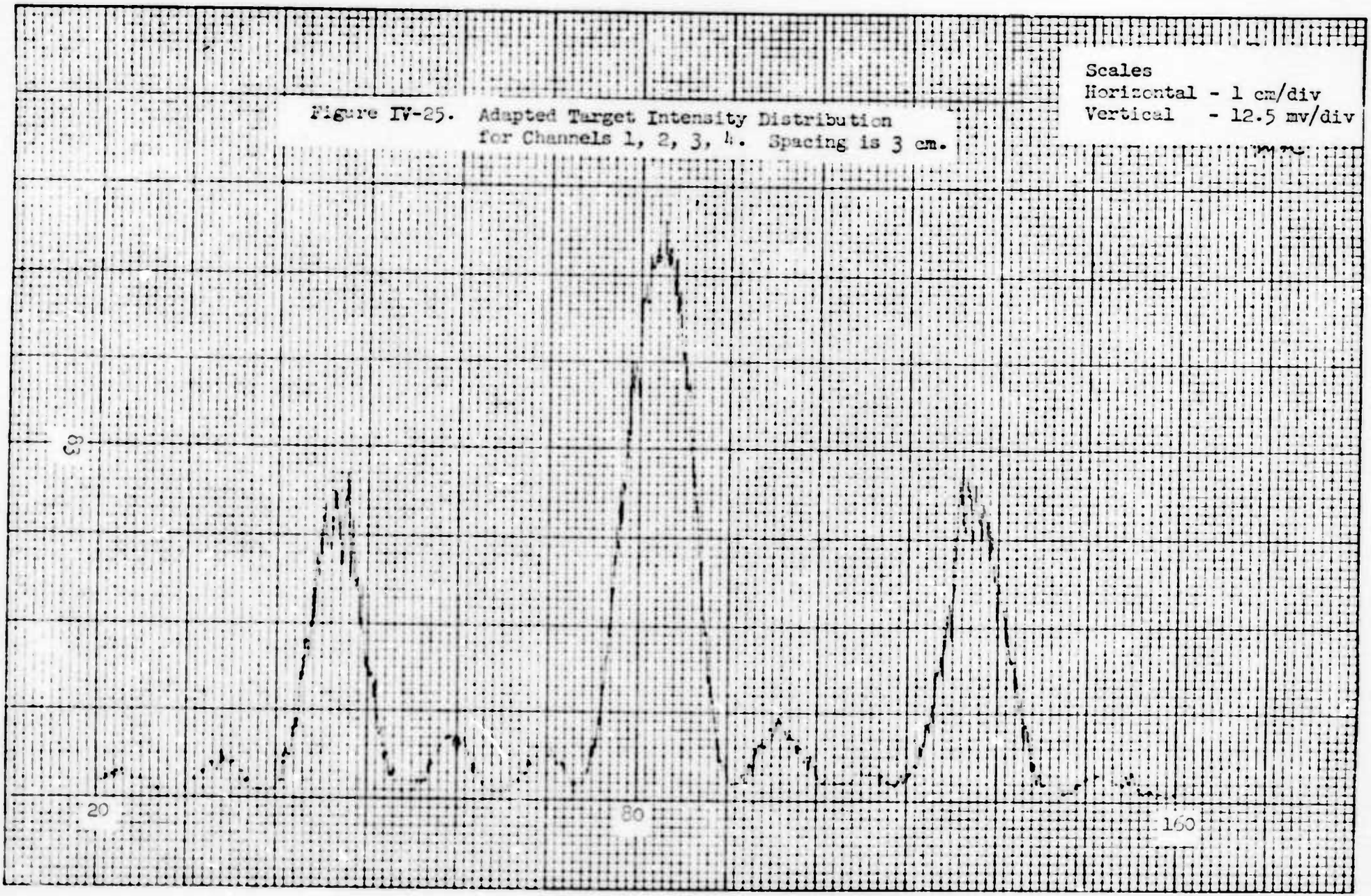

Figure IV-25. Adapted Target Intensity Distribution for Channels 1, 2, 3, 4. Spacing is 3 cm.

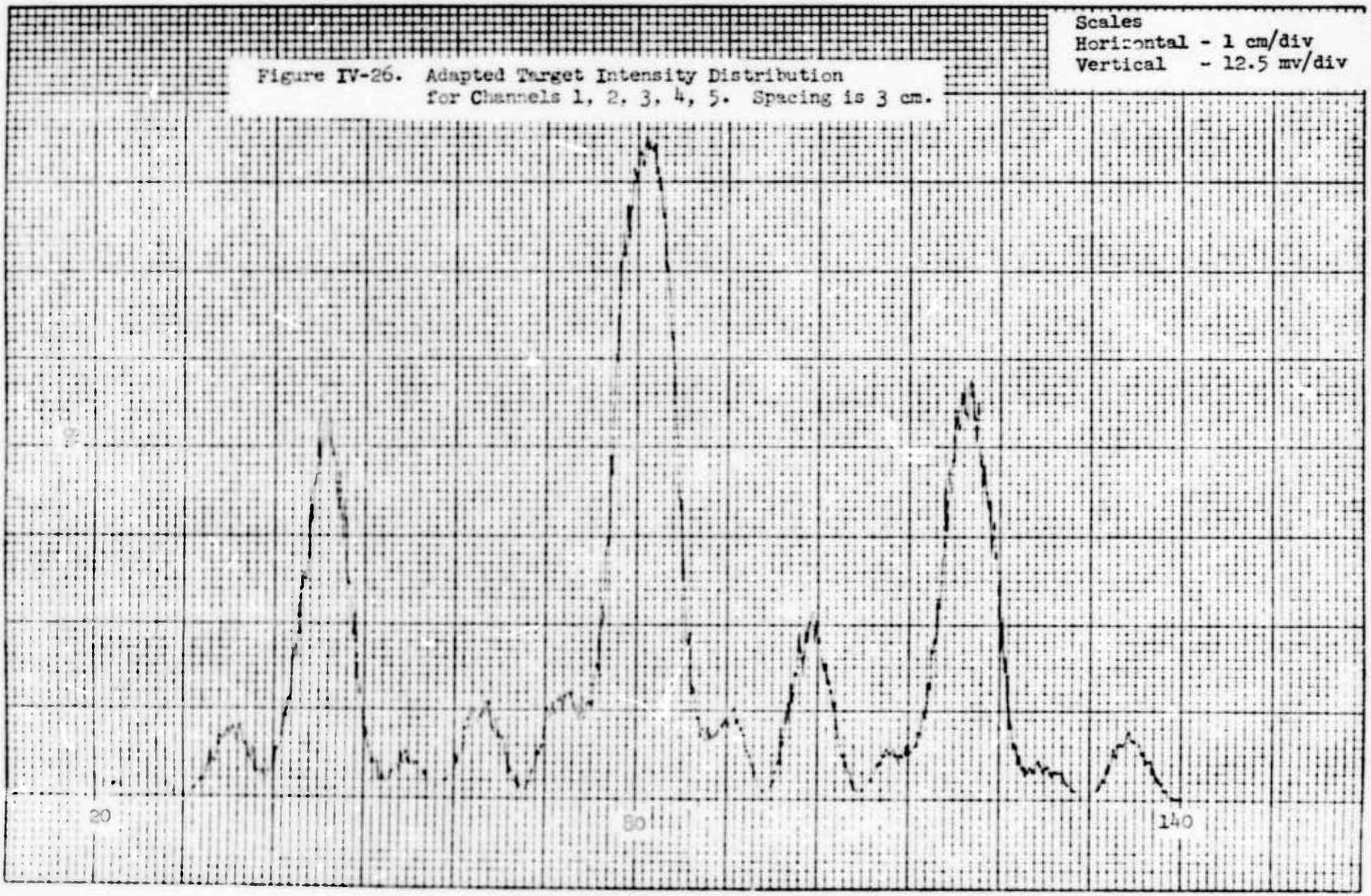

Figure IV-26. Adapted Target Intensity Distribution for Channels 1, 2, 3, 4, 5. Spacing is 3 cm.

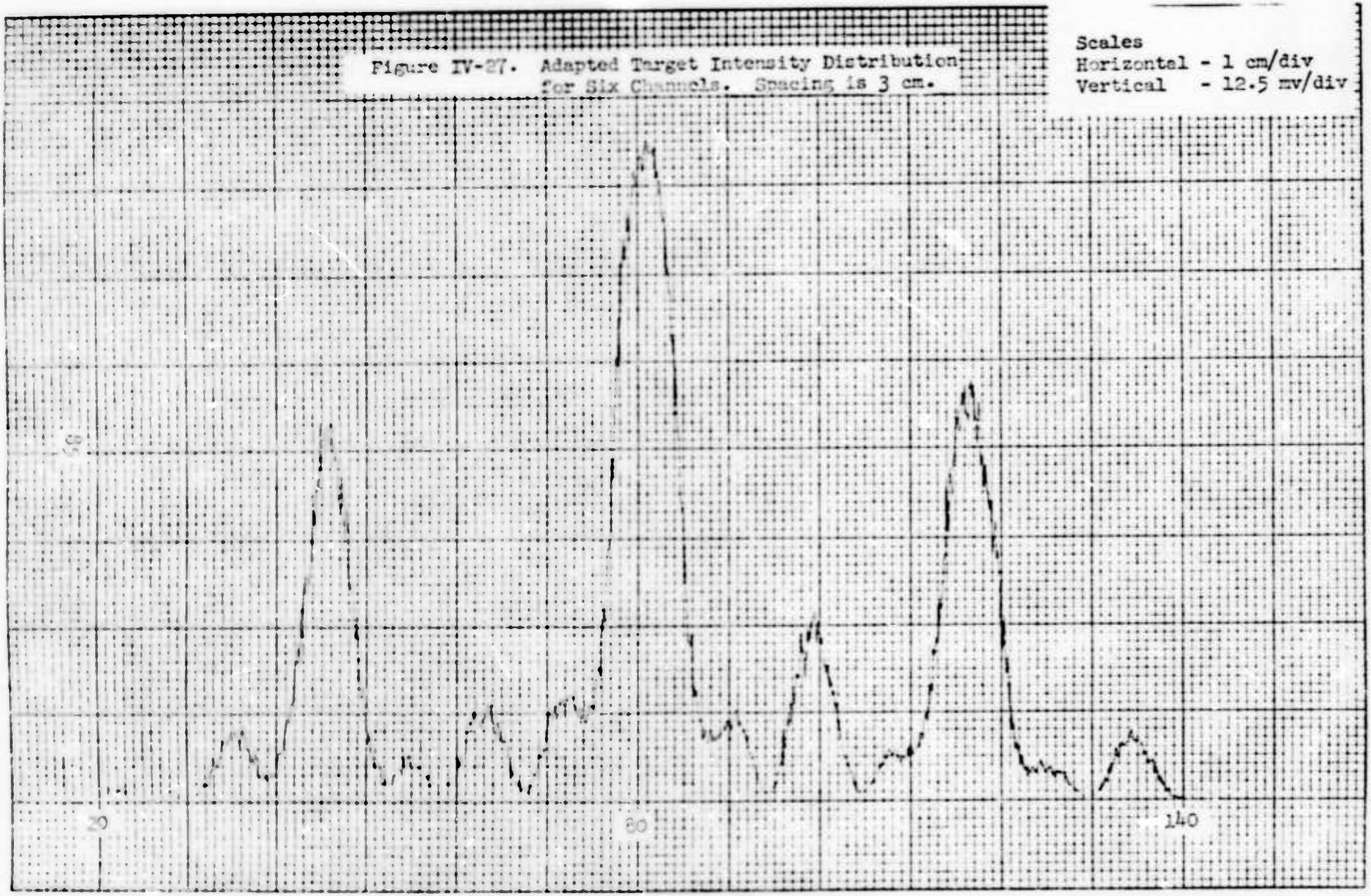

Figure IV-27. Adapted Target Intensity Distribution for Six Channels. Spacing is 3 cm.

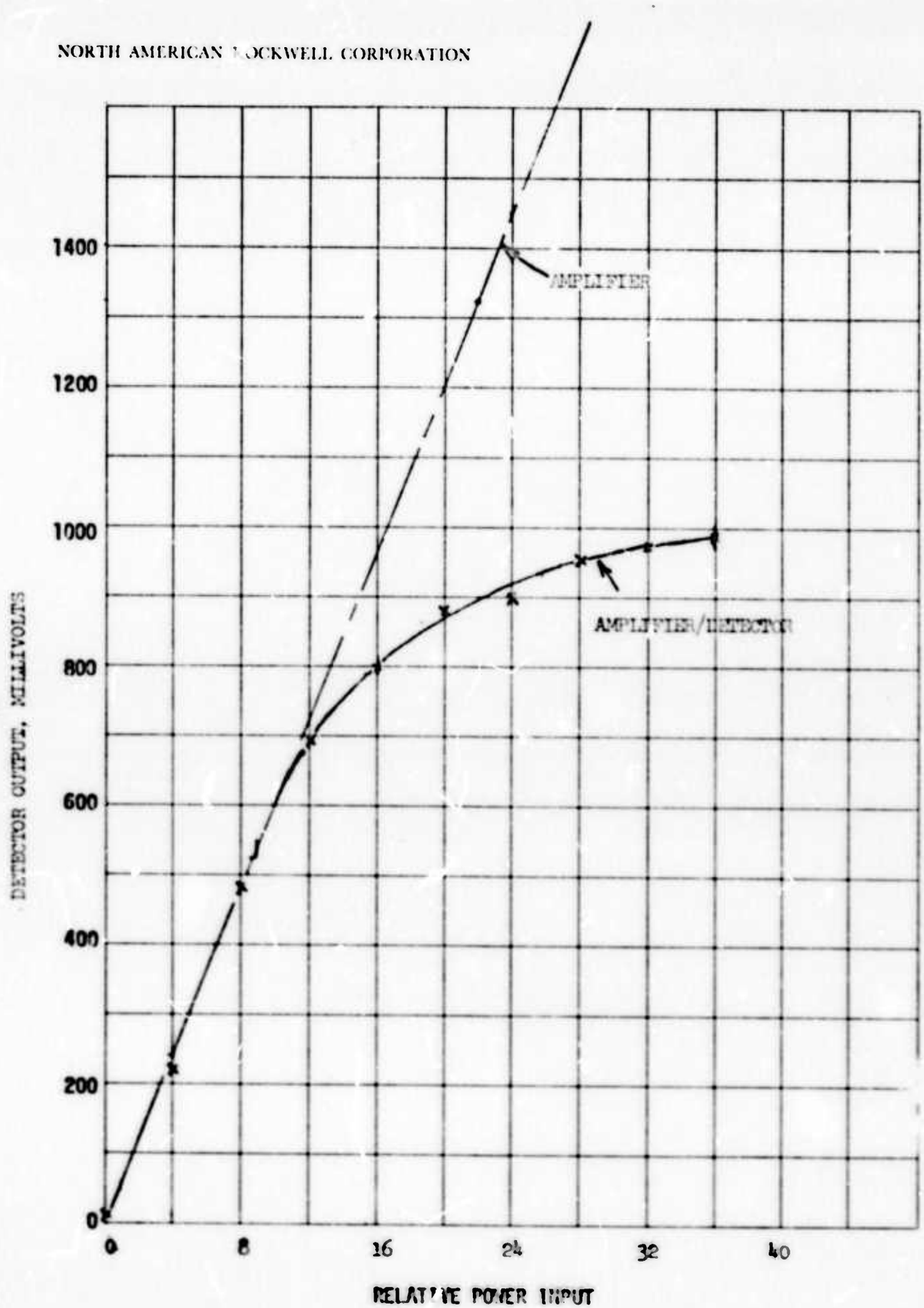

Figure IV-28. Detector Calibration Curve

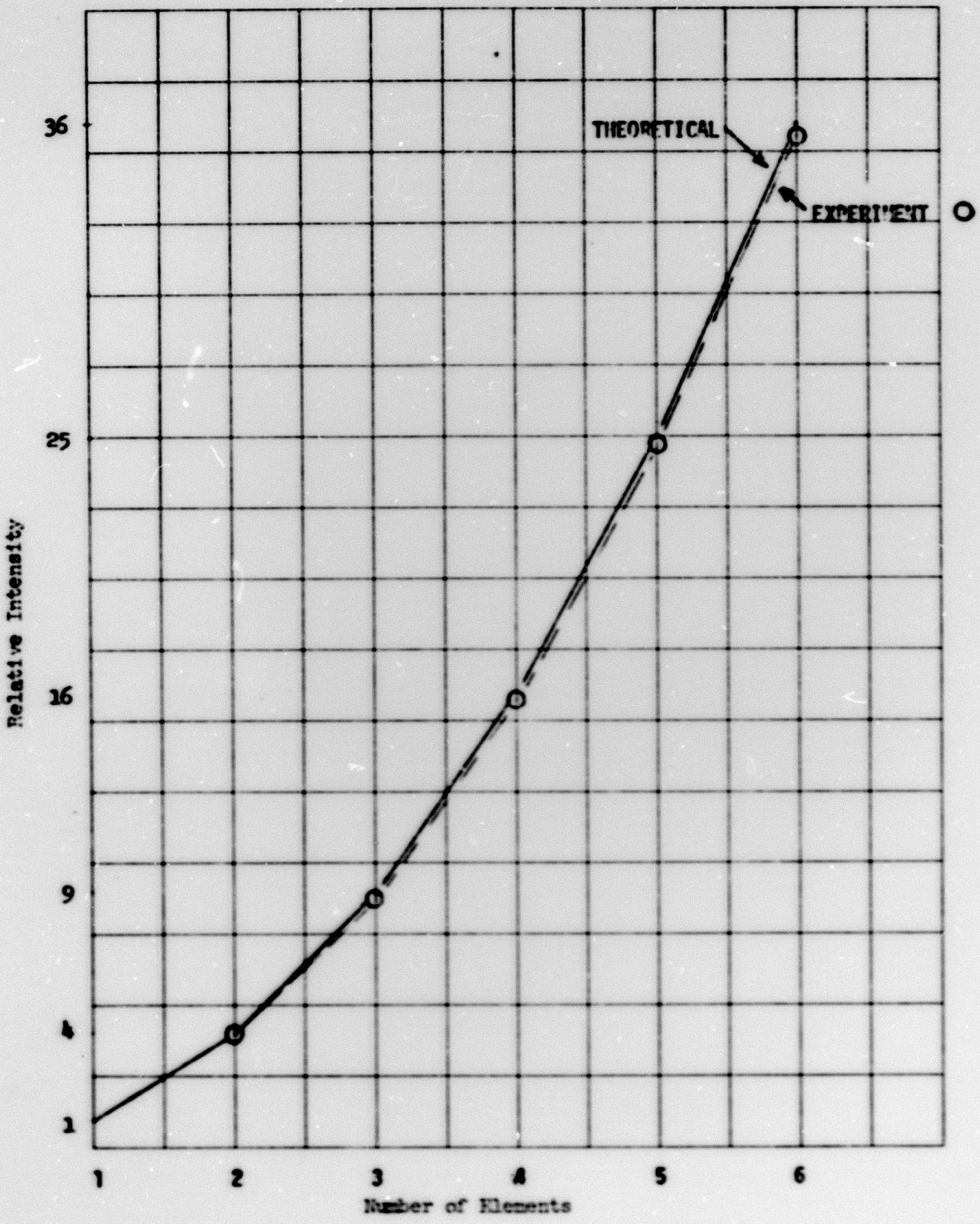

Figure IV-29. Theoretical and Experimental Comparison of the Increase of Peak Intensity at the Target

D. Variable Element Spacing

In order to assess the effect upon the target distribution of the interelement spacing, a series of tests were conducted in which different combinations of elements (1-2, 1-3, 1-4, 1-5, 1-3-5) were used. Of interest was the effect upon fringe structure, atmospheric effects, and the ability of the system to compensate under these different conditions. By this approach, operation of the system was somewhat analogous to "thinned array" testing with the only difference being the overall width of the transmitting aperture. Time was not available to rearrange the array for use of all channels with maximum interelement spacing. However, the data obtained demonstrates the system's ability to operate as predicted and some of the atmospheric effects for which the system provided automatic compensation.

To express analytically what is to be expected, the analysis of Section II must be modified to exhibit the effects of using two apertures at a time. Using this approach, the intensity distribution at the target can be written as:

$$I(X_o) \alpha \left[1 + \cos 2\pi \frac{S}{\lambda R} X_o\right] \sin^2 \frac{\pi d}{\lambda R} X_o .$$

Thus, a sinusoidal fringe pattern is expected, having a periodicity inversely proportional to the element spacing (s). Again, the amplitude of each fringe is governed by the overall envelope determined by the array element diameter (d). With this background, examination of Figures IV-30 through IV-32 indicates that operation of the system locked to a target in the center of the field is as expected. (Please note that the vertical scale was not constant during these tests in that qualitative information was of primary interest.) Figure IV-33 is of particular interest in that it provides a comparison of a distribution taken for no

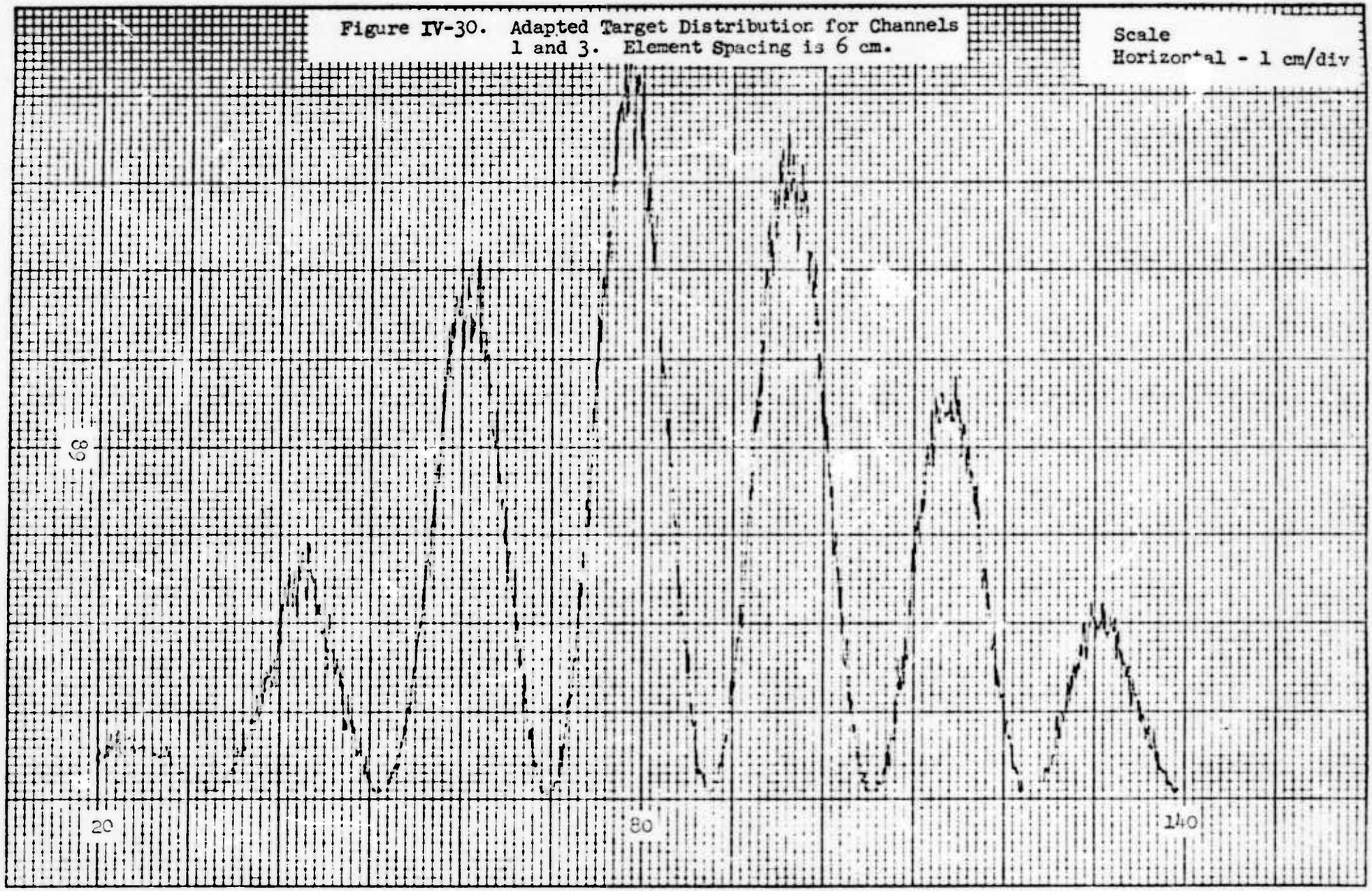

Figure IV-30. Adapted Target Distribution for Channels 1 and 3. Element Spacing is 6 cm.

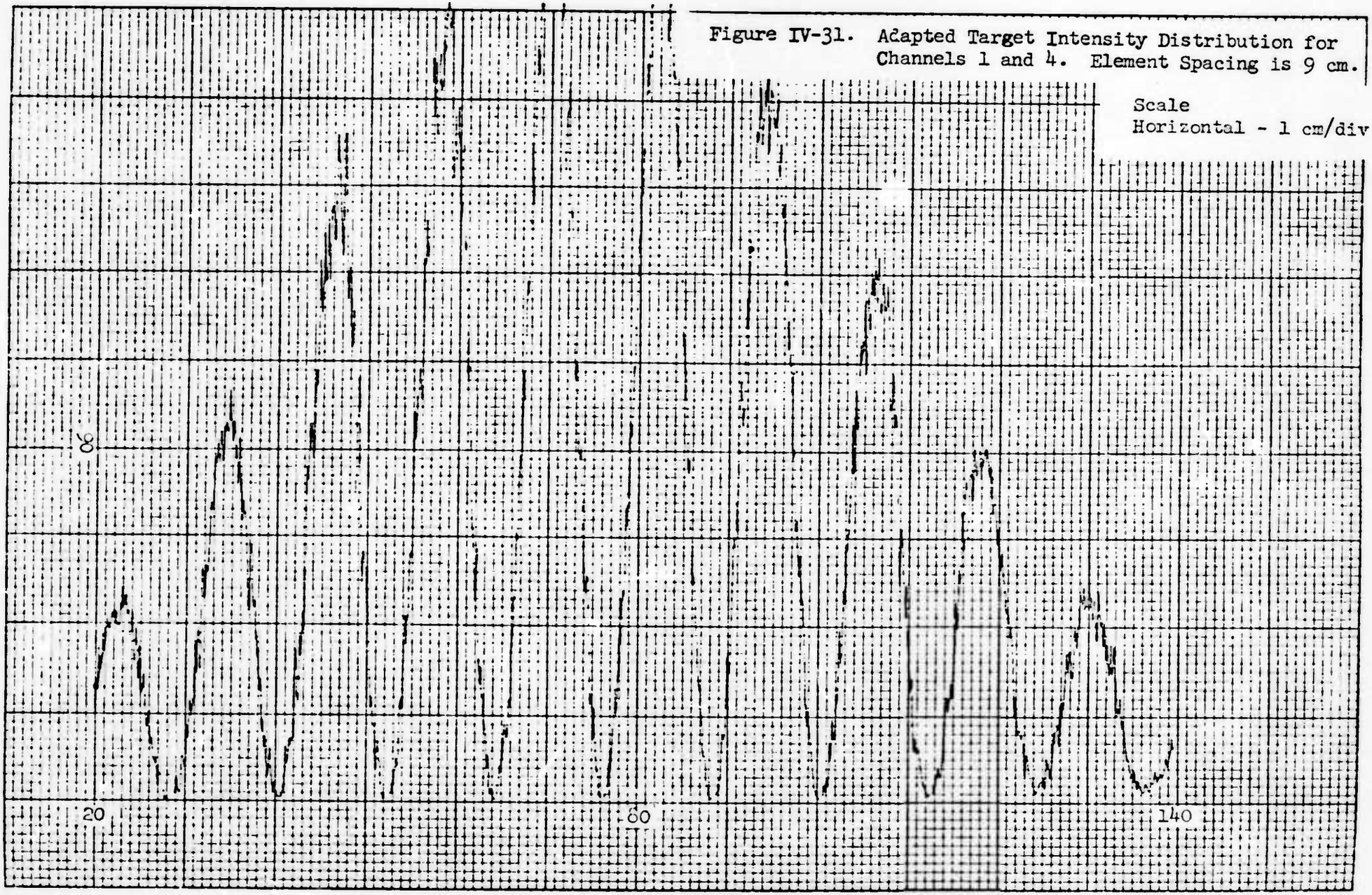

Figure IV-31. Adapted Target Intensity Distribution for Channels 1 and 4. Element Spacing is 9 cm.

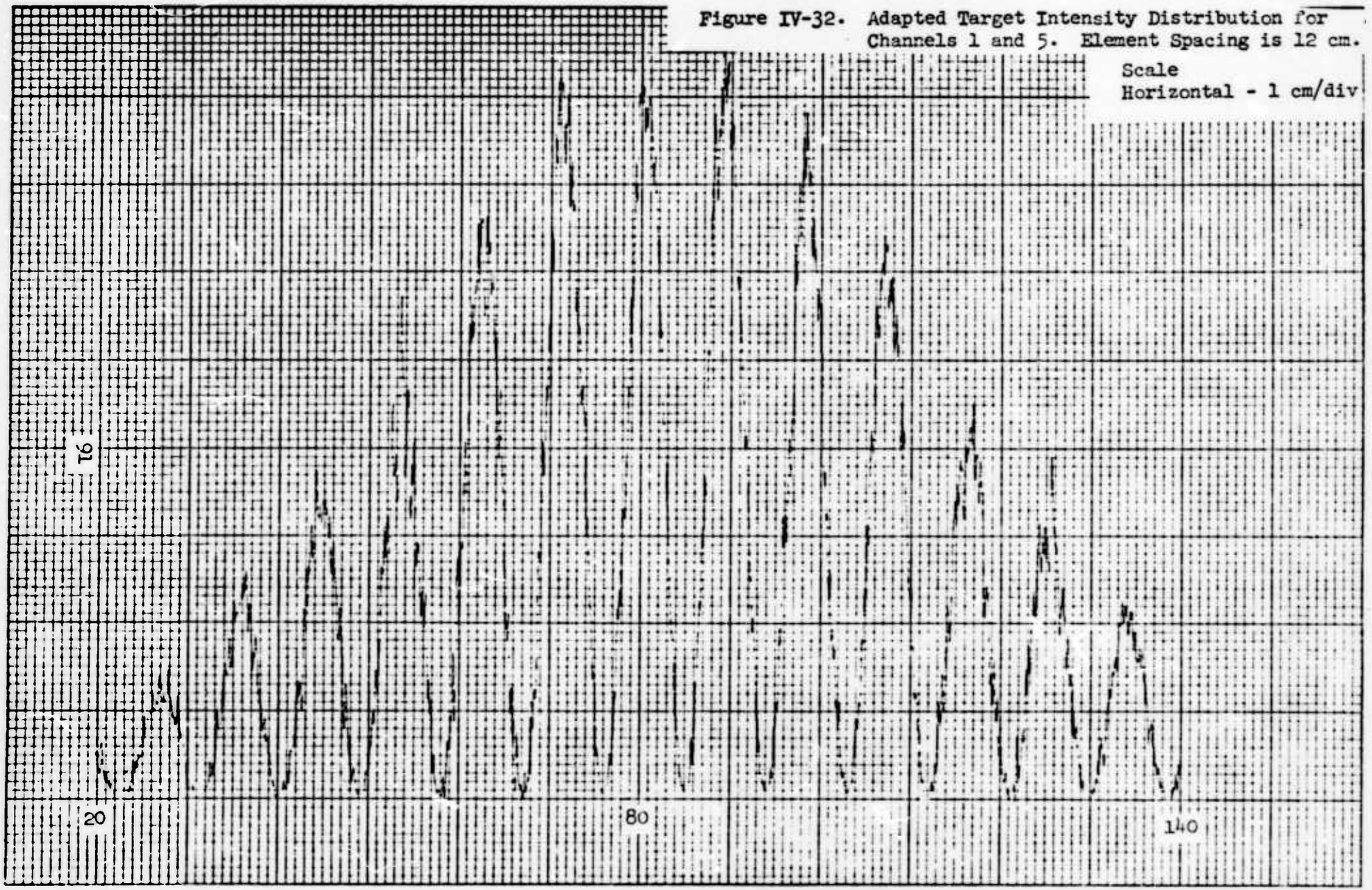

Figure IV-32. Adapted Target Intensity Distribution for Channels 1 and 5. Element Spacing is 12 cm.

Scale
Horizontal - 1 cm/div

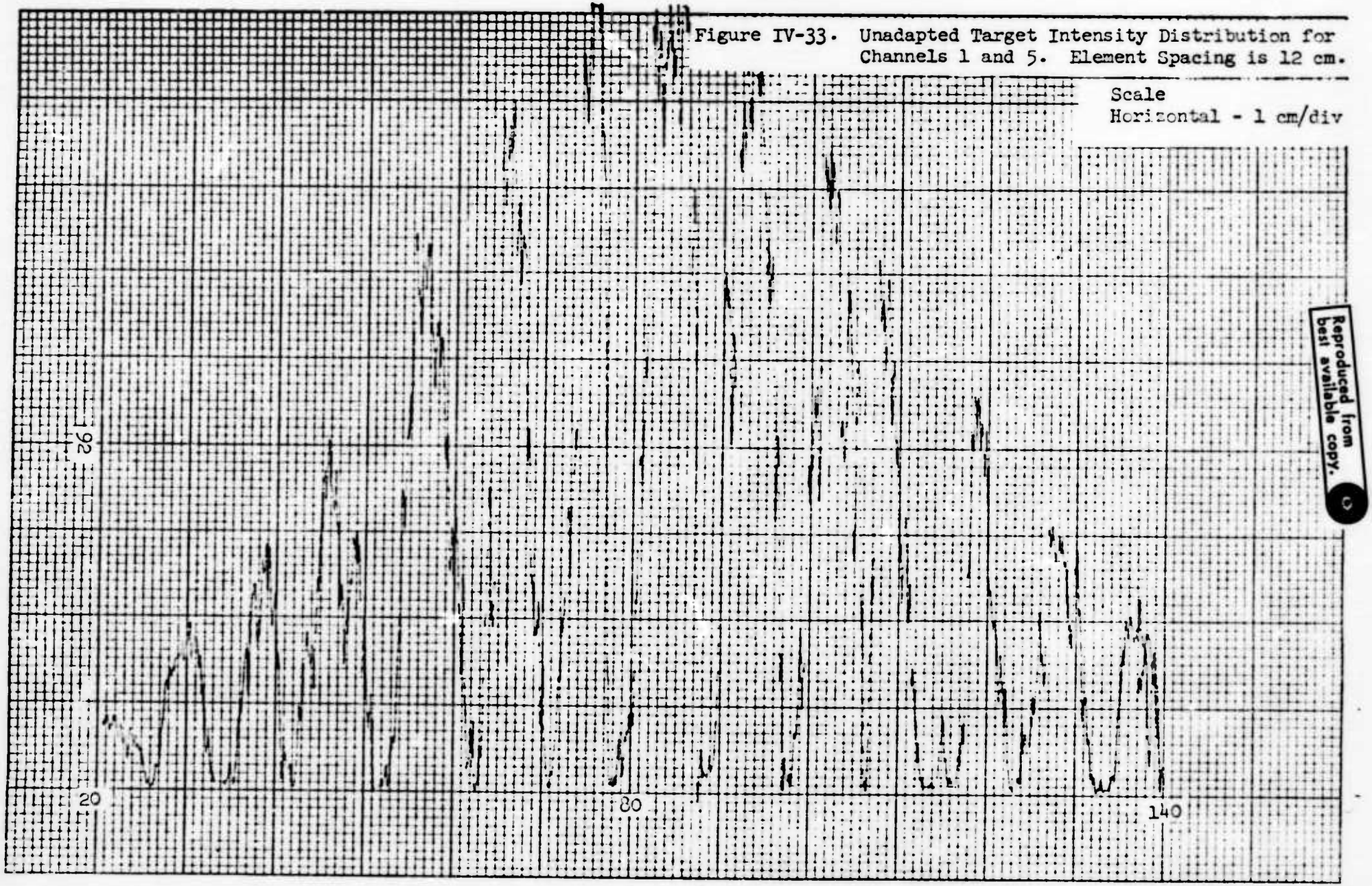

Figure IV-33. Unadapted Target Intensity Distribution for Channels 1 and 5. Element Spacing is 12 cm.

system compensation to that of the adapted condition of Figure IV-32. The effects of atmospheric perturbations are evident although not severe enough at this range (1 Km) to totally destroy the mutual coherence between the beams. However, the ability of the system to totally compensate for these effects is also equally evident.

Without repositioning the array, the "thinned" aperture having the largest overall width is made up of elements 1-3-5. The target distribution expected for this configuration reverts to the form given in Section II. Figure IV-34 shows that the fringe spacing to be about 17 cm as is required for an element separation of 6 cm. Each individual lobe takes on a $\text{sinc}^2 x$ character with a null-to-null distance of about 13 cm which is in agreement with what an array width of 15 cm should provide.

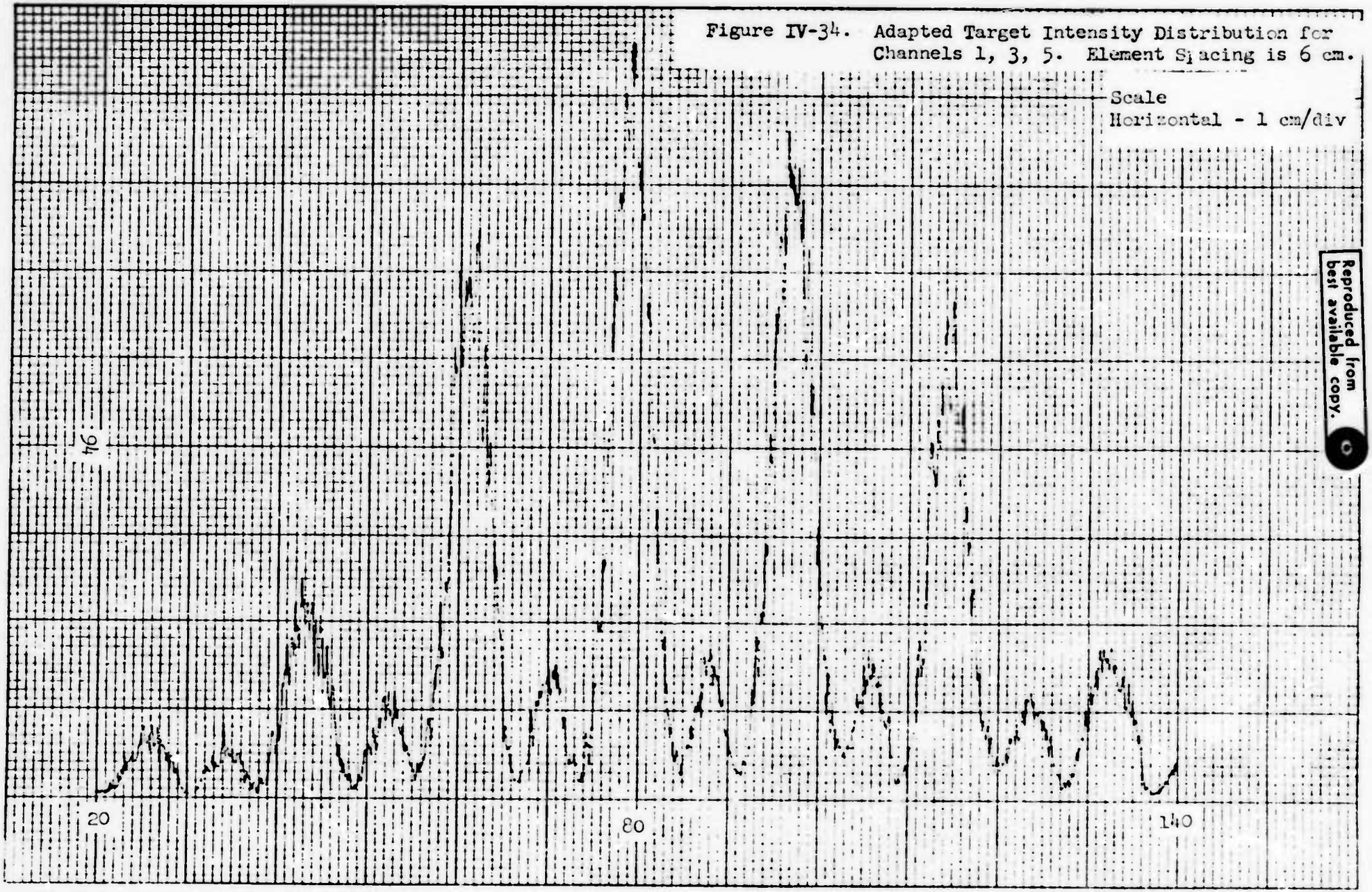

Figure IV-34. Adapted Target Intensity Distribution for Channels 1, 3, 5. Element Spacing is 6 cm.

E. 10 km Test Results

All previous data which have been presented were taken at a range of 1 km. When operating at a wavelength of 10.6 μm, extended ranges are needed in order to observe more readily the effect introduced by atmospheric perturbations. To this end, as time permitted, tests were conducted over a 10 km range. (See Section III-B). Of course, as the range increases, the array must be capable of performing with a lower signal-to-noise ratio or the return power must be increased by increasing the target size or increasing the transmitted power. In this system, the transmitter power was limited by the available power output of the single laser source. However, sufficient return signal was available to achieve an adaptive lock for a three element array. The data indicate the system performs as expected and can compensate for the perturbations introduced over this extended propagation path.

Before discussing the interesting features of the data, it is necessary to examine what intensity distribution should be expected at the target plane and what the scanner is capable of displaying. For an array with an overall width of 8.5 cm, element width of 2.5 cm; and a spacing of 3 cm, from Section II-B, the expected distribution is that illustrated by Figure IV-35. This corresponds to far-field operation with an assumed uniform plane wave illumination at the apertures. The field of view of the array is now 8 meters as shown from null-to-null. The fringe spacing is governed by the aperture spacing of 3 cm and a separation of 3.33 meters is expected at 10 km. However, the apparent spacing is less than this

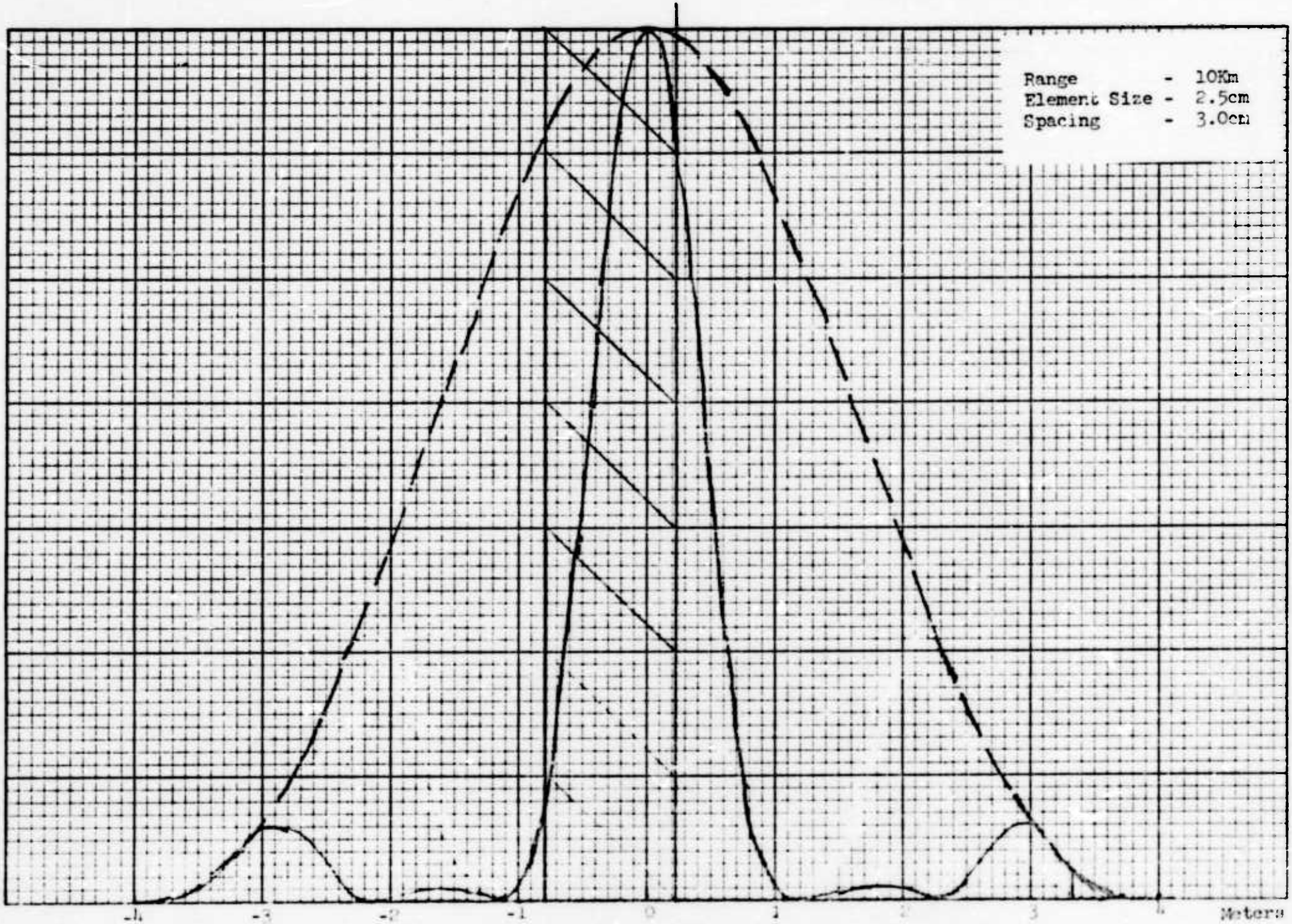

Figure IV-3. Intensity Distribution for 3 Element Array

value since the intensity envelope of the field of view materially reduces the intensity of that part of the fringe in the skirts of the overall distribution. This is also illustrated. Of prime importance is the character of the central lobe since the data to assess system operation are contained in this portion of the distribution. For an array width of 8.5 cm, a null-to-null width of 2.35 meters is expected. This exceeds the scanning range of the target plane scanning system. Thus, for the data collected, the target to which the system locked was placed close to the edge of the scanner limit in order to display most of the intensity change for one skirt of the fringe. This region of scan is shown by the shaded portion of the figure.

With this background, the data of Figure IV-36 indicate successful system operation at this range. Several interesting features are readily apparent. Foremost is the overall agreement of the distribution with the theory. The central lobe is locked to a target located 25 cm from the scanner limit. Using the 2.35 m value for the null-to-null width of the fringe, the experimental results follow very closely the $\text{sinc}^2(2\pi \frac{x}{235})$ function. One region from 90 to 105 cm deviates somewhat from the curve, but radio communication with the transmitter site established that the lock signals were somewhat unstable during this period. This was apparent from monitoring the phase error control signals at the output of the phase detectors in the control servo. Obviously, complete control was not lost during this time, but the jitter associated with the signals did not permit operation at maximum efficiency. In large part,

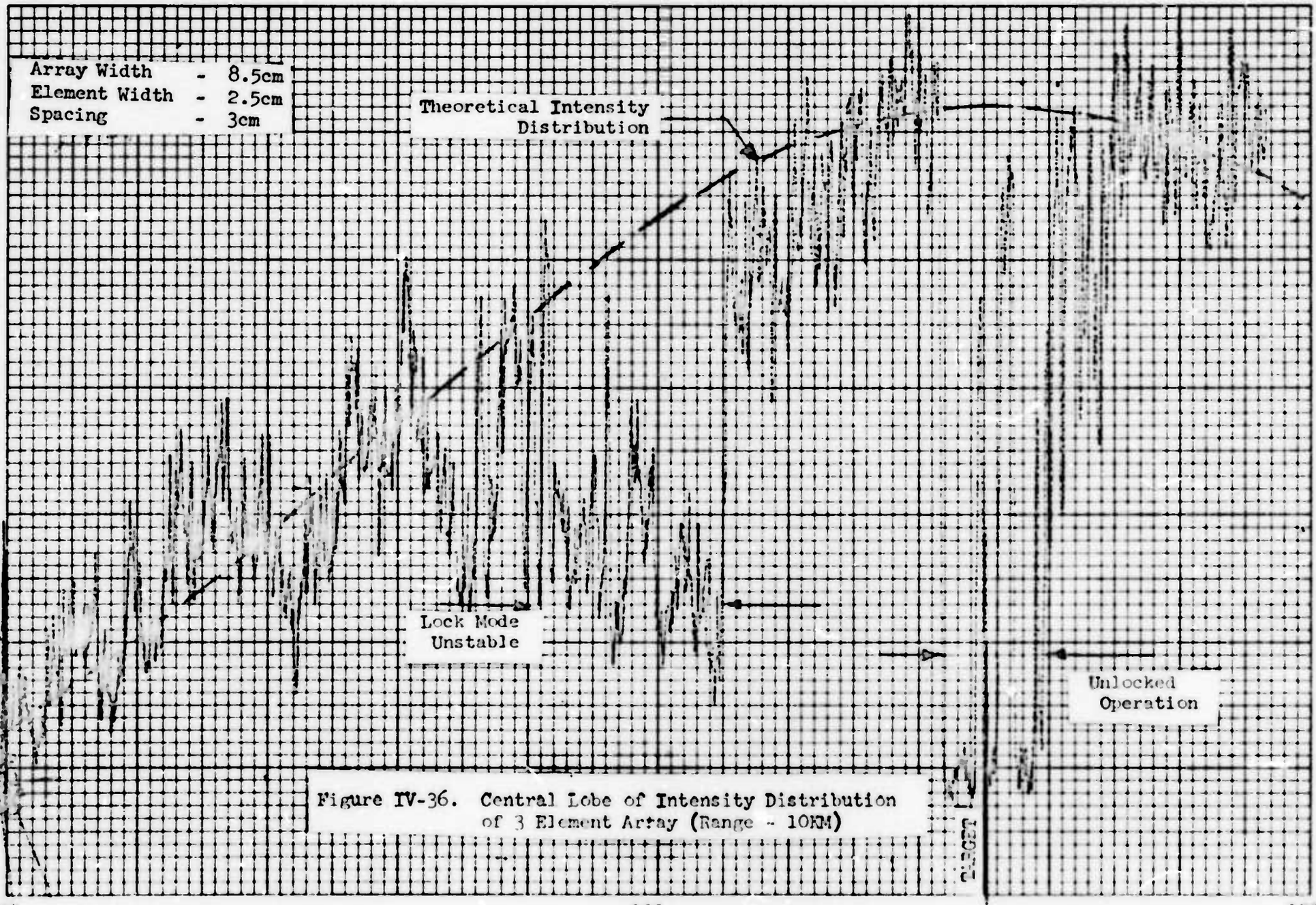

Figure IV-36. Central Lobe of Intensity Distribution of 3 Element Array (Range - 10KM)

this instability was due to the signal-to-noise ratio at which the system was operating. Computer simulation has predicted that the phase conjugation technique can provide adaptive operation at low SNR with a lower limit being about 2:1. This was about the level at which these data were taken.

When the scan had proceeded into the vicinity of the target (125cm) the system was unlocked. Readily apparent is scintillation present at this time and the general loss of energy delivered to the target area. The depth of modulation due to the atmosphere is approximately the same as that observed for each individual aperture when the system was being aligned. That is, each was characterized by an extreme amount of fluctuation. Comparing the level of scintillation during the locked and unlocked modes, an improvement (reduction) in the intensity fluctuations by a factor of five is evident. The fact that it has not totally been removed is again probably due to the low SNR. In addition, it must be remembered that correction for these effects is being accomplished in one dimension only as a consequence of the linear array. It would seem probable, then, that a certain level of scintillation should remain due to the other uncontrolled dimension.

Proceeding with the scan, upon initiating the relock command, the system recovered to the adapted mode in approximately 2-seconds (4cm of scan at 2 cm/sec). This observation was also confirmed by monitoring the error signals at the receiver. Again, the recovery time appears to be dependent

upon the SNR at which the system is operating as well as initial conditions associated with the relative phases among channels.

In summary, system operation has been accomplished at a range of 10Km. While signal-to-noise ratios were quite low, the basic function of adapting for atmospheric effects has been demonstrated and agrees with the computer simulation prediction of being able to operate at a low SNR. Table IV-1 presents a comparison of the modes of operation at this range.

TABLE IV-I

	Experiment	Theory
1. Fringe Width (null to null)	$\approx$ 2.3m	2.35m
2. Power Increase Factor (at target)	2.7	3.0
3. Scintillation Reduction Factor	5.0	-
4. SNR Improvement factor at receiver	$\approx$ 1.5	$\sqrt{3}$
5. Lock Time (SNR $\cong$ 2/1)	2 sec.	-

F. Atmospheric Data

During the collection of data on COAT performarce, measurements of atmospheric-produced scintillation were conducted using the techniques and equipment previously described in Section III. These scintillation data were then reduced to a form where the refractive index structure constant,* C_N^2, could be calculated. Our method of reducing these data, which was developed on previous programs and which has been described in detail[5,6] uses a pulse-height-analyzer to obtain the probability density of the scintillation, and from this the probability distribution. We then "best-fit" a log-gaussian distribution to the data and computed the variance of the log-amplitude ($\frac{1}{2}$ ln I). Using spherical wave propagation theory,[7] we calculated C_N^2 using the following expression:

$$C_N^2 = \sigma_1^2 / 0.124 \left(\frac{2\pi}{\lambda}\right)^{7/6} Z^{11/6},$$

where,

σ_1^2 is the log-amplitude variance

λ is the optical wavelength (m)

Z is the propagation range (m)

and

C_N^2 is the refractive index structure constant ($m^{-2/3}$).

From our measurements over the 1.0 km range, the strength of turbulence varied from 1.0×10^{-15} $m^{-2/3}$ to about 5.0×10^{-15} $m^{-2/3}$. The data gathered over the 10.0 km range indicated a strength of turbulence from 5.0×10^{-16} $m^{-2/3}$ to 1.0×10^{-14} $m^{-2/3}$. Qualitatively, this corresponds to the categories of weak to mild turbulence.

*A measure of the strength of optical turbulence.

V. COMPUTER SIMULATION AND COMPARISON

Part of this program effort was directed twoards the verification of results obtained by computer simulation. Using previously developed codes[2] which incorporate atmospheric perturbations in the propagation path as well as induced phenomena, a series of computer runs were made to simulate actual test conditions. The results show a one-to-one correspondence with experiment. In all cases, the system performed as predicted, and the ability to investigate various configurations by this computer method without fabricating hardware has been shown. Various arrays are now being investigated to optimize system performance.

Following the same chronological pattern of the experiments, Figures V-1 through V-5 illustrate the results obtained for sequencing the channels as described in Section IV-C (1-2, 1-2-3, etc.). As before the fringe spacing (grating lobe) is 33 cm as expected for an element spacing of 3 cm when measured at a range of 1 Km. The overall field of view is slightly narrower than that of the experimental array. Consequently, the amplitude of the fringes is less than that obtained by experiment. This is due primarily to the difference in truncation of the Gaussian aperture distribution used for the simulation as opposed to the truncation of the transmitted beams of the experiment. As described in Section II, this "filling" factor influences the field width and the intensity of the side fringes.

Of further importance is the manner in which the peak intensity increases as additional beams are locked to the target. Plotting this

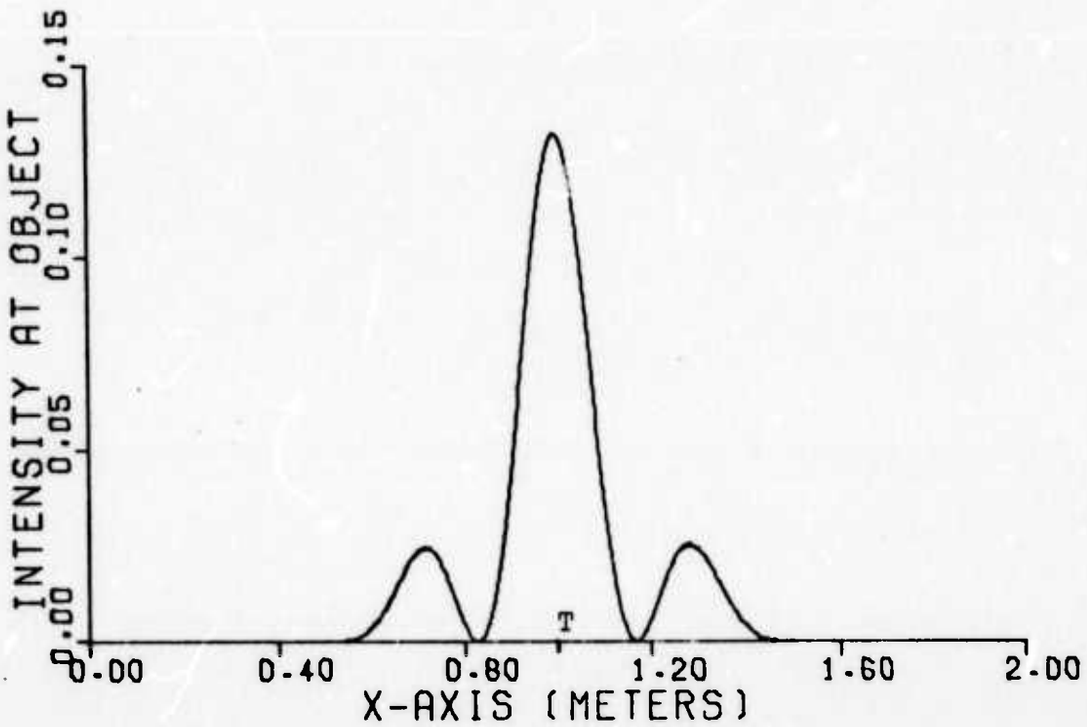

Figure V-1. Adapted Target Intensity Distribution for Channels 1 and 2. Element spacing is 3 cm.

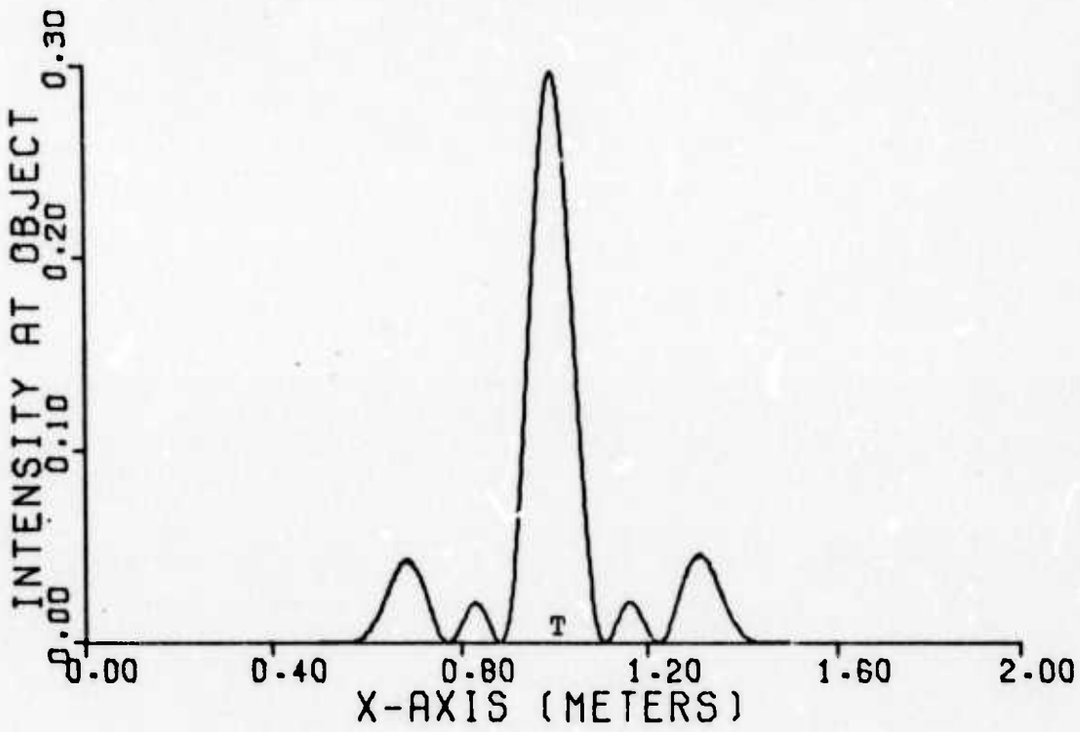

Figure V-2. Adapted Target Intensity Distribution for Channels 1-2-3. Element spacing is 3 cm.

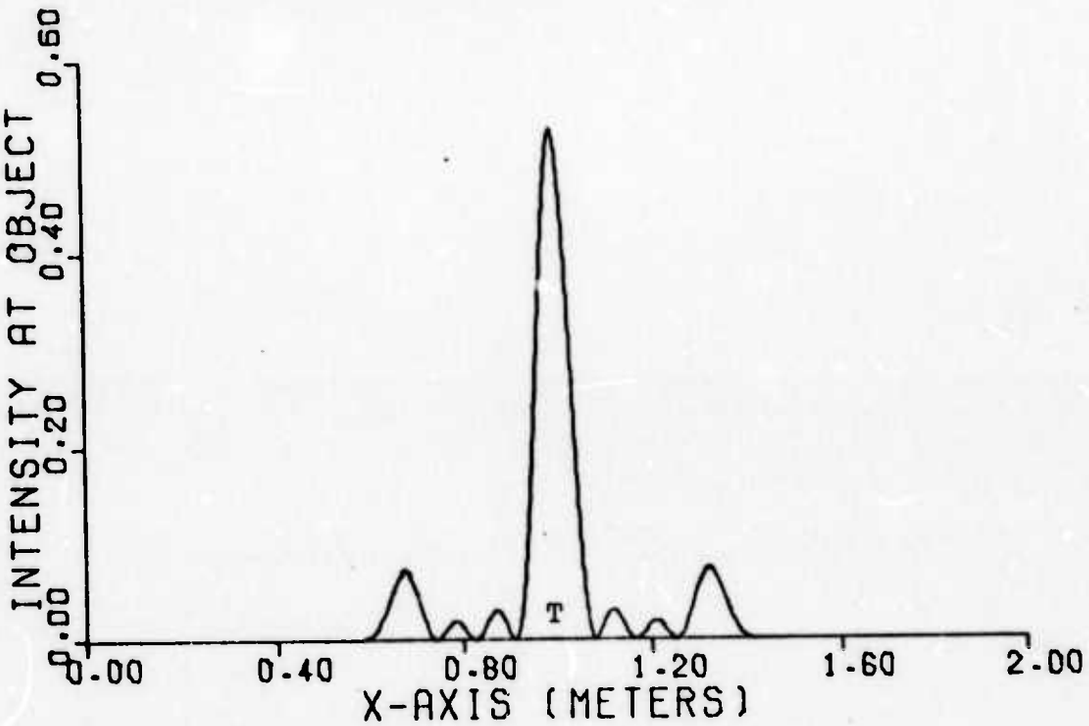

Figure V-3. Adapted Target Intensity Distribution for Channels 1-2-3-4. Element spacing is 3 cm.

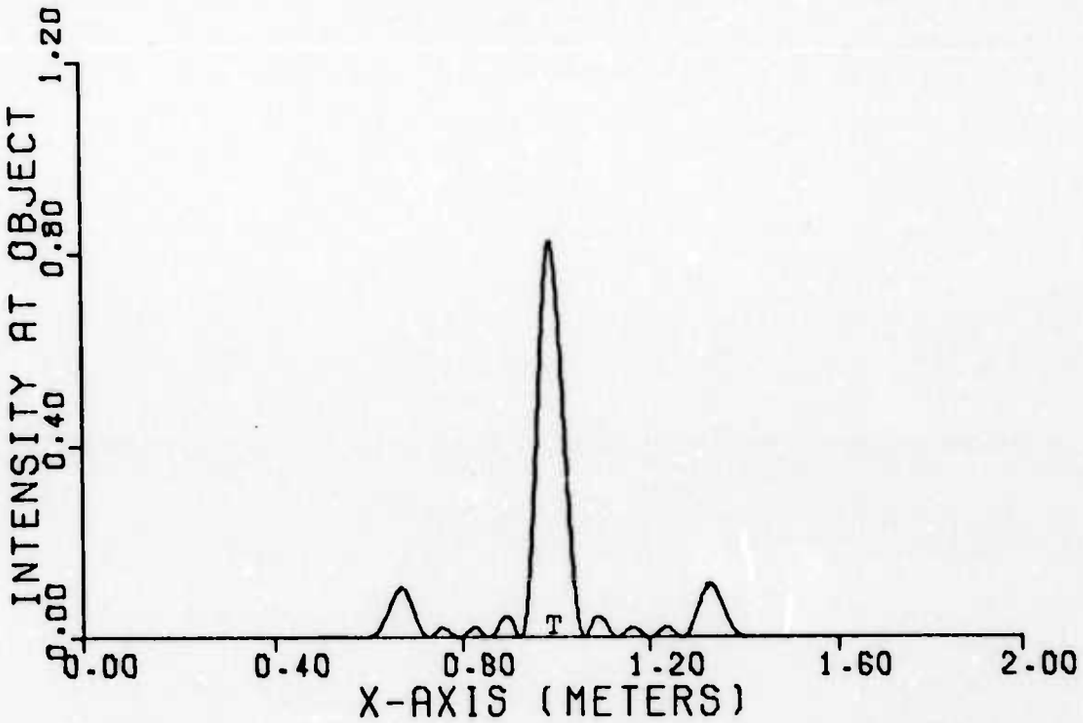

Figure V-4. Adapted Target Intensity Distribution for Channels 1-2-3-4-5. Element spacing is 3 cm.

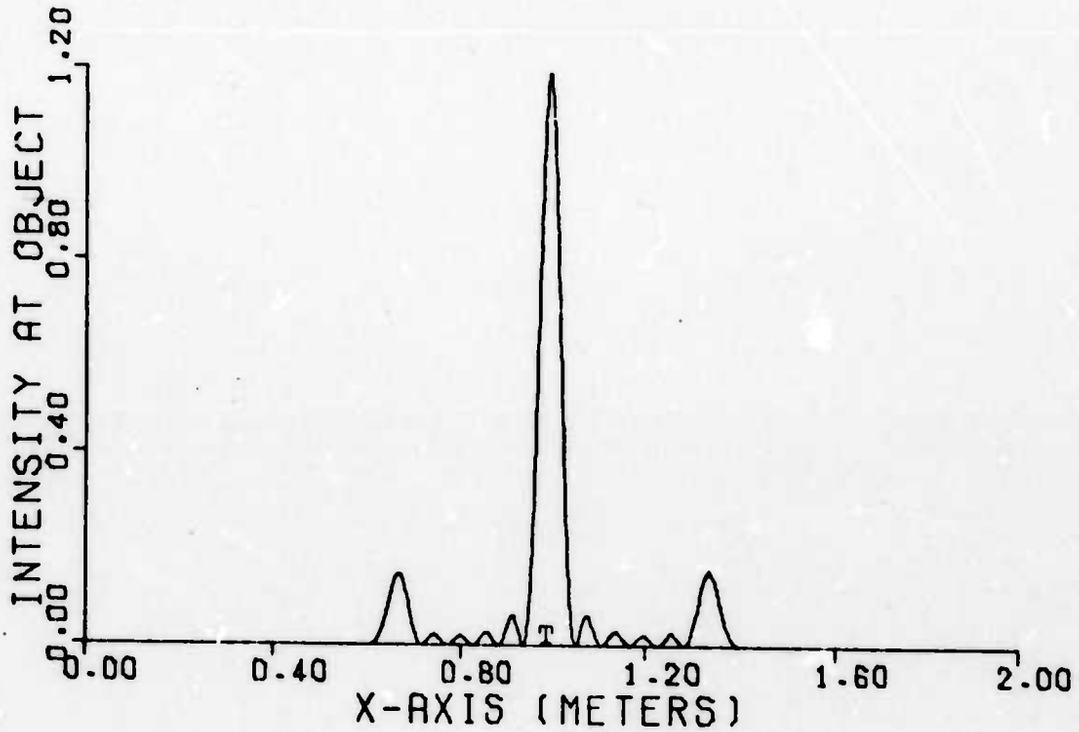

Figure V-5. Adapted Target Intensity Distribution for the Channels 1-2-3-4-5-6. Element spacing is 3 cm.

function yields the theoretical curve of Figure IV-29 and again demonstrates the agreement of experiment with theory.

In order to assess the effect of element spacing on the target plane distribution of energy as in Section IV-D, the "thinned" array results of V-6 through V-8 are presented. Several features of these distributions are of interest. First, the field of view of the array is shown to be the same for each simulation independent of element spacing. This is consistent with the analysis of Section II in that the element size solely determines this distribution parameter. Of course, the number of fringes within the field of view envelope increases as the elements are separated. Particularly noteworth is the fact that the value of peak intensity at the target is the same for all conditions of these simulations. This is a consequence of the addition of the phased field quantities at the target and can be increased only by adding more elements to the array or increasing the amount of transmitted energy.

Finally, Figure V-9 illustrates several basic features of phase conjugation COAT system operation. For this run, a target having a reflectivity of 0.9 was placed on the array axis. The adapted distribution for this condition is shown at time 1. At this time, a target of unit reflectivity was introduced at an off axis position. The system then adapted to the brighter target eventhough its initial illumination was nearly zero. Time markers 2 through 7 display the evolution of the final distribution. It is to be noted that the "dim" target has been completely ignored. This prediction is, of course, borne out by the

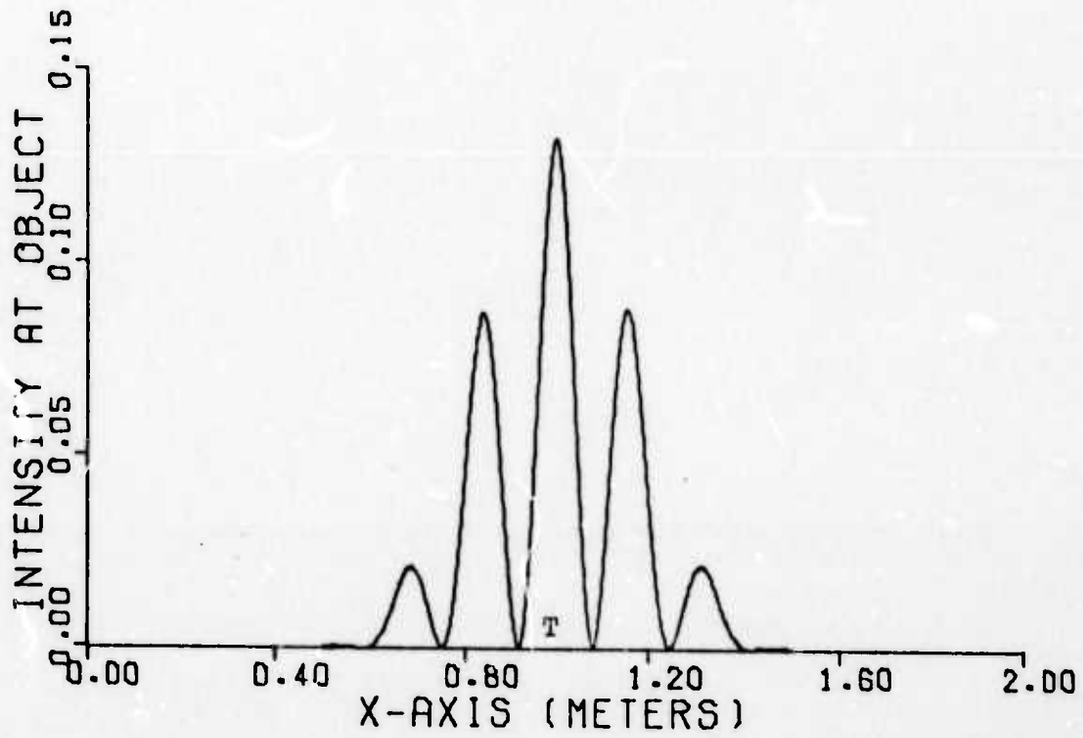

Figure V-6. Adapted Target Intensity Distribution for Channels 1-3. Element spacing is 6 cm.

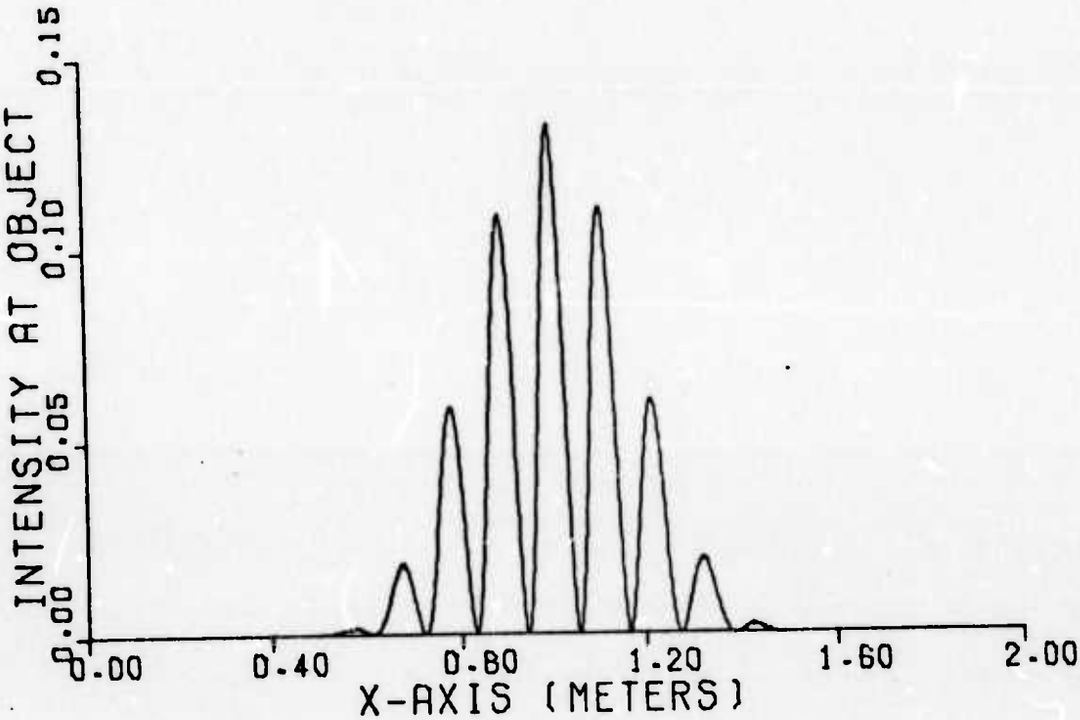

Figure V-7. Adapted Target Intensity Distribution for Channels 1-4. Element spacing is 9 cm.

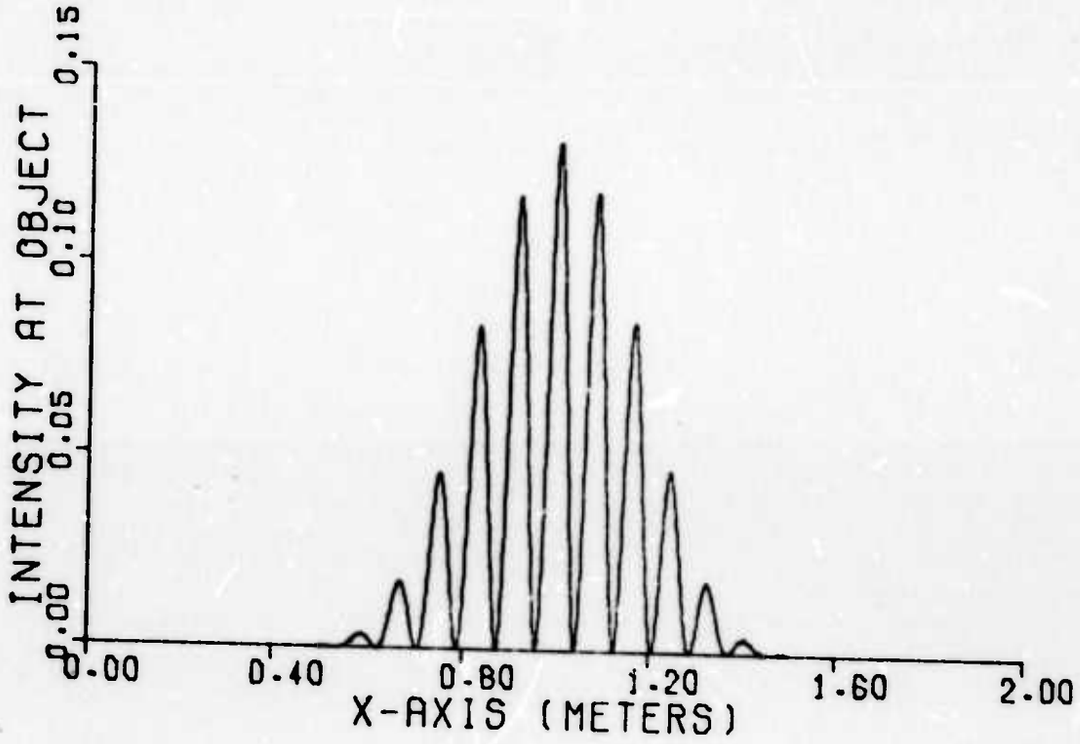

Figure V-8. Adapted Target Intensity Distribution for Channels 1-5. Element spacing is 12 cm.

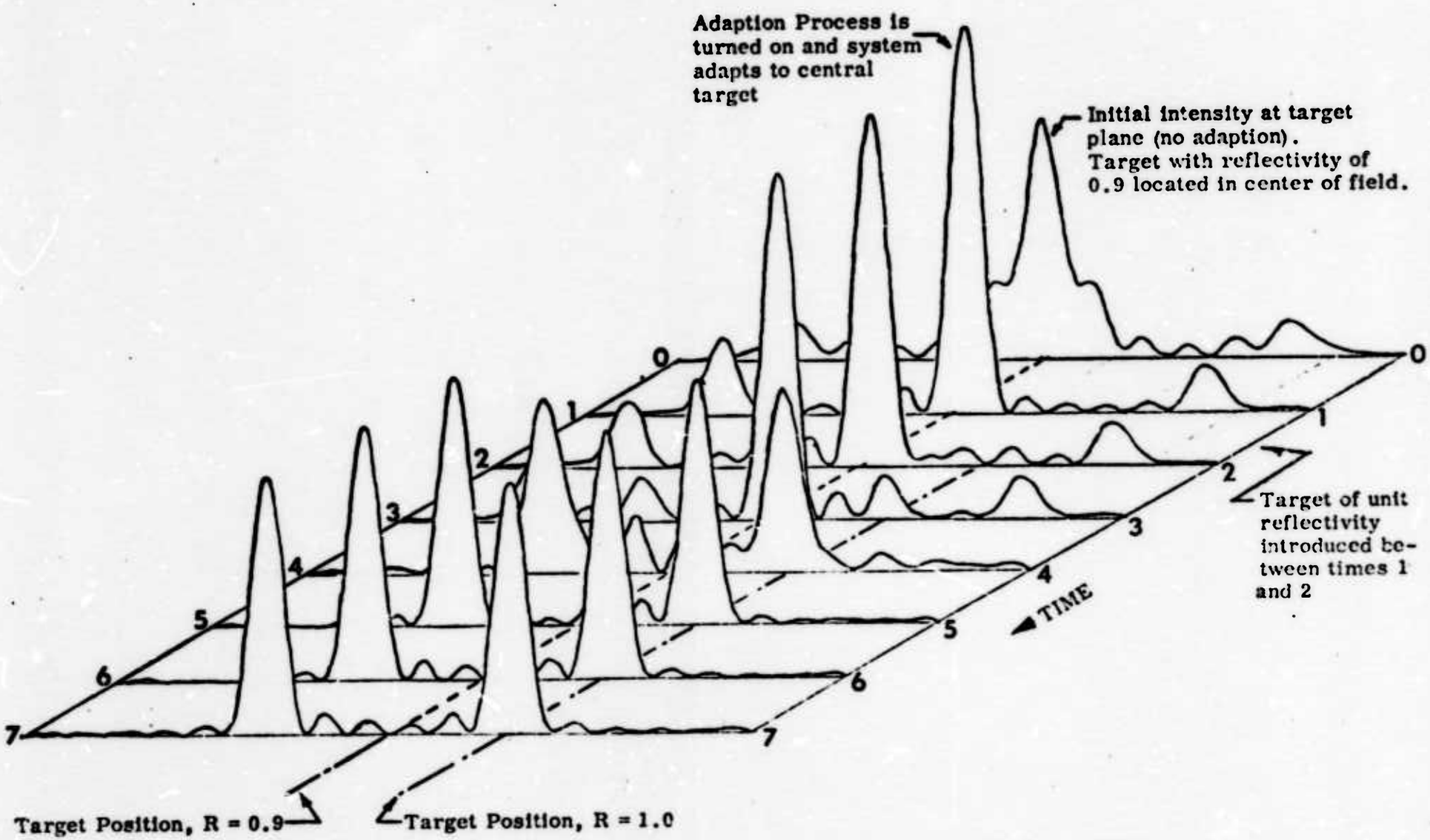

Figure V-9. Adapted Target Intensity Distribution for a Multitarget Scenario as a Function of Time

data of Section IV.

In addition to this target grabbing capability, the final distribution displays the ability of the system to lock to an off axis location with the intensity at this target being governed by the field of view envelope. The remaining energy appears in the adjacent fringe whose separation distance is a function of the element spacing.

In summary, the computer codes developed for COAT simulation predict very accurately the system characteristics. Having been verified by experimental data, these codes become a powerful tool for analysis of future systems and their applications.

VI. CONCLUSIONS

The experiments conducted during this program show conclusively that the COAT system compensates for atmospheric effects on laser radiation propagated over long paths. In addition, the system mechnization based upon the phase conjugation principal (analogous to holography) provides the ability to automatically acquire and track a target anywhere within its field of view at very high rates with high resolution. Also inherent to this operation is the ability, at the same time, to increase the power density level of the radiation at the target by the square of the number of elements of the array as a consequence of the array focusing capability. Practially speaking, all of these functions are accomplished with optical elements of limited size which are easily fabricated. Yet the full benefits of a large aperture system are realized and exceeded without having to meet attendant pointing requirements.

We believe that phase conjugation COAT will have important applications in the fields of optical radar, communications, and high energy beam power delivery to remote targets. The experimental results presented herein have conclusively demonstrated the following properties of phase conjugation COAT:

1. Compensation for atmospherically induced perturbations (both beam spreading and scintillation)
2. Lock to a single glint target centered in the field
3. Lock to a single glint target at various locations within the field of view
4. Lock to a moving glint target

5. Lock to the glint of highest reflectivity in a multi-glint target environment
6. Speed of adaptive acquisition is limited only by the transit time
7. Array focusing capability is improved.

Furthermore, the results obtained have been in excellent agreement with our computer simulation predictions. Therefore, we feel confident in using the PSYCAT simulation routine for predicting the operation of future systems.

Future work on phase conjugation COAT systems is strongly recommended, based on the experimental results which we have obtained to-date. Effort in the following areas is suggested:

(1) increase power handling capability of system
(2) extend experimental work to two-dimensional arrays
(3) study and evaluate alternate optical configurations which retain the highly desirable phase conjugation operating principal
(4) perform detailed studies of application techniques for high energy systems, infrared radar and tracking systems, and infrared/optical communications systems.

VII. BIBLIOGRAPHY

1. W. T. Cathey, C. L. Hayes, and W. C. Davis, Coherent Optical Adaptive Techniques, Final Report on Contract F30602-67-C-0227 (RADC)

2. R. P. Futrelle, G. E. Mevers, and C. L. Hayes, Coherent Optics Adaptive Techniques, RADC-TR-71-148, Final Report on Contract F30602-70-C-0298, March 1971

3. C. L. Hayes et al. Coherent Optical Adaptive Techniques, First Quarterly Report on Contract F30602-72-C-0417 R. F. Ogrodnik RADC OCTM-1-MONITOR

4. J. SooHoo, C. L. Hayes, and R. A. Brandewie, An Acousto-Optical Modulator for CO_2 Lasers, presented at EOSD Conference, New York, September 1972.

5. D. L. Fried, G. E. Mevers, M. P. Keister, Jr., J. Opt. Soc. Am. 57 787, p-101.

6. "Optical Propagation Measurements at Emerson Lake-1968," NASA Contractor Report, NASA CR-1733.

7. D. L. Fried, J. Opt. Soc. Am. 57 175 (1967).